DEPARTMENT OF ELECTRONIC & ELECTRICAL ENGINEERING

University of Strathclyde Engineering

Novel Hybrid HVDC System for Resilient and Efficient Operation of Offshore Wind Farms

Shangen Tian

A thesis presented in fulfilment of the requirements for the degree of Doctor of Philosophy

Department of Electronic and Electrical Engineering

University of Strathclyde, Glasgow, UK

2024

This thesis is the result of the author's original research. It has been composed by the author and has not been previously submitted for examination which has led to the award of a degree.

Signed:  Date: 18 May 2024

Dedicated to my family

Acknowledgements

I would like to express my thanks and respect to my supervisor Professor Olimpo Anaya-Lara for his continuous support, encouragement and technical guidance over my PhD study. His immense knowledge, enthusiasm and patience has a profound impact on my career. More importantly, Olimpo-style encouragement and humor has enlightened my life, especially during lockdown caused by Covid-19. My special gratitude goes to Dr. David Campos-Gaona, who has always been patient in providing solution when I meet a problem during the research. Every discussion we had has given me great inspiration in my research.

I would also like to thank my colleagues in the department, Dr. Rafael Pena Alzola, Dr. Dong Wang and Dr. Yin Chen, for their technical support and proofreading through my study. In addition, special thanks to my friend Dr. Vinicius Albernaz Lacerda who was an exchange PhD researcher in our research group. His advice and support helped me settle into my PhD quickly in the early stages of my career.

I would like to express my gratitude to my friends – Ming Gong, Baixiang Zhao, Weijie Ke, Yannan Xing and the rest of my friends inside and outside of the university.

My sincere thanks to my big family, my uncles and Aunts, Qingli Bu, Qingmin Bu, Haiyan Zhu, Ping Bu, Wenge Yang, and Peizhen Gao for their unlimited love and support. In addition, my brothers – Xiaonan Bu, Fan Bu and Brian Di Zhu, thank you sincerely for your dedication to our family when I was unable to be with them.

Last but not least, my greatest thanks go to my parents, Weidong Tian and Bin Bu for their unconditional support and love. I am so lucky to be your son. My special gratitude goes to my wife, Chuwei Zhang, for her trust, understanding, and encouragement during my PhD period. You are the sunshine of my life.

Abstract

As strategies to achieve Net-Zero targets are proposed by various countries worldwide, offshore wind power generation has attracted the attention of industry and academia as its advantages, like higher, less-turbulent wind speeds, no use of continental land space and energy capture capacity make it more attractive than other renewable energy solutions. However, the connection of large, distant offshore wind farms is a current challenge pressing the wind industry hard. High-Voltage Direct Current transmission is the type of connection favored for these cases. At present, HVDC using voltage source converters (VSC), has been used. To reduce the cost and land space, the diode rectifier based HVDC solution has been proposed for offshore wind farms. In this thesis, a novel hybrid converter topology is proposed for the offshore substation (wind farm) converter. The topology structure of the hybrid converter is a VSC and a 12-pulse diode rectifier (12P-DR) in a series connection. This thesis research focuses on the modelling and control of an offshore wind farm connected with an HVDC system based on this hybrid deployment converter.

Due to the control capabilities of the VSC used in the hybrid converter, two control strategies were designed and assessed. In addition, the 6-pulse diode rectifier (6P-DR) is used in the hybrid converter to reduce the complex structure of the transformer on the offshore side. The first control strategy uses the VSC converter of the hybrid converter (Hybrid-VSC) as a grid forming converter to perform the AC voltage control at the PCC point. The second control strategy uses the grid-side converter of the PMSG wind turbine to establish the offshore AC voltage. Also, a harmonics compensation controller based on Synchronous Reference Frames (SRF) tuned by PI controller is proposed in the hybrid converter to reduce the harmonic content of the hybrid topology. The harmonic compensation structure provides an easy-to-tune harmonics compensation control strategy.

An additional research contribution is the use of an advanced power electronics device, the Vienna rectifier, in the hybrid converter in order to reduce the harmonic components on the offshore side. This topology uses one switching device per phase, which reduces power losses and produces a low harmonic sinusoidal current output. The Vienna rectifier-based system uses a backup ancillary services control mode that retains harmonic-free power transfer capabilities, even in the case of a switch failure, by using the VSC converter harmonic compensation capabilities. Finally, A fast harmonics controller based on the Two Degrees of Freedom Internal Model controller (2DF-IMC) is used in the hybrid converter to reduce the harmonics compensation time. A fast harmonics controller is used in the hybrid converter and compared with the SRF-PI harmonics compensation controller.

The results of this work demonstrate the performance and feasibility of the hybrid topology and pave the way for its implementation in offshore projects, providing cost reductions and increasing efficiency.

List of Abbreviations

HVAC	High-Voltage Alternating Current
HVDC	High-Voltage Direct Current
STATCOM	Static Compensator
XLPE	Cross-linked polyethylene submarine cables
CSC	Current-Commutated Converter
LCC	Line-Commutated Converter
VSC	Voltage Source Converter
MCC	Modular Multilevel Converter
DR	Diode Rectifier
MT-HVDC	Multi-Terminal HVDC system
SCIG-WT	Squirrel-Cage Induction Generator Wind Turbine
WRIG-WT	Wound-rotor induction generator Wind Turbine
DFIG-WT	Doubly-Fed Induction Generator Wind Turbine
FRC-WT	Fully-Rated Converter Wind Turbine
PMSG-WT	Permanent Magnetic Synchronous Generator Wind Turbine
RSC	Rotor-Side Converter
GSC	Grid-Side Converter
VOC	Voltage-oriented control
PROMOTioN	Progress on Meshed HVDC Offshore Transmission Networks

PR-Controller	Proportional - Resonant Controller
PI-Controller	Proportional - Integral Controller
PCC	Point of Common Coupling
PLL	Phase-Locked Loop
PWM	Pulse-Width Modulation
THD	Total Harmonic Distortion
GPS	Global Positioning System
6P-DR	Six-Pulse Diode Rectifier
12P-DR	Twelve-Pulse Diode Rectifier
IMC	Internal Model Controller
2DF-IMC	Two Degree Freedom Internal Model Controller
SRF	Synchronous Reference Frame
LPF	Low-Pass Filter

List of Symbols

Chapter 3 Hybrid Converter Based on 6P-DR and VSC Converter Used for offshore wind farms

$C_{onshore}$	DC Capacitance between onshore converter station
C_{dr}	DC Capacitance between diode rectifier converter station
C_{vsc}	DC Capacitance between VSC converter station
E_{dc_hvdc}	DC voltage of overall HVDC system
E_{dc_dr}	DC voltage of diode rectifier
E_{dc_vsc}	DC voltage of VSC
P_{wf}	Wind farm active power
P_{dr}	Diode rectifier active power
P_{vsc}	VSC active power
K_{p_dc}	Integral gain of DC voltage converter
K_{i_dc}	Proportional gain of DC voltage converter
K_{ph}	Integral gain of harmonics current controller
K_{ih}	Proportional gain of harmonics current controller

Chapter 4 Low Harmonics Hybrid Converter Based on a Vienna Rectifier and VSC Converter Used for Offshore Wind Energy Conversion with backup capacity

P_{wf}	Wind farm active power
P_{Vie}	Vienna Rectifier active power
P_{vsc}	VSC active power
P_{pcc}	PCC point active power
Edc_{vie}	DC voltage between Vienna Rectifier station
Edc_{vsc}	DC voltage between VSC station
$Edc_{onshore}$	Onshore DC voltage
i_{d_vie}	Vienna Rectifier d current
i_{q_vie}	Vienna Rectifier q current

v_{d_vie}	Vienna Rectifier d voltage
v_{q_vie}	Vienna Rectifier q voltage
i_{d_vsc}	VSC d current
i_{q_vsc}	VSC q current
v_{d_vsc}	VSC d voltage
v_{q_vsc}	VSC q voltage
L_{vie}	Vienna Rectifier inductance
L_{vsc}	VSC inductance

Chapter 5 Fast Harmonics Compensation Controller Used for Hybrid Converter

P_{wf}	Wind farm active power
P_{Vie}	Vienna Rectifier active power
P_{vsc}	VSC active power
P_{pcc}	PCC point active power
Edc_{vie}	DC voltage between Vienna Rectifier station
Edc_{vsc}	DC voltage between VSC station
$Edc_{onshore}$	Onshore DC voltage
I_h	Harmonics current
i_{n_d}	n harmonic current d signal
i_{n_q}	n harmonic current q signal
$V_{n\_d\_inv}$	n harmonics voltage d signal
$V_{n\_q\_inv}$	n harmonics voltage q signal
THD-2DIM	Total harmonic distortion using fast harmonics compensation controller
THD-PI	Total harmonic distortion using conventional PI controller

List of Figures

List of Tables

Table of Contents

Chapter 1 Introduction

1.1 Zero Carbon and renewable energy

To reduce greenhouse gas emissions, the United Kingdom (UK) passed the law *Net Zero Emission*. This law aims to reduce all greenhouse gas emissions around the UK to net zero by 2050, a reduction of at least 80% emissions compared to 1990 levels [1]. The European Union (EU) also provides a proposal *European Green Deal* to reduce greenhouse gas emissions. The targets are at least 55% greenhouse gas emissions reduction by 2030 and no net emissions of greenhouse gases by 2050 [2].

Traditional electricity generation using coal and gas, produces CO2 (carbon dioxide) emissions. Carbon dioxide is a greenhouse gas harmful to the atmosphere, which causes global warming. Due to the *Net Zero Emission law*, the UK system operator, National Grid ESO, is moving towards a system that can operate at zero carbon by 2025 by using more renewable energy, including solar, wind and hydro [3].

Fig. 1-1 shows the Britain's electricity generation mix in 1990 and April 2021. Electricity generation is dominated by fossil fuels at 63.6%, while Zero carbon produces just 21.3% of the market, with more than 60% of electricity generation coming from fossil fuels. The 21.3% of electricity generated by Zero Carbon includes 19.9% nuclear and 1.5 % hydro. However, according to data provided by Nation Grid ESO in April 2021, electricity generated from fossil fuels fell to less than 50%, or 44.5%, which includes 43.7% of gas and 0.8% of coal. This represents a decrease of 62.1% compared to 1990, with 62.9% of electricity generation coming from coal. In addition to nuclear and hydroelectric power, solar and wind power are beginning to participate in power generation, with solar power accounting for 6.4% and wind power

for 15.8%, and the capacity of wind power is only 0.3% lower than nuclear power. This shows that wind power is gradually becoming a major force in power generation by zero carbon [4].

This image has been removed by the author of this thesis for copyright reasons.

Fig. 1-1 Comparison of Britain's changing electricity generation mix 1990 between 2021 [4]

1.2 The development of wind energy

Fig. 1-2 shows the new wind energy installations from 2013 to 2022. The year with the fewest installations was 2018, with 9.5 GW of onshore wind and 2.7 GW offshore wind installed, respectively. the highest number of installations was in 2022, with a total of 19.2 GW, of which onshore wind accounted for 16.7 GW [5]. In 2022, onshore wind accounted for 87% of all new installations. The largest number of onshore wind turbines were built in Sweden, Finland, Germany, and France. At present, Europe has a 255GW wind capacity.

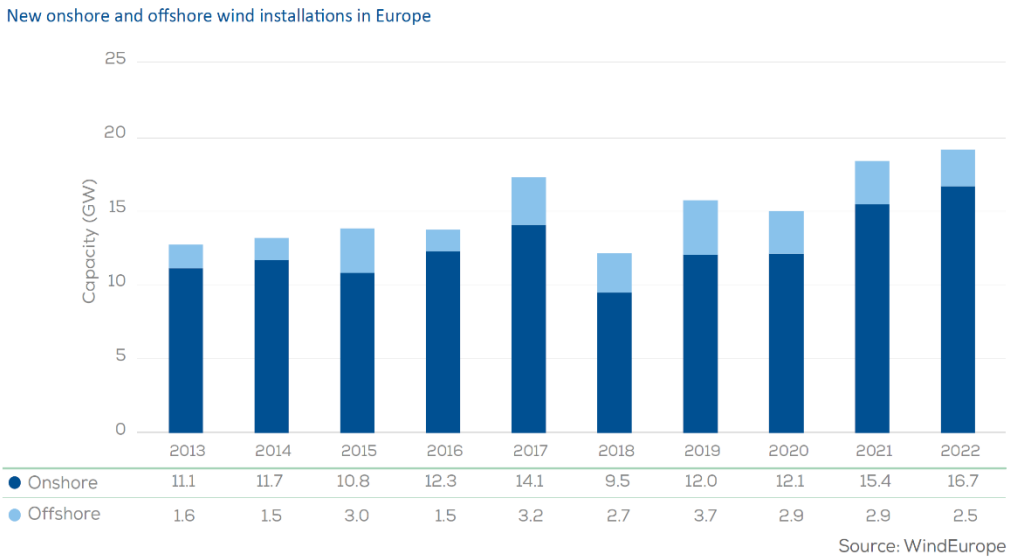

Fig. 1-2 New onshore and offshore wind installations in Europe [5]

Fig. *1-3* presents the new installation, including onshore and offshore wind farms in 2022. Most countries in Europe are focusing on onshore wind, but the UK has 1,179MW of new installations offshore in 2022, which is more than two times the number of new installations onshore. The UK is a world leader in offshore wind with more installed capacity than other countries. The generated offshore wind power is

supposed to serve 4.5 million homes, which facilitates the reduction of carbon emissions to achieve the emissions goal of 2050 [6].

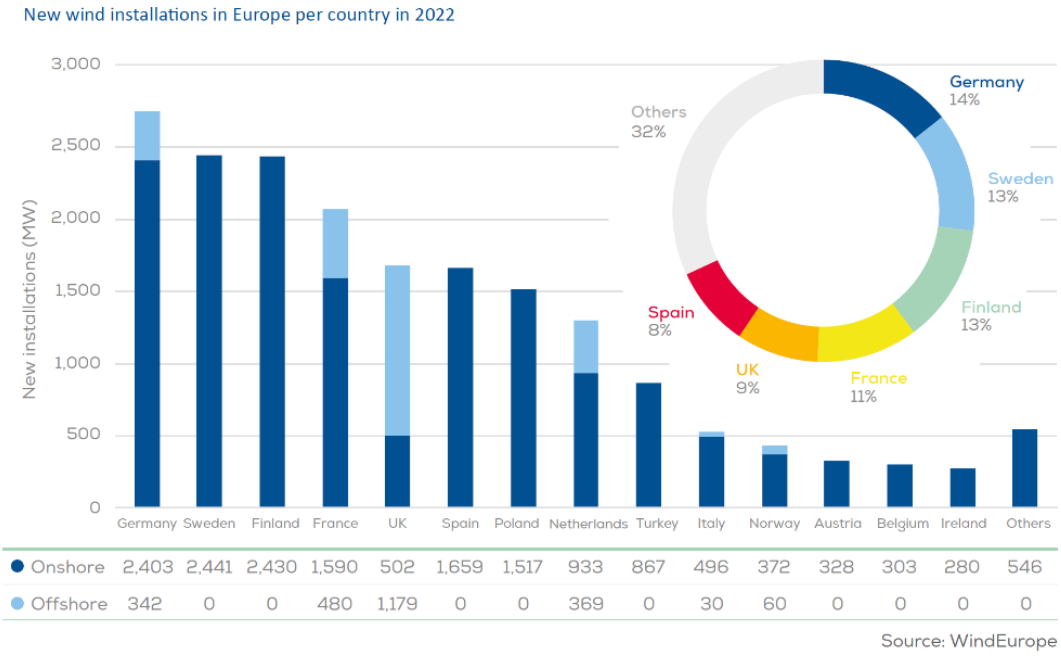

Fig. 1-3 New installation including Onshore and Offshore in EU-28 in 2022 [5]

The number of wind turbines expected to be installed in Europe between 2023 and 2027 is shown in Fig. 1-4. The installation of onshore wind is still countered as the main part, but compared with the previous data, the installation of offshore wind is also gradually improving, in the planning of 2027, the installation of offshore wind in that year is 11.6GW, which is closed to the general installation of onshore in that year. Offshore wind installations are also continuing to grow.

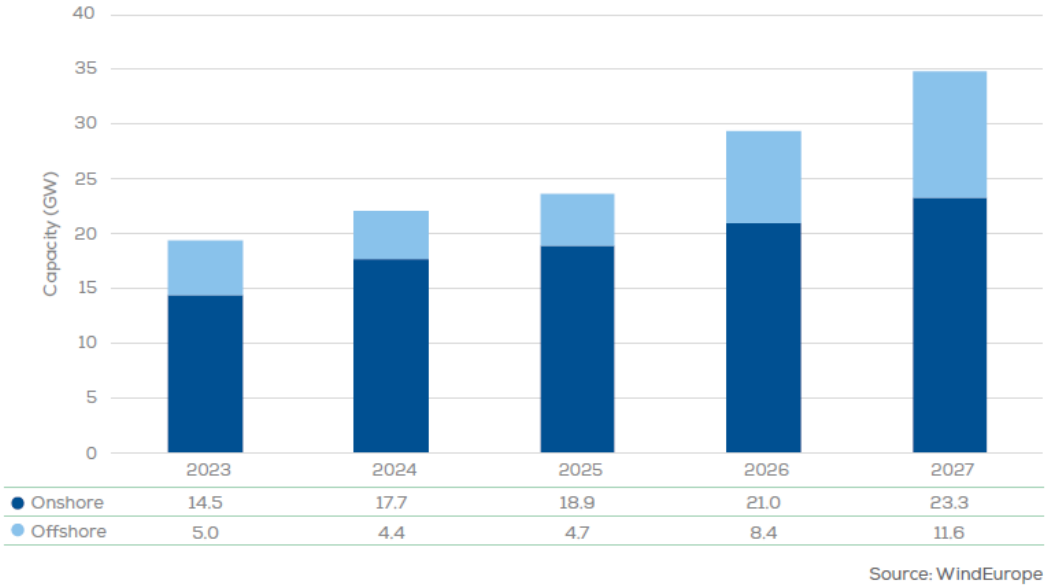

Fig. 1-4 Expected New Installation in 2023 to 2027[5]

Offshore wind has attracted considerable attention. Transmission solutions to connect offshore wind power plants to the onshore grid are a popular topic in research and industry, particularly about the significant challenges of connecting wind farms located far away from shore. Presently, there are two solutions to transport electricity from offshore wind farms to shore, namely, the HVAC system and the HVDC system. These are reviewed in the following section.

1.3 Offshore wind energy transmission system

1.3.1 High-Voltage Alternating Current (HVAC) Transmission System

HVAC systems are widely chosen for larger offshore wind farms to transmit power to the onshore grid due to their simple structures and economical connections. However, they have several limitations especially when the transmission distance is significant [7]. The basic structure of an offshore HVAC system is shown in Fig. 1-5.

The offshore and onshore substations link the offshore wind farm and onshore grid. In addition, transformers of substations provide voltage step-up. Therefore, reactive power compensators, such as static compensators (STATCOMs) and Static Var Compensators, are generally used to improve transmission efficiency [8-10].

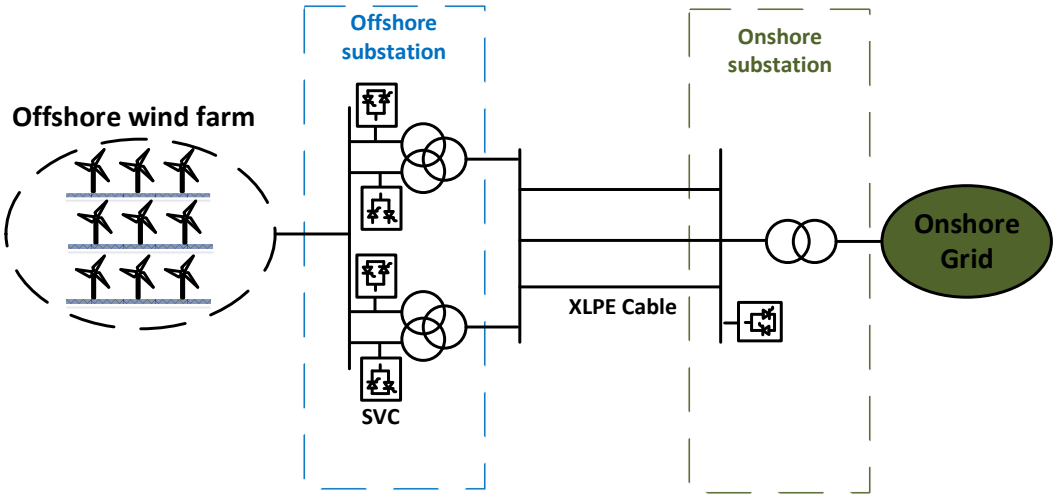

Fig. 1-5 Layout of Offshore HVAC system [9]

The components of the offshore HVAC system (Fig. 1-5) are as follows:

- Offshore wind farm
- Offshore substation
- Cross-linked polyethene submarine cables (XLPE)
- Static Var compensator/static compensator
- Onshore substation

HVAC transmission has many disadvantages when used in offshore wind farm applications. High power losses and larger reactive power compensators are required over long connection distances. A wind farm can only synchronously couple with the onshore grid. Any offshore wind farm faults can affect the onshore grid. Additionally, the voltage profile is easily affected because of the high capacitance of long AC submarine cable [9, 11].

1.3.2 High-Voltage Direct Current (HVDC) transmission system

HVDC transmission systems have been widely used to interconnect non-synchronous networks through long distance submarine and underground cables. The two converter types are used in the HVDC system: Current Source Converter (CSC) and Voltage Source Converter (VSC). The CSC-HVDC uses line-commutated switching devices, such as Thyristors, and the VSC-HVDC uses self-commutated switching devices, such as IGBTs, MOSFETs and GTOs [12, 13].

The function and location of converter stations have serval configurations that can be used in both converter station schemes, such as Monopolar, Bipolar, Homopolar, Back-to-back and Multi-terminal [14, 15].

- Monopolar HVDC system

Two converters are separately connected by a single pole line and a positive and negative DC voltage. Submarine cables are widely used in this transmission system, which connects two AC systems. The current return path is via grounding, sea, or a metallic conductor.

- Bipolar HVDC system

The bipolar configuration is composed of two monopolar systems, namely, one flows with a positive polarity and the other with a negative polarity, as shown in Fig. 1-6 (b). Two converters of equal-rated voltage have series connections on the DC side of each terminal. Both pole currents are equal and have zero ground currents during normal operations. This HVDC configuration is commonly used in CSC-HVDC via an overhead line to transmit power between AC systems. The highlight of this configuration is that the other pole can continue to transmit power with high reliability despite a pole failure.

- Homopolar HVDC system

Homopolar HVDC systems have two or more conductors with negative polarity, which can be operated with ground or metallic return paths. These two poles can be operated in parallel. The homopolar configuration has the advantage of lower installation costs. However, the return current is the major drawback.

- Back-to-back HVDC system

Back-to-back HVDC systems are the common choice for two asynchronous AC systems because the two converters are located at the same or nearby sites. The two-AC system may have the same or different nominal frequencies. A short length line or no line is used for this configuration because of the location of the converters.

- Multi-Terminal HVDC system

In the multi-terminal HVDC (MT-HVDC) configuration, two or more sets of converters have the option to be connected in parallel or series. The layouts are shown in Fig. 1-6 (e) and (f). Over the last two decades, MT-HVDC control and communication between sets of converters have developed significant complexity, particularly in CSC converters. With increased research in VSC converters, the improvement of control strategies design plays an essential role in MT-HVDC [2].

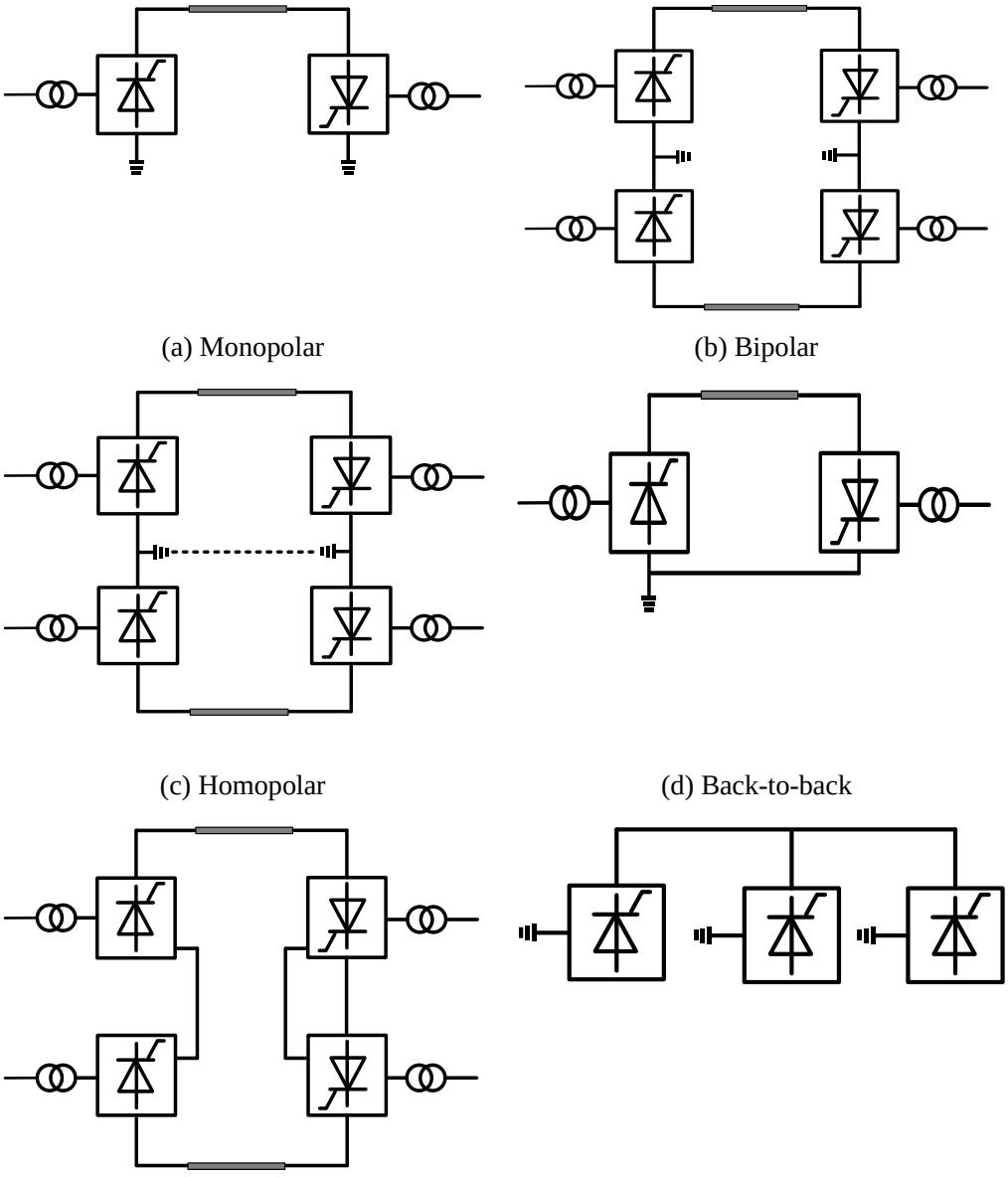

Fig. 1-6 Different HVDC configurations [9, 12-15]

According to the Siemens overview report, Siemens is involved in 43 HVDC projects with LCC converters in operation or nearing completion in 18 different countries and regions. In addition, there are 23 HVDC projects in 121 countries with VSC or MMC converters [16]. Rte International regularly updates their newsletter on industrial projects related to HVDC. The following two tables are from data they have collated [17].

Table 1-1 Summary of the worldwide LCC-HVDC project from 2019 to 2022 [17]

Name	Year commissioned	Power (MW)	Nominal Voltage (kV)	Converter Manufacturer
Raigarh-Pugalur, India	2019	6000	800	Hitachi ABB
HVDC MON.ITA Project, Italy	2019	1000	±500	Toshiba
Xingu-Rio, Brazil	2019	4000	800	NARI, XD,CET
Wudongde multi-terminal UHVDC demonstration project	2021	6000	800	/ 3-Terminal, Yunan (Thyristor), Guangdong and Guangxi (IGBT)
Ethiopia–Kenya HVDC Interconnector	2022 (Ongoing)	2000	500	Siemens

Table 1-2 Summary of the worldwide VSC-HVDC project from 2019 to 2022 [17]

Name	Year commissioned	Power (MW)	DC Voltage	AC Voltage	Converter Manufacturer

			(kV)	(kV)	
Hokkaido-Honshu, Japan	2019	300	±320	275	Toshiba
Yu'E, China	2019	4×1250	±420	/	RXGK, XuJi Electric and C-EPRI
COBRAcable, Denmark-Netherland	2019	700	±320	400/400	Siemens
BorWin3, German	2019	900	±320	400/400	Siemens
NEMO, UK-Belgium	2019	1000	±400	400/380	Siemens
ALEGrO, Germany-Belgium	2020	1000	±320	380/380	Siemens Energy
Zhangbei Phase1, China	2020	2×3000	±535	500/500	NR Electric, XuJi Electric, C-EPRI, SiFang and Hitachi ABB
Krieger-Flak Combined Solution, Germany-Denmark	2020	410	±140	150/400	Hitachi ABB
NordLink, Norway-Germany	2020	1400	±525	0/400/380	Hitachi ABB
KunLiuLong/ Wudongde CSG, China	2020	5000 3000	±800	525	RXHK, XuJi, TBEA, NARI,

					Xidian
IFA2, UK-France	2021	1000	±320	400/400	Hitachi ABB
SW Link, Sweden	2021	2×720	±300	400	GE
Rudong offshore wind farm, China	2021	1100	±400	220/500	RXHK, XJ Group
North Sea Link, Norway-UK	2021	1400	±515	420/400	Hitachi ABB
Pugalur – Thrissur, India	2021	2×100	±320	/	Siemens Energy
ElecLink, UK-France	2022	1000	±320	400/400	Siemens Energy
Guangdong (partial), China	2022	2×1500	±300	/	RXHK and Partners

Compared to HVAC transmission, the HVDC system can cover long distances and has low transmission losses. At the same time, the transmission lines of the HVDC system require less space, which reduces the environmental impact. More importantly, HVDC systems have better control of voltage and current, which improves the stability of the interconnected grid and allows for the interconnection of two asynchronous grids [12, 13]. Due to these characteristics, the HVDC system is a solution for connection to offshore wind.

1.4 Motivation and contribution

1.4.1 Research question

The previous section describes the HVDC as an attractive solution used for offshore HVDC system transmission. However, this research addresses certain questions. The problem of offshore HVDC systems is summarized by many research studies in the works of literature [12, 18, 19] including the cost, footprint and efficiency. Many converter topologies are used for offshore converter station as explained later and detailed reviewed Chapter 2. This thesis is intended to improve the topology of a series-connected hybrid converter used on the offshore side by providing a cost-effective and smaller footprint offshore converter station option for academic and industrial use.

1.4.2 Research motivations and objectives

Among the commercial applications used in HVDC systems, the LCC-HVDC and VSC-HVDC have a large market share. LCC HVDC system is a mature technology used to transmit power over long distance, with larger capacity, high reliability and low power loss. Besides, the external voltage source needs to communicate, and the larger passive filter needs to eliminate harmonics. Compared to LCC-HVDC, the VSC-HVDC system can provide a robust control ability to regulate the offshore AC voltage and frequency. However, high installation costs and high switching loss are the main drawbacks of the VSC-HVDC system.

To reduce the cost of HVDC systems, the DR-HVDC has been proposed for offshore transmission systems. The frequency and AC voltage regulation in this configuration relies on the wind turbine controller, since the diode rectifier is an uncontrollable device. DR-HVDC system provides low-cost, low power loss, high

reliability, and small footprint features to an HVDC system.

In addition, the HVDC system based on a hybrid converter has been proposed for offshore converter stations. Such hybrid converters comprise a reduced-power 2-level VSC converter connected in series with a higher-power 12-pulse diode rectifier. In this configuration, the series connection of this hybrid converter combines two kinds of power electronics converters and reduces the overall investment, cost, footprint, and power loss. The VSC converter can also regulate frequency, AC voltage, DC voltage and harmonic current at the offshore PCC.

Compared to other technologies, the HVDC system based on a hybrid converter shows a low investment cost, small footprint, and high efficiency and reliability. However, the current offshore hybrid converter lacks the standardization of control strategies, for example, the selection of the control system of wind turbine and hybrid converter when the hybrid converter is connected to the offshore wind farm. In addition, there are still other power converter options available in the market. This thesis will investigate the potential improvement of hybrid converters in terms of design, control and operation. And test their performance on the PSCAD/EMTDC environment. Two control strategies for offshore converter station will be investigated. The development of the improved hybrid converter will focus on the power electronic structures and controllers to improve steady state and dynamic performance. In addition, a fast harmonics compensation controller is also proposed in hybrid converter applications.

1.4.3 Thesis contributions

The contributions of this thesis are shown below:

- A hybrid converter based on 6 pulse diode rectifier and a VSC converter

is proposed, which includes two control strategies that suit different situations. Two control strategies are investigated and discussed, frequency and voltage controller enables the proposed hybrid converter functions to perform as a grid forming converter to provide fixed frequency and voltage. The other proposed control strategy uses the wind turbine side converter to serve as a grid forming converter. The proposed converter structure and control system avoid complexity, which reduces initial cost and footprint while providing a test bed for hybrid converter design.

- Vienna rectifier is proposed to be a part of the hybrid converter, which is series connected with 2-level VSC converter. The proposed hybrid converter provides a low cost and low harmonics feature. As the Vienna rectifier replaces the diode rectifier of the hybrid converter, the harmonic current compensation controller can be a backup option when the switching fault occurs at the Vienna rectifier. In other words, the VSC of the hybrid converter performs as a built-in active power filter, which provides a backup capability for harmonic current compensation.
- An easy-to-tune harmonic current compensation controller is used in hybrid converter applications, including a hybrid converter based on 6 pulse diode rectifier and VSC converter and a hybrid converter based on a Vienna rectifier and VSC converter, which uses the synchronous reference frame (SRF) based on PI controller in the proposed control system. The proposed controller reduces the complexity of the hybrid converter control system.
- A two-degrees-of-freedom internal model controller is proposed in the hybrid converter to replace the PI controller used in the SRF harmonic compensation approach, which provides fast harmonics compensation

response time due to the elimination of the low-pass filter during the control process when switching the control mode of the hybrid Vienna-VSC converter.

1.5 Author's publication

[1] **S. Tian**, D. Campos-Gaona, V. A. Lacerda, R. E. Torres-Olguin, and O. Anaya-Lara, "Novel Control Approach for a Hybrid Grid-Forming HVDC Offshore Transmission System," *Energies*, vol. 13, no. 7, p. 1681, Apr. 2020. **(Chapter 3)**

Abstract: This article describes a hybrid topology of high-voltage direct current (HVDC) for offshore wind farms using a series connection of a voltage source converter (VSC) and 6 pulse diode rectifier (6P-DR). In this topology, the offshore side VSC (OF-VSC) acts as a grid-forming converter to maintain the PCC (point of common coupling) voltage of offshore wind farms (WF) and frequency. In addition, the OF-VSC functions as an active power filter to suppress the 5^{th}, 7^{th}, 11^{th}, and 13^{th} order harmonic current components produced by the 6P-DR, making it almost sinusoidal. Due to the 6P-DR being used in the hybrid converter, this new configuration reduces the total cost of the converters and losses, while preserving the power flow to the onshore gird. Compared to the fully-rated converter and hybrid converter based on a 12-pulse diode rectifier, the power loss and cost are reduced, and in addition, the proposed hybrid converter does not require a phase shift transformer nor a high number of diodes. A 200 MW in an HVDC transmission system using the hybrid configuration was simulated in PSCAD. The results show that the system operated correctly and the harmonic components were filtered.

[2] **S. Tian**, D. Campos-Gaona, R. Pena-Alzola, and O. Anaya-Lara, "Fast Harmonic compensation in hybrid HVDC offshore system," *Journal of Physics: Conference Series*, vol. 2362, no. 1, p. 012040, 2022/11/01 2022, doi: 10.1088/1742-6596/2362/1/012040. **(Chapter 5)**

Abstract: Hybrid HVDC systems have been proposed as an alternative for nominal VSC-Based HVDC for offshore applications. Hybrid HVDC systems consist of an offshore power station composed of the connection of high-power diode rectifiers in series with a fractional power VSC-HVDC. This hybrid configuration allows large power transfer from offshore sites, with the added robustness, simplicity and efficiency of uncontrolled rectifiers. In this research, a robust and fast-acting controller, the Two Degrees of Freedom Internal Model controller (2DF-IMC), is used to control the active power filter features of the fractional-power VSC-HVDC system, resulting in a much faster overall THD reduction in the offshore AC currents in dynamic conditions (i.e. time-varying wind power) when compared with standard active power filter controllers. This improvement is the direct consequence of the fast closed-loop dynamics of the 2DF-IMC controller that do not require filtering stages. Additionally, the increased closed-loop response time did not affect the overall robustness of the control system, thanks to the enhanced disturbance rejection capabilities of the 2DF-IMC configuration.

[3] **S. Tian**, D. Campos-Gaona, R. Pena Alzola, and O. Anaya-Lara, “Low Harmonics Offshore Hybrid HVDC System Based on Vienna Rectifier and Voltage Source Converter with Back-up Capability,” Submitted to IEEE Transaction on Energy Conversion (under second review) **(Chapter 4 & 5)**

Abstract: High voltage direct current transmission system is attractive solution for transmit power from offshore to onshore, offshore HVDC system has been used to

reduce the carbon emission to achieve the Zero Carbon goal. However, the high installation cost and low reliability impose few challenges for the offshore wind development. To address these challenges, few low-cost topologies for offshore converter station is proposed, such as, the HVDC system based on diode rectifier (DR) and the HVDC system based on hybrid converter. In this paper, a hybrid converter based on Vienna rectifier and Voltage Source Converter (VSC) is proposed for offshore HVDC system, which provide a low-cost, low-harmonics and high reliability option. In addition, VSC of hybrid converter can be operated as an active power filter to suppress the harmonic current at PCC point in case of the IGBTs of Vienna rectifier is fault. The harmonics compensation controller is used serval synchronous reference (SRF) technique tuned by two-degrees-of-freedom internal model controllers(2DF-IMC) for reducing harmonics cancellation process time. All the results in PSCAD/EMTDC verify the proposed hybrid converter operated in its control strategy.

1.6 Thesis Structure

This thesis is organized as follows:

Chapter 2 presents the general review of offshore HVDC systems based on different converter topologies, including the basic structure and control system LCC-HVDC, VSC-HVDC, DR-HVDC and hybrid converter based HVDC. In addition, the types of wind turbines are reviewed.

Chapter 3 presents a control system including a fundamental control system and harmonic compensation control for the proposed converter based on 6P-DR and VSC converter. Two control strategies are proposed and verified in the PSCAD environment. In addition, PSCAD simulation results verify the performance of the hybrid converter and the effect of the harmonics compensation controller using the synchronous reference frame technique.

Chapter 4 develops the hybrid converter, which uses advanced power electronics. The Vienna rectifier series connects with the VSC converter. It shows enhanced performance, including low cost, low harmonics and high reliability. In addition, the VSC converter of the hybrid converter has the ability to multifunction control, which provides different control strategies to deal with different dynamic events.

Chapter 5 proposes a fast harmonics compensation controller used in the hybrid converter control system. Two Degrees of Freedom Internal Model Controller (2DF-IMC) replaced the conventional PI controller, used in harmonics compensation controller in hybrid converter application. The proposed converter provides a fast response to set-point, an easy-to-tune process and a strong disturbance rejection solution for hybrid converter harmonics current compensation controller.

Chapter 6 draws a conclusion and future work suggestions.

Chapter 2 Literature Review

2.1 Introduction

This chapter provides an overview of HVDC connected offshore wind farms. Firstly, this chapter briefly introduces the types and development of wind turbines (WTs), and secondly, the AC/DC converters currently used for energy. In addition to the well-known Line-Commutated Converter (LCC), Voltage Source Converter/Multi-Level Modular Converter (VSC/MMC), and diode rectifier, this thesis also discusses the Vienna rectifier's typical topology and operation. This Vienna rectifier will be one of the contributions to this thesis. Subsequently, this chapter outlines the HVDC scheme currently discussed in offshore wind farm, which includes the operation and control, along with part of the required equipment and advantages and disadvantages of this HVDC scheme. Though the discussion of the converter and HVDC scheme are outlined and summarized, as the hybrid converter can functions as controllable converter while reducing investment and footprint in offshore, it will be a main topic of discussion in the rest of thesis. Towards the end of the chapter, potential enhancements that can be made to the hybrid converter are discussed. These include the selection of power electronic compensation, the choice of harmonics controller and strategies to expedite the compensation of harmonic controllers.

2.2 Wind turbine generator types

The four types of wind turbines (WTs) are divided into two categories according to whether they are the variable speed type. Type I squirrel-cage induction generator wind turbines (SCIG-WT) are defined as fixed-speed WTs. Categories of variable-speed WTs include Type II wound rotor induction generator WTs (WRIG-WT), Type III doubly-fed induction generator WTs (DFIG-WT), and Type IV fully-rated

converter WT (FRC-WT)[8, 9, 20]. The diagram of WT topologies is shown in Fig. 2-1.

- Type I SCIG-WT

A SCIG-WT is driven by the WT through a gearbox and directly connected with a soft starter and step-up transformer. Additionally, a larger capacitor bank is needed in SCIG-WT to consume reactive power caused by the induction generator. The induction generator provides an almost constant rotational speed, which varies by generator slips (maximum of 1%). Owing to its simple structure and low cost, SCIG-WTs were used in early wind farms. In recent years, they have been gradually eliminated from the wind market share because of low energy conversion [21].

- Type II WRIG-WT

The variable resistance of WRIG-WT is controlled for variable speed during operation, and the diagram of its topology is shown in Fig. 2-1 (b). The variable resistance is a series connected with an induction generator; it is also known as OptiSlip [22]. Since the mid-1990s, products from the Danish manufacturer Vestas have been used in wind power markets. Due to the controlled variable resistance, the range of rotating speed is typically 0%–10% above the synchronous speed. However, the high loss caused by additional rotor resistance is a limitation of WRIG-WTs.

- Type III DFIG-WT

The typical DFIG topology diagram is shown in Fig. 2-1 (c). Its structure compares a wound rotor induction generator and back-to-back converters. Its structure has a wound rotor induction generator and back-to-back converters. The windings of the induction generator are directly connected to the grid through a back-to-back converter that consists of a rotor side converter (RSC) and grid side converter (GSC).

Its power rating is about 20%–30% of the DFIG rating. Owing to the back-to-back converter of DFIG-WT, active power can be generated at a constant frequency and voltage over a wide of synchronous speeds. In addition, the active power magnitude and direction between the induction rotor and grid can be controlled. The rotational speed of DFIG decoupled with the synchronous frequency can be varied at a range of ±25% by controlling the injected rotor current. The main shortcomings of DFIG-WT are the slip-rings and complex external fault solutions [20, 23, 24].

- Type IV FRC-WT

The basic structure of FRC-WT is shown in Fig. 2 3 (d), and it includes the induction or synchronous generators connected via back-to-back converters to link AC grids. The back-to-back converter consists of RSC and GSC, which play an important role in FRC-WT. Owing to the back-to-back converter, independent control can be applied to the WT, including active power control, reactive power control, and voltage control. Among all FRC-WTs, permanent magnetic synchronous generators attract much attention in the wind market, because of low maintenance costs, high reliability, and easy controllability. The main drawback of Type IV WTs is the high cost of fully rated back-to-back converters [25, 26].

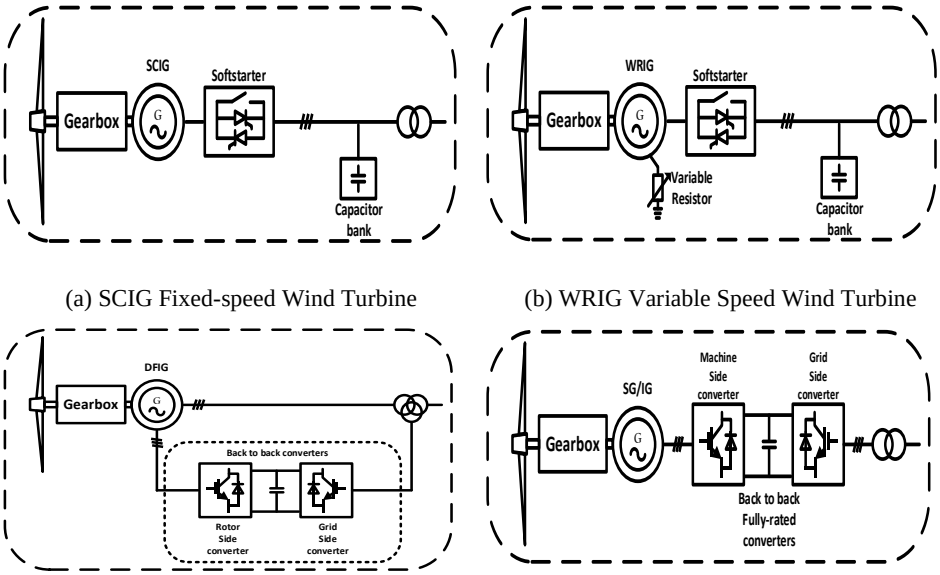

(a) SCIG Fixed-speed Wind Turbine (b) WRIG Variable Speed Wind Turbine

(c) DFIG Wind Turbine (d) FRC Wind Turbine

Fig. 2-1 Diagram of Wind Turbines: (a) SCIG-WT, (b) WRIG-WT, (c) DFIG-WT, (d) FRC-WT [8, 9]

2.3 Review of AC/DC Converters Used for Offshore Wind

2.3.1 Line-Commutated Converter

The first commercial HVDC project, Gotland 1, was built in 1954. It used two 6pulse converters in a series connection operated as a twelve-pulse converter to link Gotland to Sweden mainland grid. LCC converters have attracted more attention and development over the past years. The first completed LCC-HVDC based on thyristors was constructed by General Electric (GE) in Eel River, Canada, and started service in 1972 [27]. The LCC converter has been widely used in HVDC systems owing to high reliability, low maintenance requirements, reduced power losses, and lower costs [13, 14].

Fig. 2-2 shows the six-pulse thyristor bridge and twelve-pulse thyristor bridge.

The twelve-pulse bridges are more widely used in HVDC systems than the six-pulse thyristor bridges. The 5^{th} and 7^{th} harmonic currents are eliminated at the AC side because the twelve-pulse thyristors bridges are connected with three winding transformers in a Y/Y/Δ connection, and there is a 30-degree phase shift between two current waves caused by two windings at the secondary side. Additionally, an AC filter is required at the AC side to consume harmonics at the AC side and provide reactive power to the LCC converter.

Although they are the more mature converters in HVDC systems, the LCC is not suitable for all offshore HVDC applications. For example, a weak grid cannot provide the strong external voltage required for LCC commutation, which results in commutation faults. In addition, larger reactive power compensation devices are needed for the AC side, which leads to larger footprints in offshore substations.

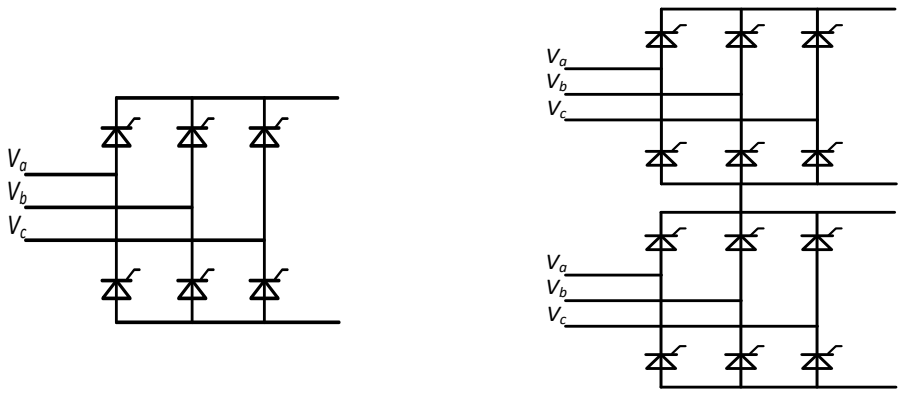

(a) (b)

Fig. 2-2 Diagram of LCC converter: (a) six-pulse bridge LCC converter and (b) twelve-pulse bridge LCC converter

2.3.2 Voltage Source Converter

A VSC converter consists of insulated gate bipolar transistors (IGBTs) known as self-commutated switching devices and anti-parallel diodes. The three-phase two-level VSC converter is shown in Fig. 2-3. The switching devices of VSC can open and close

periodically, and VSC current can operate leading or lagging the AC system. Therefore, VSC can consume or supply the reactive power of its connected AC grid, and there is no need for a reactive power compensator unlike LCC-HVDC [13, 14]. VSC is the most competitive technology for offshore HVDC system because of the following advantages [28].

- ✓ VSC-HVDC enables the pulse-width modulation (PWM) control strategy, which provides independent control of current, voltage, active power, and reactive power
- ✓ VSC-HVDC limits fault current during AC current faulting
- ✓ Bidirectional power flow without DC voltage reversal
- ✓ Small size AC filter
- ✓ Black-start capability

In 1997, the first HVDC system based on a two-level VSC converter was tested in Sweden. The first commercial VSC-HVDC was operated by ABB, which was a 50 MW ± 80 kV system with a submarine cable linked to Gotland, Sweden [29]. After the development of the VSC converter, there are various weak points of the 2-level VSC converter used in the HVDC system.

- × Difficult to operate in high power applications
- × Harmonic current filter is required
- × High power loss
- × Overcurrent is discharged by DC capacitors when DC faults

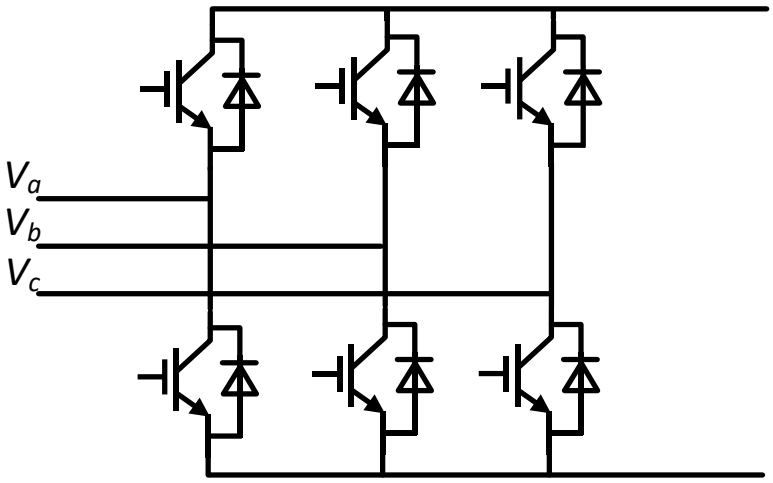

Fig. 2-3 Two-level VSC converter

Modular Multilevel Converter (MMC) was first proposed in 2001 to overcome the drawbacks of a 2-level VSC converter. In recent years, academic and industrial research has made extensive improvements in developing attractive converter topologies for HVDC applications. Fig. 2-4 shows the MMC schemes and its sub-modules (SMs), including the half-bridge, full-bridge, clamp-double, three-level flying-capacitor converter (FC), three-level neutral-point-converter (NPC), and five-level cross-connected SM. Each phase leg of MMC consists of series SMs and series inductances SMs of the arms are controlled to AC voltage, and the inductance suppresses inrush and high-frequency currents. Generally, PWM techniques are used in VSC, such as selective harmonic elimination, space-vector modulation (SVM), and sinusoidal PWM (SPWM). These can be employed in MMC converters but are not the best choices for MMC converters. To overcome the more significant number of cells per arm modulation in MMC converters, staircase modulation is used. Each output voltage of the sub-modules can be regulated, and the overall output voltage of the arms can form almost ideal sinusoidal waveforms [30, 31].

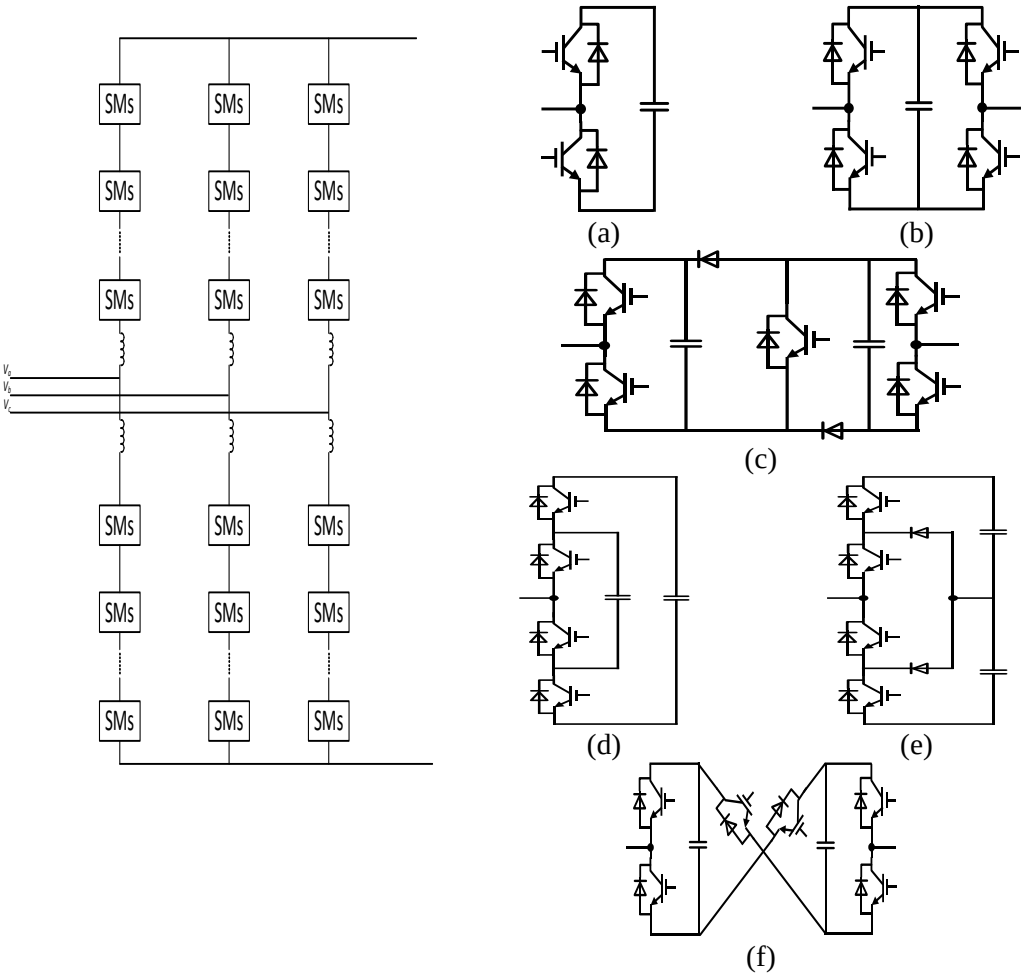

Fig. 2-4 MMC converter and its SMs: (a) Half-bridge, (b) Full-bridge, (c) The clamp-double, (d) The three-level FC, (e) The three-level NPC, and (f) The five-level cross-connected SM [13, 30-32]

A few studies have summarized the highlights of MMC converter over VSC[13, 30-32]:

- ✓ Low power losses
- ✓ High modularity, fast response and controllability
- ✓ No AC filter or small AC filter is required
- ✓ An ability to ride when DC faults

2.3.3 Diode Rectifier

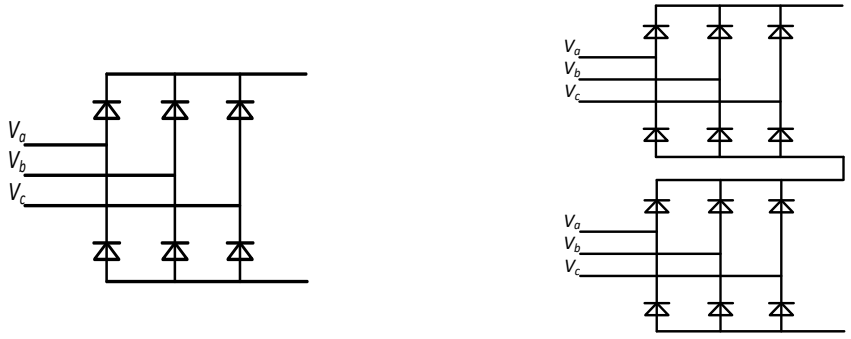

(a) (b)

Fig. 2-5 Diagram of diode rectifier: (a) six-pulse bridge diode rectifier and (b) twelve-pulse bridge diode rectifier

Fig. 2-5 shows the diagram of a 6 pulse diode rectifier bridge and a twelve-pulse diode rectifier bridge. Similar to the 12 pulse LCC bridge, the AC side of the twelve-pulse diode rectifier connects with a three-winding transformer, and the 5^{th} and 7^{th} harmonic currents are suppressed by the voltage phase shift of the secondary winding. In recent years, the 12-pulse diode rectifier bridge has been proposed for offshore HVDC systems where the AC side connects to the offshore wind farm and the DC side connects with onshore DC networks. The larger harmonic filter bank is connected to the AC side to filter the harmonic current. Compared with other power electronics used in offshore wind HVDC systems, it has several advantages and disadvantages [33].

- ✓ Simple structure and small footprint
- ✓ Low initial cost
- ✓ High reliability
- ✓ Low power losses

- × Uncontrollable device. Its AC voltage and frequency depend on the converter of the WT
- × A larger harmonics filter bank is required

2.3.4 Vienna Rectifier

The Vienna rectifier is a three-phase three-level boost AC/DC converter with PWM modulation. The Fig. 2-6 shows the original topology of the Vienna rectifier. This topology was first proposed in 1997 by Professor Kolar [34, 35]. It is widely used in telecommunication applications to implement a 12-kW telecommunications power supply. Compared to other AC/DC power electronics, Vienna rectifiers have several advantages:

- ✓ Low harmonics, approximately sinusoidal current
- ✓ Controlled power devices
- ✓ Low-blocking voltage stress
- ✓ High power density, high efficiency and high reliability
- ✓ Simple control system and circuit structure

The Vienna rectifier attracts more attention in other applications, for example, an electrolyzer based on a Vienna rectifier and an electric vehicle (EV) charger [36, 37]. In addition, a few studies investigate the possible applications of the Vienna Rectifier in renewable energy systems. The reference takes a survey of the Vienna Rectifier used in the HVDC system [OBJ], and the Uses of the Vienna rectifier have been considered for WT technology in [39, 40].

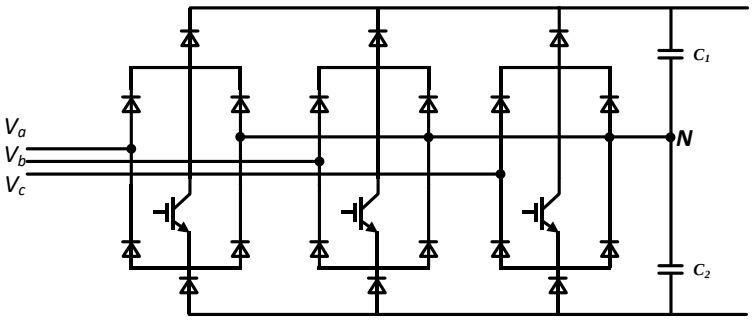

Fig. 2-6 Original Vienna Rectifier topology

There are two Vienna rectifier topologies (I-Type Vienna rectifier and T-type

Vienna Rectifier) developed from the original topology, and its circuit structures are shown in Fig. 2-7 and Fig. 2-8 [38]. The Vienna rectifier can work as a three-phase, three-level, neutral point converter with unity power control. In this thesis, the utilization of the Vienna rectifier as a part of the hybrid converter used for the offshore HVDC system will be discussed in Chapter 4.

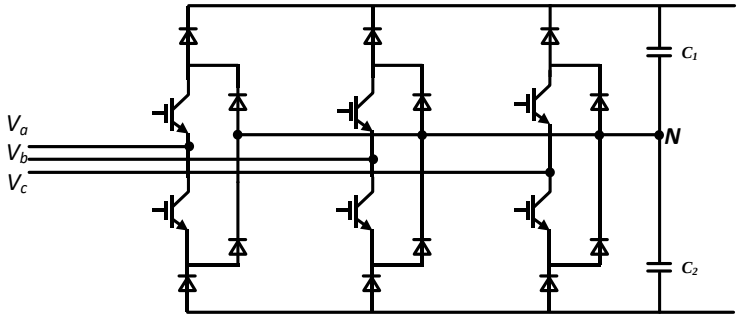

Fig. 2-7 I-type Vienna Rectifier topology

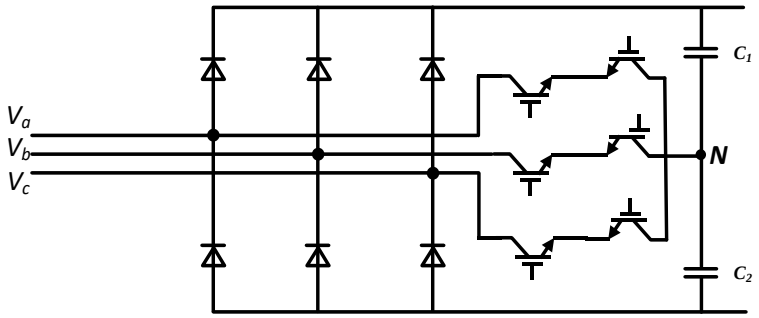

Fig. 2-8 T-type Vienna Rectifier topology

2.4 Control and operation of existing Offshore HVDC System

2.4.1 LCC-HVDC

HVDC systems based on LCC converters are a mature technology for connecting with offshore wind farms. LCC-HVDC can connect with wind farms based on DFIG-WTs or PMSG-WTs. The following section introduces the LCC-HVDC operation and control with different types of WTs.

a) LCC-HVDC connect to DFIG-WTs Offshore wind farm with STATCOM

As a mature technology, the LCC-HVDC can be operated at high power levels, a submarine cable can be used, and the maximum transmitted power can reach 1200 MW. However, the LCC-HVDC requires a communication link at the PCC point with offshore wind farms. The synchronous compensator (SC) or STATCOM could be implemented in LCC-HVDC systems. Reference [41] presents the LCC-HVDC system connections for DFIG-WTs, and the topology and control system are shown in Fig. 2-9.

The STATCOM device can perform as a grid-forming converter to control the offshore AC voltage at a constant magnitude. Additionally, the phase angle and frequency are controlled with fixed values by STATCOM. The LCC converter can be used in offshore converter stations with the AC side of the LCC converter connected to DFIG-WTs at the PCC point and the DC side of the LCC converter connected with the onshore converter station that controls the DC voltage to regulate onshore DC networks for power balancing between offshore to onshore [41, 42].

When DFIG-WT is operating while connected to an HVAC system, the MSC converter controls the torque and reactive power to regulate the rotor current, and the GSC converter controls the DC voltage of the WT and reactive power.

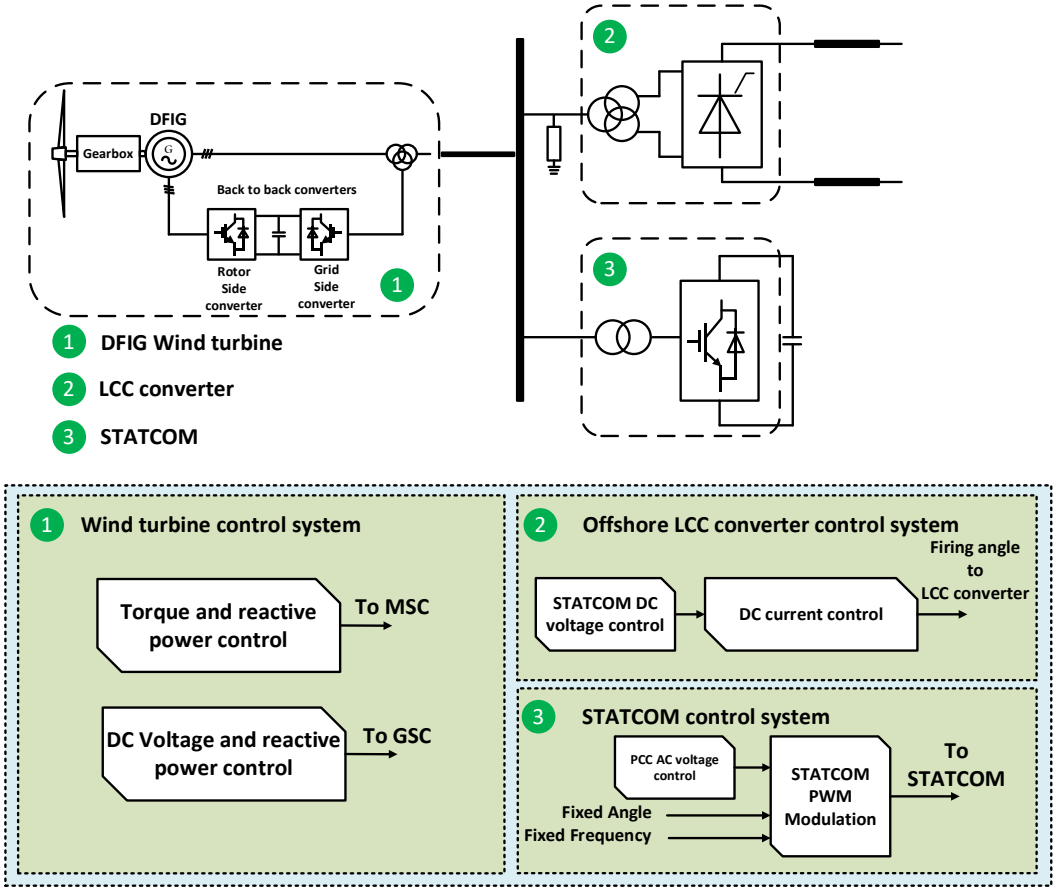

Fig. 2-9 Layout of LCC-HVDC with STATCOM connected DFIG-WTs and control system [41, 42]

b) LCC-HVDC connect to DFIG-WTs Offshore wind farm without STATCOM

Fig. 2-10 shows the LCC-HVDC connected to DFIG-WTs without STATCOM devices. Compared to LCC-HVDC with STATCOM, the control system of DIFG-WTs has different control strategies. DFIG-WTs are used for maintaining the PCC AC voltage for communication. The MSC converter controls the stator flux and torque while the GSC converter controls the DC voltage and reactive power. The offshore LCC converter controls the offshore AC network frequency by regulating the firing angle. The offshore AC voltage is controlled in the desired range because the DFIG-WT stator voltage combines the stator flux controlled by the MSC converter and the

offshore network angular frequency controlled by the LCC converter [43, 44].

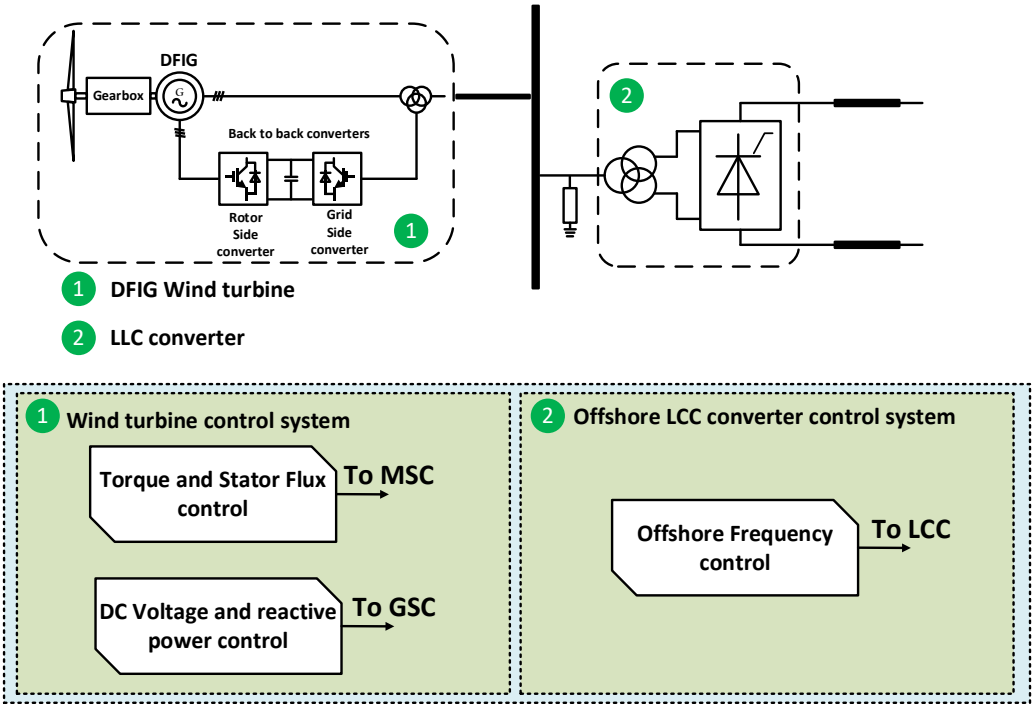

Fig. 2-10 Layout of LCC-HVDC without STATCOM connects with DFIG-WTs and control system [45, 46]

c) LCC-HVDC connect to PMSG-WTs Offshore wind farm

Fig. 2-11 shows the configuration and control system that provides a solution for LCC-HVDC connected to PMSG-WTs. The MSC converter of PMSG controls the torque and stator flux, and the GSC converter controls the DC voltage of the WT and Q-f control. The Q-f controller provides the correct offshore AC network frequency by tuning the reactive power of PMSG-WTs. Therefore, the offshore LCC converter controls the PCC AC voltage magnitude by its firing angle. In this configuration, PMSG-WTs provide a simple structure and reduce the cost of HVDC systems because they do not require additional STATCOMs. However, PMSG-WTs need to remotely measure the voltage at the PCC point, which reduces the robustness of the control system. This is the main disadvantage of this configuration and control strategy [47, 48].

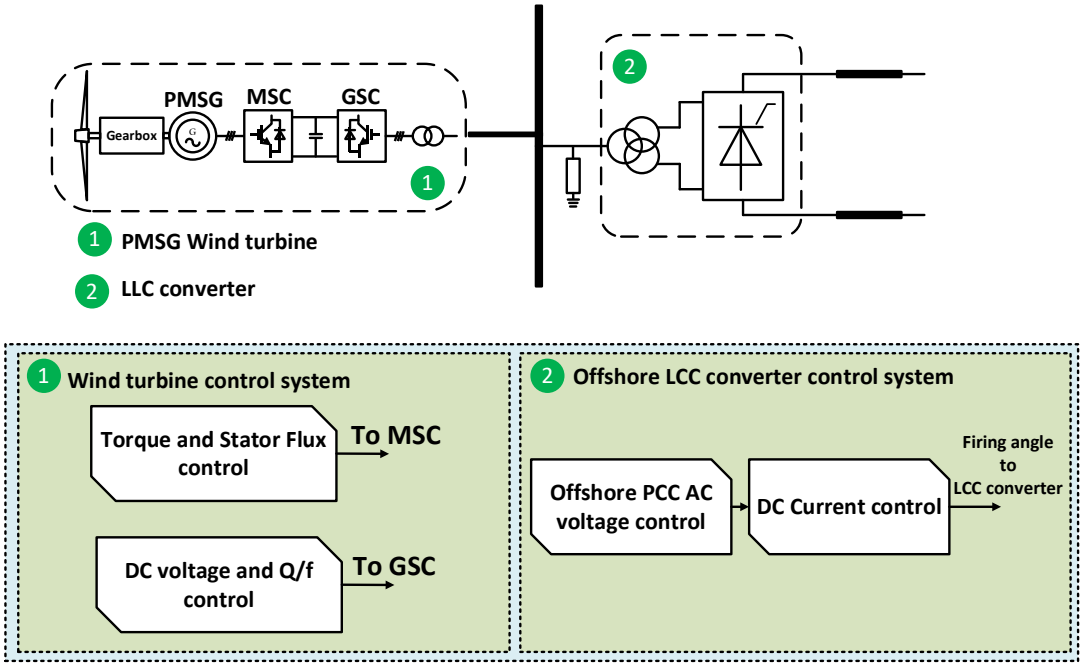

Fig. 2-11 Layout of LCC-HVDC without STATCOM connected PMSG-WTs and control system[47]

2.4.2 VSC-HVDC

Fig. 2-12 shows the VSC-HVDC connected to an offshore wind farm based on PMSG-WTs. The control system of the WTs is similar to the control system connected to the HVAC system. The active power and reactive power are controlled by the MSC converter, and the GSC converter controls the overall DC voltage of WT and the reactive power. If the offshore VSC converter can be assumed to be an infinite AC voltage source to regulate offshore AC voltage and frequency, then the power generated by the wind farm is absorbed by the VSC converter and transmits active power from the offshore wind farm to the onshore station. The onshore VSC converter is similar to the other transmission methods, i.e., controlling the overall HVDC DC voltage to connect the two networks. In addition, the VSC-HVDC system has the ability to black-start and limit the current during faults [49, 50].

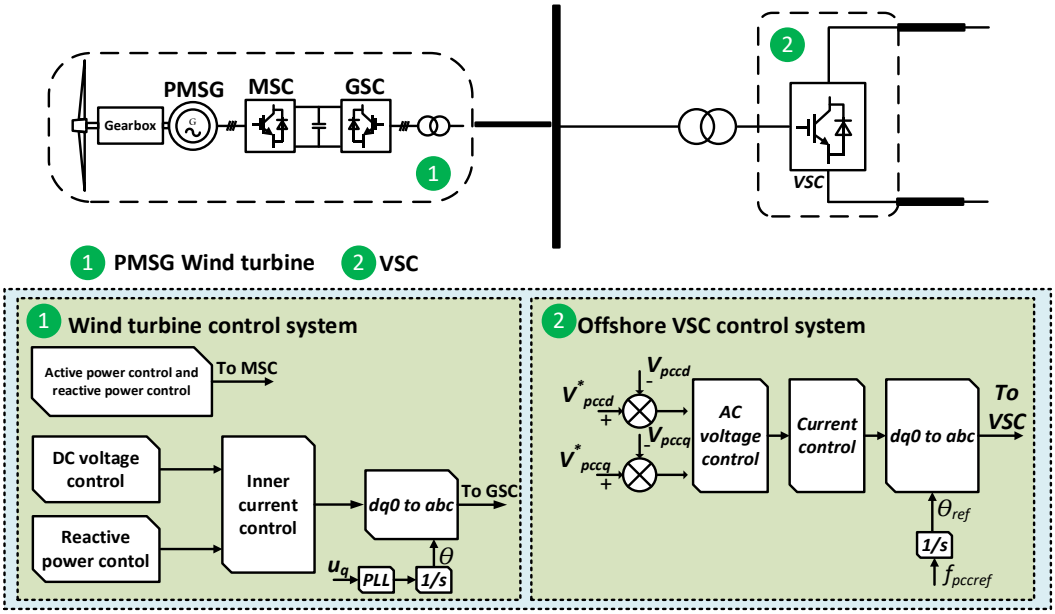

Fig. 2-12 Layout of VSC-HVDC system connected with PMSG-WT and control system [49, 50]

2.4.3 DR-HVDC

To reduce the costs and footprints of offshore converter stations, DR-HVDC is being investigated by many researchers. Compared to other technologies, the diode rectifier is an uncontrollable converter, and the offshore AC voltage relies on the GSC of the WT. Other barriers need to be discussed, such as the frequency of the offshore AC network needing to be regulated by the WT. In this configuration, the diode rectifier transmits power from offshore to the onshore grid, and the AC side of the offshore diode rectifier connects to FRC-WTs (e.g., PMSG-WTs)[33]. The DC side is connected to the onshore converter station based on VSC converters or MMC converters to control the DC voltage and regulate the overall DC voltage of the HVDC system [50, 51]. In this section, several typical control strategies of DR-HVDC will be introduced.

a) Control system based on FixRef system

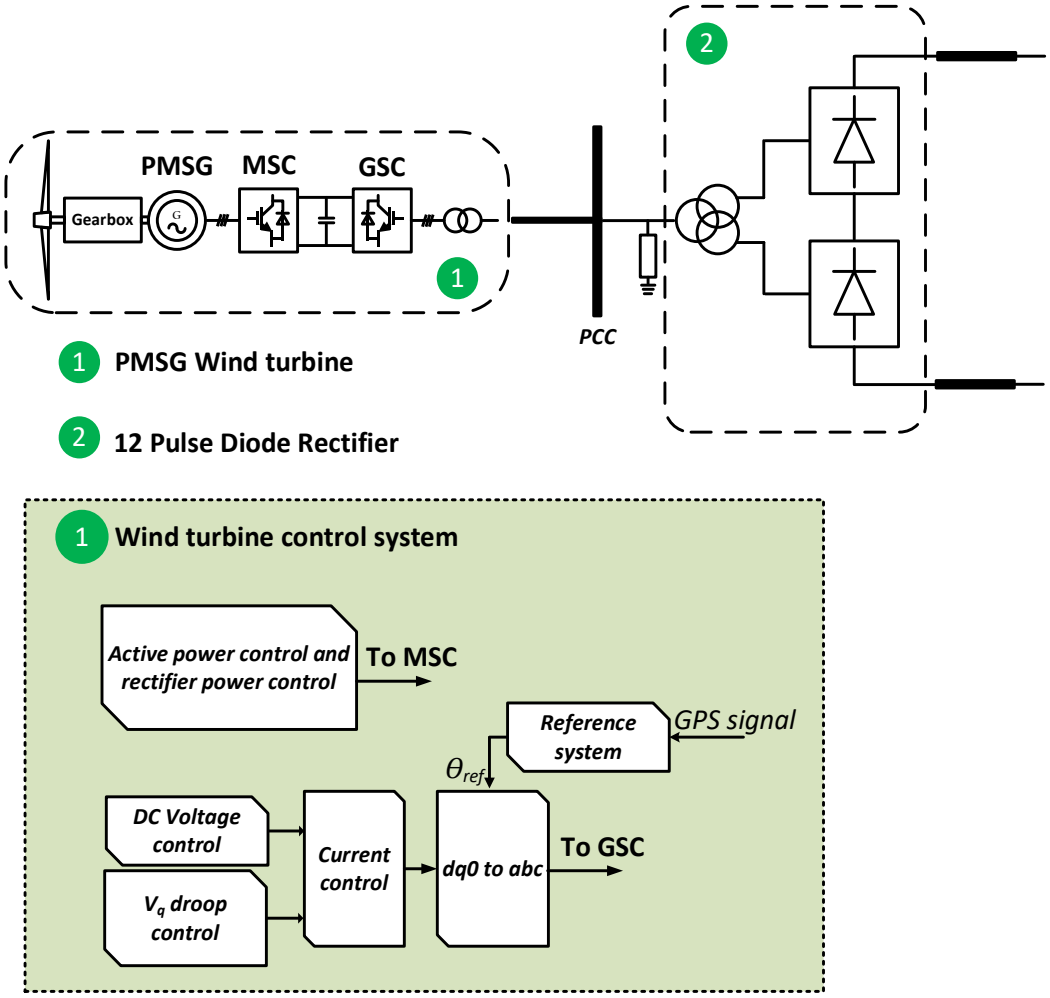

Fig. 2-13 WT control system of DR-HVDC based on FixRef frame [52]

A FixRef technique is proposed for offshore WTs that connect with a DR-HVDC system. This technique was proposed in [52] for a weak grid using power electronics as a voltage-oriented control (VOC) method. The global position system (GPS) external system provided a fixed frequency and common angular reference for the WTs, which replaced the phase-locked-loop (PLL). The configuration of DR-HVDC used on FixRef is shown in Fig. 2-13. The MSG converter controls the active and reactive power, while the GSC converter controls the DC voltage in the d-axis and the *Vq/iq* droop in the q-axis.

b) Control system of WT without the communication device

The decentralized control system without a communication device was proposed in reference. The configuration and control system are shown in Fig. 2-13. The MSC converter controls the active power and reactive power, while the MSC converter controls the DC voltage of WT. The DC link voltage is aligned with the rotating d-axis reference by controlling reactive current. In addition, the reactive power-frequency droop (Q/f-droop) control loop is used to regulate the WT phase angle according to the formula $\omega^* = K_p(Q_{wf} - Q^*_{wf})$. However, the phase regulation without the PLL technique proposes a few challenges, such as synchronization issues during initial start-up, and difficulty in controlling the AC voltage without an AC voltage controller when it operated in an isolated mode and low wind conditions [44, 53].

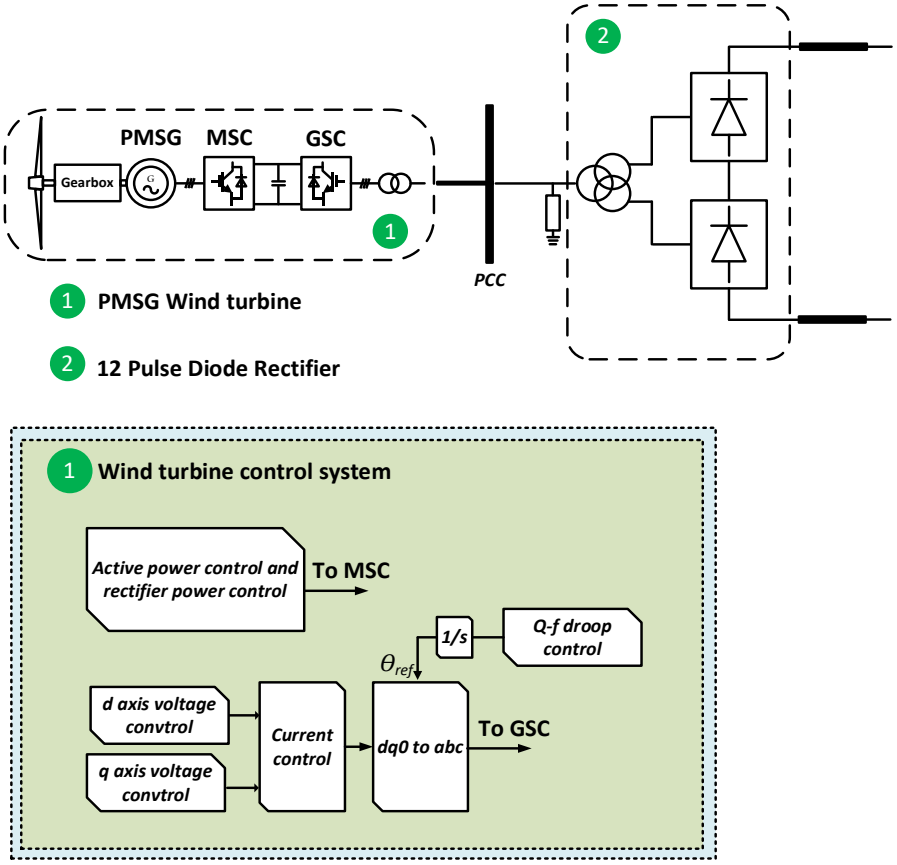

Fig. 2-14 Control system of WTs in DR-HVDC [44, 54, 55]

c) Control system of WT used the distributed-PLL technique

The control method based on a distributed-PLL technique is proposed [56], which was a part of the EU PROMOTioN Project. PROMOTioN project is funded by the EU Horizon 2020 Research Program, which took a holistic approach to address the design, development, and deployment of EU's energy infrastructure in technical, financial, regulatory, managerial and policy areas [57]. The distributed PLL technique does not require an additional communication device or GPS, and it can be considered an automatic synchronization process. In addition to the phase angle regulation shown in Fig. 2-15. An additional frequency controller is used in q-axis control. as shown in Fig. 2-15. In the GSC control system, the signal that is regulated through the active power controller is sent to the d-voltage and d-current control loops. The signal tuned by the reactive power sharing and frequency controllers is forwarded to the q-voltage and q-current controllers. The distributed PLL technique provides a simple and fast frequency regulation method.

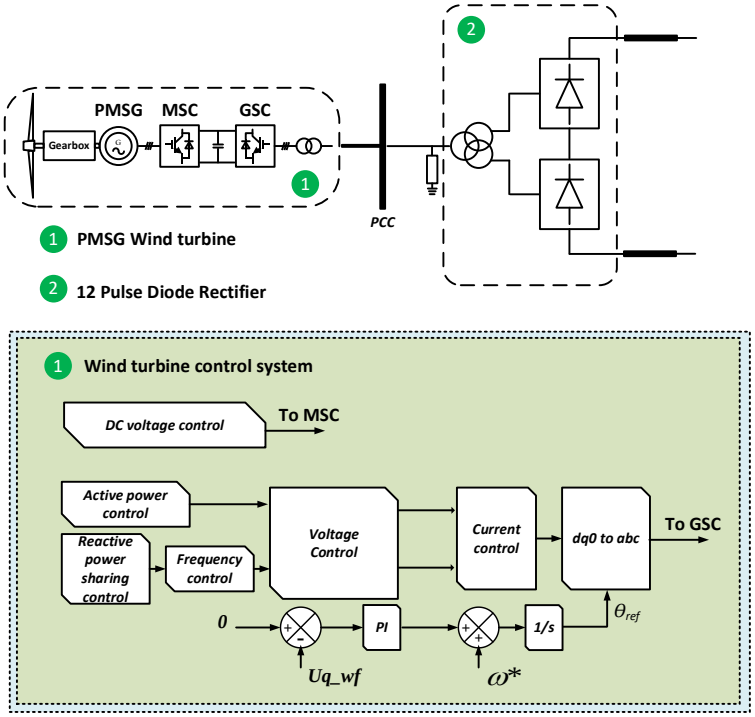

Fig. 2-15 Distributed PLL Control system of WTs in DR-HVDC system [56]

2.4.4 Hybrid-HVDC

A hybrid converter topology in series connections with a Diode Rectifier and a VSC is proposed in 2014, which was used for offshore HVDC systems. The HVDC configuration based on the proposed hybrid converter is shown in Fig. 2-16. In this configuration, DR is series connected with VSC at an offshore converter station to transmit power from OWF to the onshore grid via cables. The AC side connects with the offshore wind farm PMSG, whereas the DC side of the hybrid converter connects to the onshore converter station. The onshore converter station is based on the VSC or MMC, which controls the DC voltage of the HVDC system[58]. In a series connection topology, the transmitted power by each converter section is relevant to the DC voltage of the hybrid converter, and the transmitted power is proportional to the DC voltage. Because DR is an uncontrollable power device, the VSC of a hybrid converter regulates the offshore AC voltage magnitude and frequency, as well as the DC-link

voltage of the VSC. In addition, the VSC functions as an active power filter at the PCC point to filter out the harmonic current caused by the diode rectifier. The 11th and 13th harmonic currents are tuned by a proportional-resonant (PR) controller with PWM modulation in the main control system [59, 60].

Compared to other techniques in HVDC systems, a series connection topology provides a potential solution for offshore wind farms. The hybrid converter aims to combine the advantages of different power electronics converters and overcome their disadvantages by control strategies. The efficiency of a hybrid converter based on 12-P DR and VSC is almost 99.07%, which is higher than the 98.4% of a fully rated VSC-HVDC system, and the cost of a hybrid converter is lower than the VSC-HVDC. In addition, the footprint of a hybrid converter is also smaller than VSC-HVDC, and a smaller AC filter is required due to VSC functions as active power to filter low frequency currents[60].

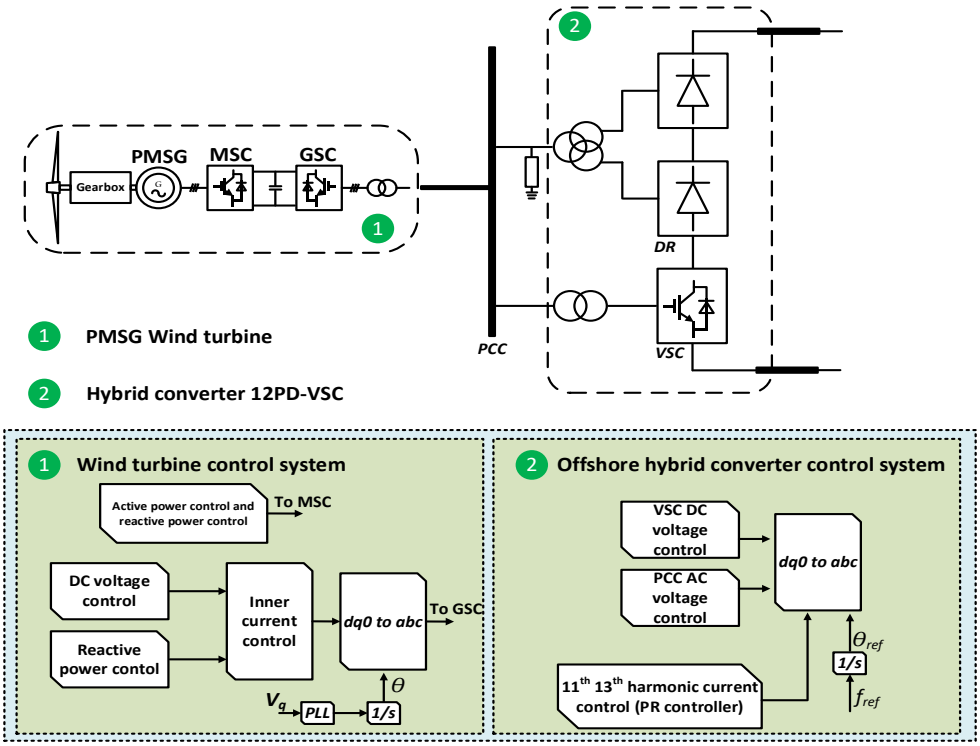

Fig. 2-16 Control system for offshore hybrid converter [59]

2.4.5 Comparison of HVDC technology

Table 2-1 Comparison of offshore HVDC technology

HVDC transmission solutions	Converter component	Controllability	Filter bank size	Transformer	Initial cost	Footprint	Advantage	Disadvantage
LCC-HVDC	LCC Converter	Limited	Larger filter bank	Three windings transformers are required for 12 pulse	High	Large footprint	-Large capacity -High reliability and low power losses	-Need an external voltage source for commutation -large footprint required as the breaker-switched passive filter
Two-Level VSC HVDC	Two-Level VSC converter	High	Small/Medium filter bank	Two windings transformer	High	Large footprint	-AC offshore form ability	-High Switching frequency and converter loss -large numbers of IGBTs in series
MMC-HVDC	MMC Converter	Highest	Small/no AC filter	Two windings transformer	Highest	Large footprint	-Enhanced power quality	-Higher cost and complex control

							-High Voltage and power rating -Better controllability	system -System complexity increased -High Harmonic Switching losses
DR-HVDC	Diode Rectifier converter	No	Larger filter bank	Three windings transformers are required for 12 pulse	Lowest cost	Smallest footprint	-Low cost and small footprint -easy maintenance and operation -complex three-winding transformer required	-Larger AC filter required -No control ability -WTs need to form offshore AC network
Hybrid-HVDC	Diode rectifier converter and VSC converter in series connections	High	Smallest AC filter or No AC filter Built-in active power filter	Three windings transformers are required for 12 pulse	Low cost	Small footprint	-Variable control strategies -Increased transmission capacity and reduced cost	- Control strategies between WTs and Hybrid converter is not clear -Harmonics compensation method needs to be discussed

Table 2-1 shows a comparison table of HVDC technology, including control capabilities, filter size, cost, footprint and advantages and disadvantages. From the perspective of power control, MMC-HVDC exhibits strong control capabilities and does not require large filters. However, its high cost and large physical footprint necessitate additional investment when utilized as an offshore converter. Additionally, the complex control system associated with MMC adds complexity to the overall system. DR-HVDC provides the most cost-effective solution and has a smaller converter footprint compared to other HVDC technologies. However, this technology lacks control capability, as all control is reliant on offshore wind turbines. Additionally, DR-HVDC employs extremely large filters to mitigate harmonics, which increases both the physical footprint and cost. Hybrid-HVDC technology, utilizing a series structured hybrid converter, presents a viable alternative for bridging the gap between MMC and DR technologies. It boasts a relatively lower cost and physical footprint, eliminating the need for excessively large filters for harmonic filtering. Moreover, hybrid-HVDC possesses control capabilities and a control system that is less complex compared to MMC-HVDC. However, there are still certain aspects of this technology that require further improvement, including the control strategy, converter selection, and harmonic current controllers. These aspects will be elaborated upon in detail in the following paragraphs

2.5 Potential improvement of HVDC systems based on Hybrid converter

Based on the previous discussion, HVDC systems based on hybrid converters provide an attractive solution for offshore wind energy, which decreases the initial cost and footprint. However, there are still some limitations that can be improved. This section will discuss these issues.

2.5.1 Control strategies and harmonics compensation controller

In the pervious paper, the control system of the hybrid converter was not described in detail, including the offshore wind turbine control system and hybrid converter system. There is no detailed discussion of the control strategy for a hybrid converter in connection with an offshore wind farm. Offshore wind turbine and offshore hybrid converter have the potential to maintain AC voltage and frequency, Chapter 3 in this thesis provides two control strategies for offshore hybrid converter.

In [60], the hybrid converter produced a harmonic current due to the diode rectifier bridge, and an AC filter was required to suppress the higher harmonic currents. In addition, the VSC converter functioned as the 11^{th} and 13^{th} harmonic current controllers. In its harmonic current compensation control system, the PR controller was used for tuning. The fast set-point change is the highlight for the PR controller, which is able to follow the sinusoidal harmonic current references at the desired resonant frequency. However, there are some drawbacks to use a PR controller, especially for its complex tuning process and stability issues[61, 62]. Additionally, due to its narrow infinite gain band, the PR controller is easily influenced by the grid frequency. The potential solution of using the second-order generalized integrators to construct a nonideal PR controller will lead to a wider band, which could increase tracking errors.

The harmonic current compensation is the main barrier for hybrid converters, especially in offshore energy transmission. Thus, improving the harmonic controller is one of the motivations of this thesis. The synchronous reference frame (SRF) controller will be introduced in a hybrid converter to cancel the harmonic current at the PCC point, which provides an uncomplicated control system with an easy-to-tune function [63-65]. This technique will be used in the hybrid converter based on the

diode rectifier and VSC converter and the hybrid converter based on the Vienna rectifier and VSC converter in Chapter 3 and Chapter 4.

2.5.2 The Choice of Power electronic devices

The hybrid converter in series connections is a novel topology that combines the advantages of two or more power devices, and the incorporation of each type of power electronics addresses their advantages. In reference [59], a 12-pulse diode rectifier connected with a VSC was proposed to reduce the cost and footprint. The power loss is lower than a fully rated VSC-HVDC due to the use of a diode rectifier as part of the hybrid converter. However, the harmonics were filtered by the harmonic compensation controller of the VSC, and an AC filter was still required on the AC side of the VSC. The MMC controller was used instead of a VSC converter in [58]. In this choice, the AC filter was not necessarily required on the AC side. However, the increased number of SMs increased the cost of the hybrid converter.

In recent years, a few advanced power electronics devices have started to be involved in offshore technology. A few converter topologies can be applied in a hybrid converter for offshore wind energy transmission. In this thesis, the hybrid converter based on 6 pulse diode rectifier and a VSC is proposed to reduce the complexity of structures used to reduce initial investment cost and footprint. In addition, the advanced power electronics Vienna Rectifier is proposed in offshore converter stations to transmit power from offshore wind farms to onshore grids. This improvement will be discussed in Chapter 4

2.5.3 A fast response controller for harmonics compensation at hybrid converter

The built-in auxiliary mode is the advantage of a hybrid converter compared to

other converter topologies. The VSC converter functions as active power to cancel out the harmonics produced by the series connected converter of the hybrid converter. Reference [66] proposed a hybrid converter using the harmonic compensation based on a PR controller to eliminate the harmonic components. In addition to this technique, the SRF based on a PI controller can provide an easy-tuning solution for harmonic compensation [61, 65]. Due to the use of a low pass filter in the SRF control process, the response speed of harmonic compensation is reduced. Control processing based on two degrees of freedom internal model controller does not require the low pass filter, which can be implemented in the hybrid converter, which can provide a fast response compensation time for harmonics cancellation [65, 67]. This controller will be introduced in Chapter 5,

2.6 Summary

In this chapter, four AC/DC converters were outlined and discussed, i.e., LCC converter, VSC/MMC converter, diode rectifier and Vienna rectifier. LCC-HVDC, VSC-HVDC, DR-HVDC and hybrid-HVDC were reviewed, respectively. The advantages and disadvantages of these HVDC links were compared. Although LCC-HVDC and VSC-HVDC are commercially used for offshore transmission systems, DR-HVDC and hybrid HVDC have gained significant attention due to their lower investment cost and footprint at the offshore substation. However DR-HVDC is based on uncontrollable power electronics and cannot provide the required control functions at the offshore side, which needs to be relied on the WTs. However, the hybrid converter can act as a controllable device located at the offshore side. Additionally, the hybrid converter has a built-in active power filter in order to reduce the size of the AC filter on the offshore side, which can reduce the investment cost and footprint further. Through the review of the HVDC system based on the hybrid converter, the potential improved points were discussed, i.e., power electronics choice, harmonics

converter choice and harmonic compensation time reductions.

Chapter 3 Hybrid Converter Based on 6P-DR and VSC Converter Used for offshore wind farms

3.1 Introduction

Chapter 2 has discussed several converter topologies used in offshore HVDC systems, such as LCC-HVDC, VSC-HVDC, and DR-HVDC. In addition, the series connection hybrid converter combines two types of converter topologies used in offshore systems to improve power capacity and reliability and reduce power loss, cost, and footprint.

The hybrid converter has a series connection of 12-pulse diode rectifier (12P-DR) and VSC. In this configuration, the three-winding transformer connects 12 P-DR to the PCC point, and the two windings transformer connects VSC to the PCC point. The DC side of both converters is in a series connection [59]. The 12P-DR is an uncontrollable device; the hybrid converter control depends on the VSC converter. Despite the advantages of hybrid converters, such as cost efficiency and lower power loss, the harmonic current remains an unsolved issue. LCC-HVDC and DR-HVDC use a larger filter to suppress the harmonic components. There is also an additional device for the offshore transmission system. For harmonic currents, the hybrid converter has a built-in filter to cancel out the harmonics, and the VSC converter functions as an active power filter to estimate the harmonics. The proportional-resonant controller (PR controller) is used as a harmonic compensation controller [60].

This chapter proposes a hybrid converter based on a 6-pulse diode rectifier (6P-DR) and VSC as an offshore converter station to reduce the complex transformer structure and costs. In addition, two converter control strategies are introduced, where

the VSC of the hybrid converter functions as a grid-forming converter to regulate the AC voltage at the PCC point, while the grid side converter of the WT (WT-GSC) regulates the AC voltage at the PCC point as a grid-forming converter. The Synchronous Reference Frame (SRF) technique is also used to monitor the harmonic compensation and suppress harmonics[63]. The onshore converter station uses a two-level VSC converter controlled by a generic control system based on the onshore grid requirement [68, 69]. Reference [70-72] discusses the solutions the onshore converter station connects to a weak grid.

This chapter will introduce the hybrid converter topology, including the two types of control systems and harmonic compensation controller based on the SRF technique, and one of the DC voltage controllers for the onshore converter station will also be described. Simulation results demonstrate the operation of the hybrid converter and the effective elimination of harmonic performance using the proposed controller.

3.2 Advanced hybrid converter based on 6P-DR and VSC

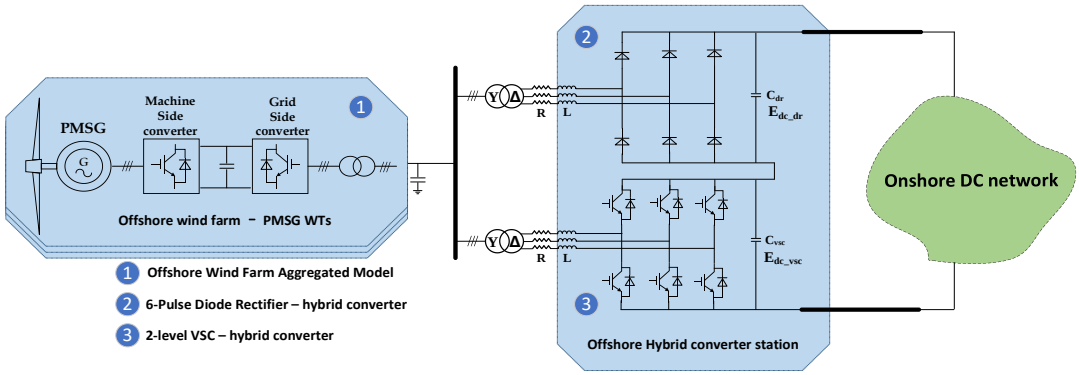

Fig. 3-1 Topology diagram of hybrid converter based on 6P-DR and VSC

The proposed hybrid converter topology is shown in Fig. 3-1. The 6P-DR series connects to a two-level VSC converter at the offshore converter station, and the DC side of the hybrid converter connects with the onshore DC network via a DC cable. A

two-level VSC converter is used in the onshore converter to regulate the onshore DC network.

The offshore hybrid converter is connected to the offshore wind farm at the PCC point. The uncontrollable 6P-DR device and controllable VSC converter connect with a Y/D transformer to the PCC point at the AC side. In addition, the DC side of the 6P-DR and VSC is in a series of connections. Two types of aggregated PMSG-WTs models are used in this chapter. The following section introduces two control strategies according to different wind farm models. Additionally, the onshore converter and harmonic compensation control systems are discussed in the following part.

3.3 Control system of hybrid HVDC system connected with offshore wind farms

3.3.1 Control system of the onshore converter

A two-level VSC converter is used in the onshore converter station for simplicity and is designed to regulate the DC voltage of the HVDC system [73]. The relationship between the offshore hybrid converter components and onshore converter components is shown below.

$$C_{onshore} = C_{dr} + C_{vsc} \tag{3.1}$$

$$E_{dc\_hvdc} = E_{dc\_dr} + E_{dc\_vsc} \tag{3.2}$$

The cascade control system is used for the control in the onshore converter station [73, 74]. There are four typical outer controllers as choices in this offshore HVDC system: active power, reactive power, DC voltage, and AC voltage controllers. To maintain the DC voltage of the overall hybrid HVDC system, the DC voltage controller is the choice for the d-axis control. In addition, the reactive power controller is used in the onshore converter station, which is able to control the reactive power for onshore

grid support.

The inner control loop is implemented in the *dq*-axis frame using the following equations:

$$u_{oncd} = u_{ond} - i_{onq}\omega L + u^*_{ond} \tag{3.3}$$

$$u_{oncq} = u_{onq} + i_{ond}\omega L + u^*_{onq} \tag{3.4}$$

The DC voltage controller aims to allow DC power to be transferred from the offshore wind farm to the onshore grid by regulating the DC voltage of the HVDC system. As shown in Fig. 3-2, the relationship between measured value and reference value can be calculated as

$$i^*_{ond} = K_{p\_dc}(E^*_{hvdc} - E_{hvdc}) + K_{i\_dc}\int (E^*_{hvdc} - E_{hvdc}) \tag{3.5}$$

Where K_{p_dc} and K_{i_dc} are the proportional gain and integral gain of the PI controller of the DC control loop, respectively. The reactive power controller can be described by

$$q(t) = \frac{3}{2}[-u_{ond}(t)i_{onq}(t) + u_{onq}(t)i_{ond}(t)] \tag{3.6}$$

$$i^*_{onq} = \frac{-2Q^*_{on}}{3u_{ond}} \tag{3.7}$$

Fig. 3-2 displays the overall control system of the onshore DC network that is implemented by the VSC converter.

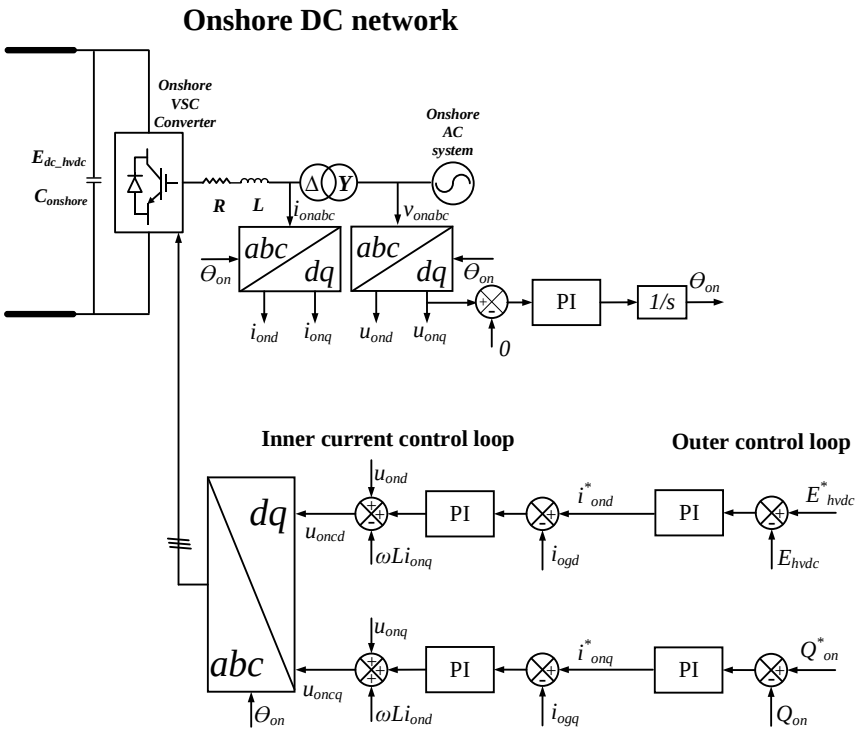

Fig. 3-2 Control system of onshore converter station

3.3.2 Grid forming capability of the proposed hybrid converter

Fig. 3-3 shows tow equivalent wind farm model diagrams to verify different control strategies used in offshore hybrid converter. Fig. 3-3 (a) displays a controlled *abc* current source, while Fig. 3-3 (b) shows the GSC control with an initial DC source. The main difference between the two equivalent models is the control role in the hybrid HVDC system.

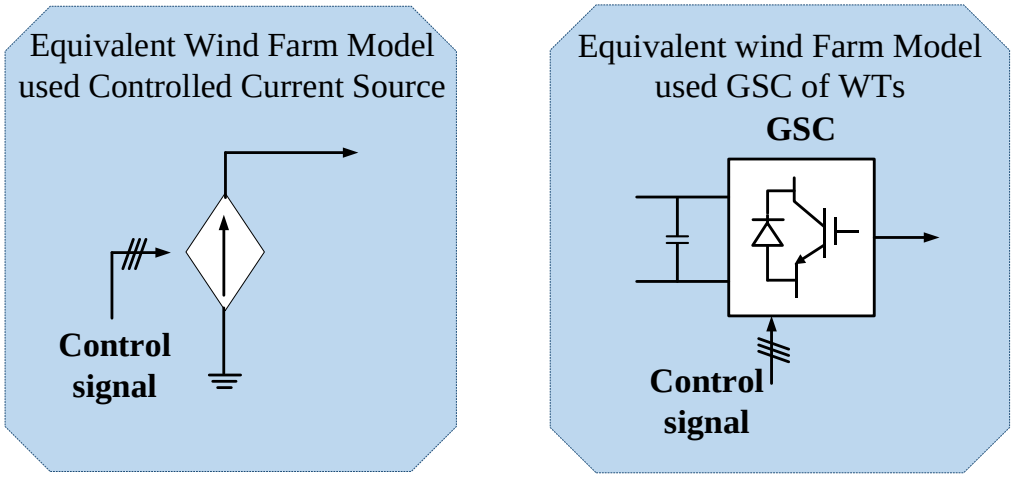

(a) (b)

Fig. 3-3 Equivalent aggregated wind farm model: (a) Wind farm model use a controlled current source and, (b) wind farm model uses GSC converter

When using a controlled *abc* current source model to describe offshore wind farms, the hybrid converter can function as the grid-forming converter to regulate the AC voltage magnitude at the PCC point. The overall control system is illustrated in Fig. 3-4. In this case study, the VSC of the hybrid converter controls the offshore AC voltage and performs harmonic cancellation. The relationship between the transmitted power and PCC voltage magnitude can be expressed as

$$P = \frac{|V_{vsc\_ac}|\, sin\, \gamma}{X_L} \cdot n|V_{pcc\_ac}| \tag{3.8}$$

$$Q = \frac{|V_{vsc\_ac}|\, cos\, \gamma}{X_L} \cdot n|V_{pcc\_ac}| \tag{3.9}$$

$$X_L = \omega_{pcc} L_{vsc} \tag{3.10}$$

where $|V_{vsc\_ac}|$ and $|V_{pcc\_ac}|$ are the magnitudes of the hybrid-VSC converter and PCC, respectively. Further, L_{vsc} is the inductance of hybrid-VSC, ω_{pcc} is the angular frequency of the PCC voltage, n is the voltage ratio of the transformer, and γ is the phase shift between the hybrid-VSC and PCC voltages.

Additionally, the VSC of the hybrid converter is designed to maintain frequency

control at the offshore AC side. The desired frequency is constant (angle Θ_{pcc} after integral) flowing into *abc/dq* transformation. The overall control system of the hybrid HVDC system, including the wind farm control system and hybrid-VSC control system, is shown in Fig. 3-4

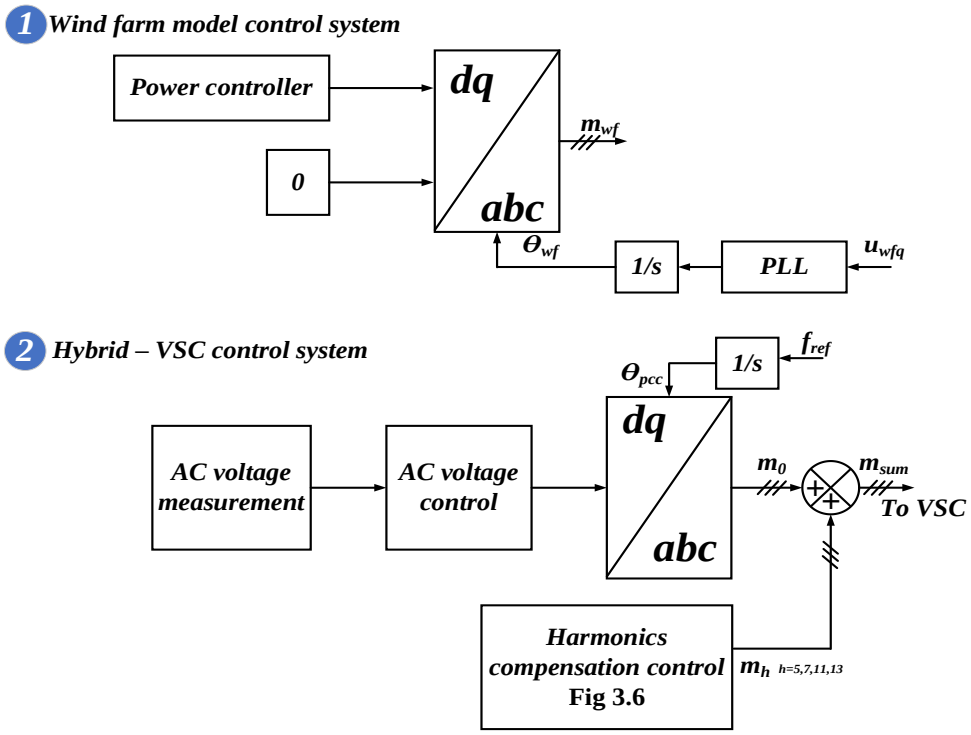

Fig. 3-4 Hybrid converter control system when hybrid converter functions as Grid forming converter

3.3.3 Offshore wind turbine functions as grid-forming converter

The previous study on hybrid converters used the hybrid converter to regulate the DC and AC voltages without an inner current controller. Additionally, the PCC voltage and frequency are maintained by the VSC of the hybrid converter. Reference [56] introduces the improved control system of the hybrid converter and WT model control system that are usually used in DR-HVDC.

The WT-GSC converter regulates the AC voltage to function as the grid-forming converter for releasing the control capacity of the hybrid converter. As the 6P-DR is an uncontrollable converter, the transmitted power by the hybrid converter components is proportional to its DC-link voltage. In this case study, the active power, *Q-f* reactive power controller, voltage controller, and inner current controller are used in GSC-WT, as shown in Fig. 3-5. In this proposed control system, the voltage magnitude is regulated by the d-axis, the u_{q_wf} set as 0, and as input to maintain the frequency output to control u_{q_wf} to equal zero in the q-axis. The relationship between u_{q_wf} and ω is denoted below.

$$\omega = \omega_0 + Kpu_{q\_wf} + Ki\int u_{q\_wf}dt \tag{3.11}$$

$$U^*_{q\_wf} = Kp(\omega^* - \omega) \tag{3.12}$$

In this control strategy, the hybrid VSC maintains the power transfer between the offshore AC side and the DC cable by regulating its DC-link voltage. The control system, including the outer DC voltage, reactive power, and inner current controllers, is used in the hybrid VSC, which is a control system widely used in VSC controllers. The diagram of a hybrid VSC control system is shown in Fig. 3-5. To reduce the size of the hybrid VSC converter, the DC voltage controller is designed to control half of the overall HVDC system to maintain the same ratio of the overall HVDC DC voltage.

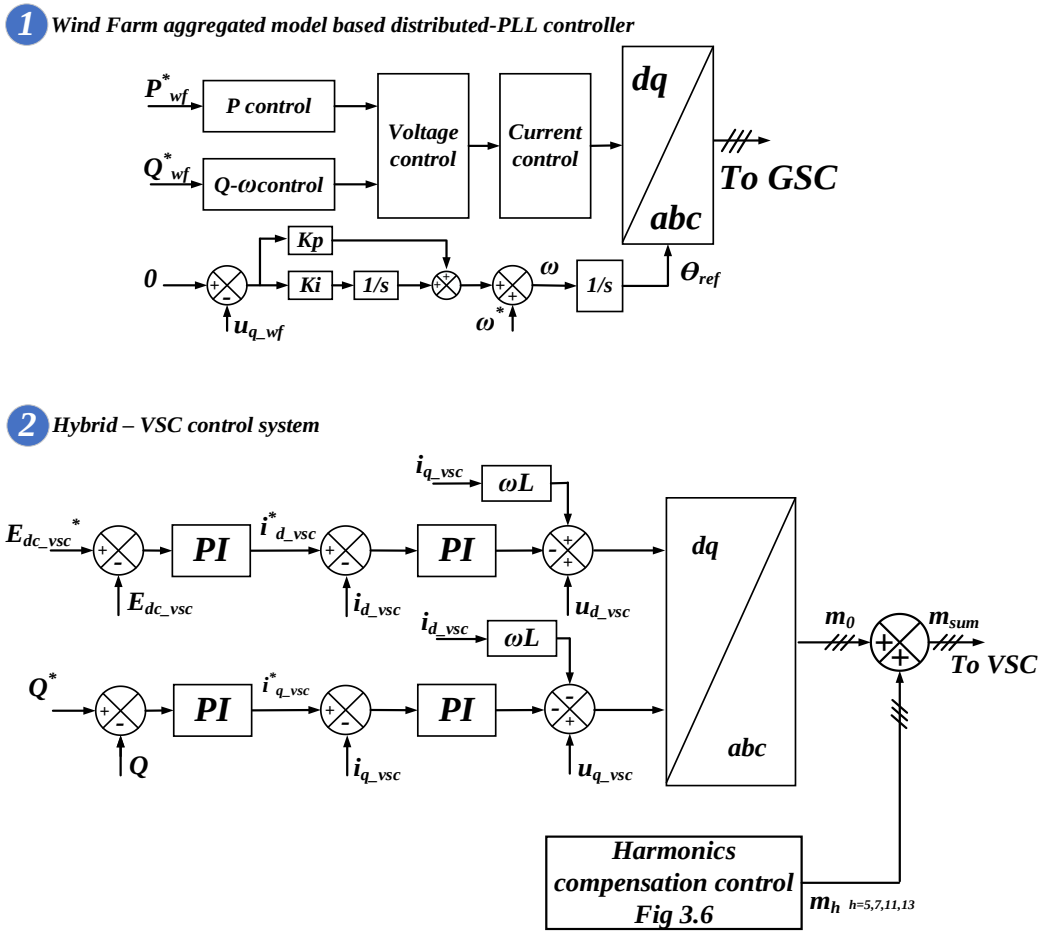

Fig. 3-5 Hybrid converter control system as GSC-WTs as grid forming converter

3.3.4 SRF-harmonics compensation control system

There are a number of research studies, including the hybrid converter and active power filter, which have used proportional-resonant (PR)-based controllers to provide active power capability to a voltage source converter. PR-based controllers are used in hybrid converters that have a 12P-DR series connected with a VSC to cancel the harmonic current produced by the 12P-DR. They can follow the sinusoidal harmonic references at their individual resonant frequencies by imposing an infinite frequency without steady-state errors. Although a PR-based controller provides a fast response to setpoint, the complex tuning process is challenging for the implementation of the

control systems. The reason for this situation is that the resonant frequency should be well tuned to the reference frequency. The narrow infinite gain band makes this control method susceptible to changes in grid frequency. Non-ideal PR-based controllers use a second-order integrator, producing a wide resonant band but increasing tracking errors.

Synchronous Reference Frames (SRF) - based controller applies several synchronous *dq* harmonic frames and Low-Pass Filters (LPF) to detect harmonic currents. The control signal is fed through an LPF to the PI controller. The benefit of using SRF-based controllers is that each harmonic component is mathematically converted into two *dq* DC signals, where the easy-to-tune PI controller provides stable control without tracking errors. In addition, active power filters using SRF-based controllers are unaffected by variations in grid frequency. In hybrid converter applications, an SRF-based controller is preferred, which provides robustness and easy deployment.

Fig. 3-6 shows the conventional process of detecting the harmonic generated by the 6P-DR. The current harmonics are fed into different harmonic *dq* transformations, which rotate at specific harmonic frequencies (i.e., the 5^{th}, 7^{th}, 11^{th}, and 13^{th} harmonic frequencies). The output of the harmonic *dq* transformations is a signal consisting of DC and AC values. The DC value represents the *d* and *q* components of the harmonic current, while the AC signal contains the remaining harmonic components and the fundamental AC signal.

The objective of using LPF is to remove the AC part of the detected current by the harmonic *dq* frame. The filtered *dq* component of harmonic currents is used as a reference signal for the corresponding PI controllers of the control system. The harmonic *dq* modulator signals produced by PI controllers drive the hybrid VSC

converter to generate the same magnitude harmonics for compensation. Accordingly, harmonic currents from the 6P-DR of hybrid converters will be cancelled out by the hybrid VSC at the PCC point. To generate these harmonic modulator signals in the hybrid VSC controller, a multiple of the synchronous frequency is used as its input for the *dq* to *abc* transformation. To ensure that each harmonic current does not exceed the allowed range, each PI controller has a saturation limit. Without the PI saturation limit, an unwanted harmonic signal will be generated and affect the PCC current quality. This is because the magnitude of the hybrid VSC reference voltage would be greater than the allowed capacity of the DC voltage. In addition, this control technique can be selected to perform cancellations based on grid requirements, either single or a group of harmonics. However, the disadvantage of the SRF technique is the slow response time to setpoint caused by the LPF filter process.

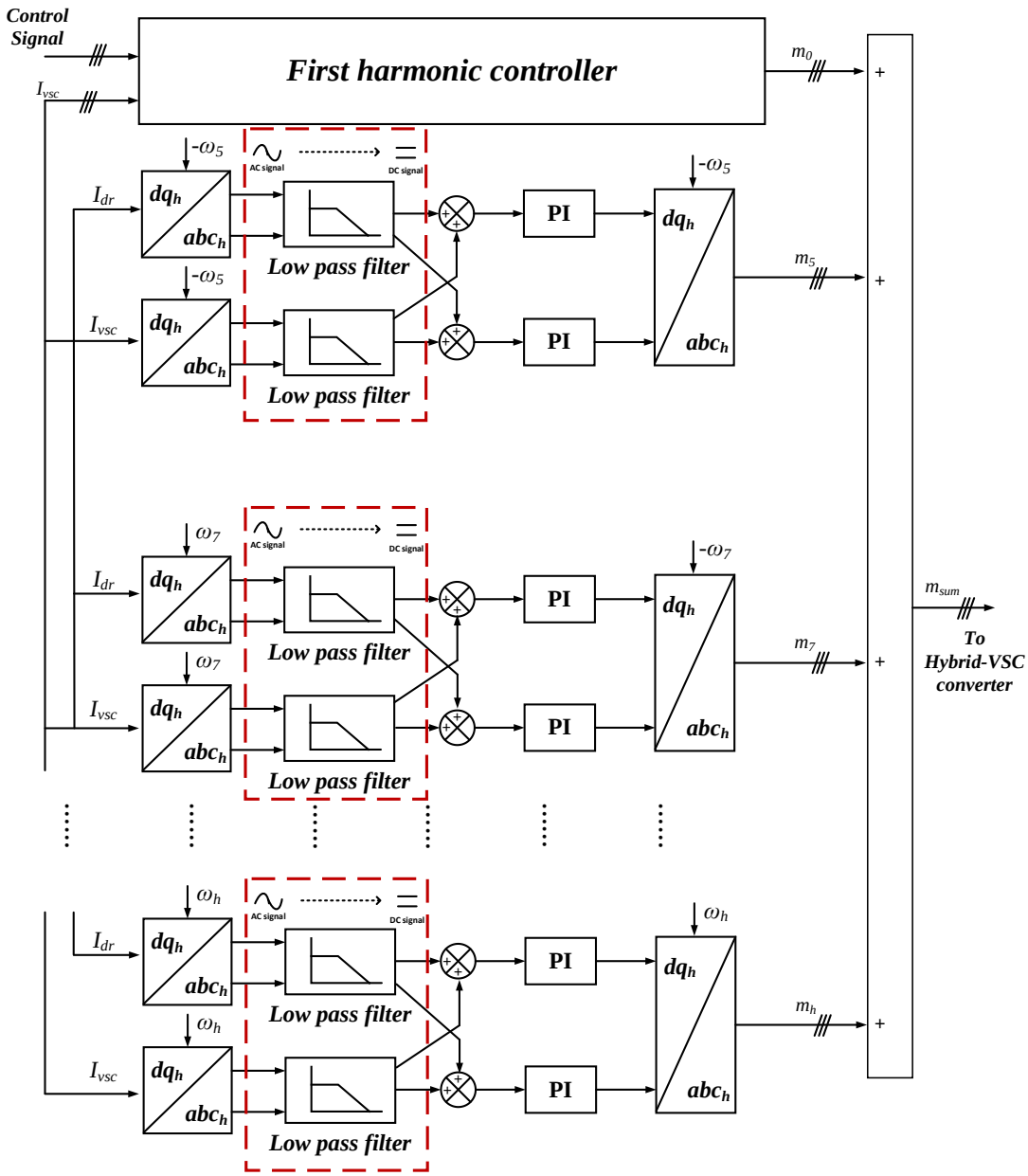

Fig. 3-6 Harmonic currents compensation control system using SRF-technique

Equation (3.13) expressed the generalized harmonic *dq* transformation T_n based on the SRF technique to obtain the *dq* components of the *n* harmonic current.

$$T_n = \frac{2}{3}\begin{pmatrix} sin(\Gamma_n n(\omega_s t)) & sin(\Gamma_n n(\omega_s t - \frac{2\pi}{3})) & sin(\Gamma_n n(\omega_s t + \frac{2\pi}{3})) \\ cos(\Gamma_n n(\omega_s t)) & cos(\Gamma_n n(\omega_s t - \frac{2\pi}{3})) & cos(\Gamma_n n(\omega_s t + \frac{2\pi}{3})) \\ \frac{1}{2} & \frac{1}{2} & \frac{1}{2} \end{pmatrix} \quad (3.13)$$

Where Γ_n = sign[sin(2π*n*/3)] represents the sequence of the *n* time harmonic currents. Applying T_n to a given three-phase AC signal produces a DC *dq* signal that represents the *n* time harmonic current, as well as an AC component that includes the remaining harmonic currents. These non-*n* harmonics are converted to frequencies that depend on the order of the *n* time harmonic currents and the order of the rest of the harmonic components. The *dq* harmonic currents can be calculated as

$$i_{n\_d} = \Gamma_n i_n \, cos(\beta_n) + \sum_{k=1,k\neq n}^{\infty} \Gamma_k i_k \, cos(-\Gamma_k[(\Gamma_n n - \Gamma_k k)(\omega_s t) + \beta_k] \quad (3.14)$$

$$i_{n\_q} = i_n \, sin(\beta_n) + \sum_{k=1,k\neq n}^{\infty} i_k \, sin(-\Gamma_k[(\Gamma_n n - \Gamma_k k)(\omega_s t) + \beta_k] \quad (3.15)$$

Where i_{n_d} and i_{n_q} represent the *d* and *q* of *n* harmonics, respectively. β_n is the phase shift of the *n* harmonic current; β_k is the phase shift of the *k* harmonic current; i_n and i_k are the magnitude of *n* and *k* harmonic currents, respectively; ω_s is the synchronous frequency in radians; and Γ_k = sign[sin(2π*k*/3)] represents the sequence of the *n* time harmonic currents and as an algebraic symbol. Equations (3.16) and (3.17) express the dynamics of the *dq* fundamental and harmonic components between the PCC point and VSC, as expressed below.

$$u_{n\_d\_vsc} = r i_{n\_d} + L\frac{di_{n\_d}}{dt} - \omega_s L i_{n\_q} - u_d \quad (3.16)$$

$$u_{n\_q\_vsc} = r i_{n\_q} + L\frac{di_{n\_q}}{dt} - \omega_s L i_{n\_d} - u_q \quad (3.17)$$

Where *r* and *l* are the equivalent resistance and inductance between the hybrid VSC and OWF; i_{n_d} and i_{n_q} are the average *dq* current of n harmonic components;

$u_{n\_d\_vsc}$ and $u_{n\_q\_vsc}$ are the dq components of the average VSC voltage; and u_d and u_q are the *dq* components of the PCC voltage. When the grid voltage u_d and u_q and the cross-coupling term in (3.16) and (3.17) are considered disturbances, the transfer function between the *dq* fundamental and harmonic currents can be represented the same as the transfer function with the *dq* fundamental and harmonic voltage. The relationships between the current and voltage in the *dq* frame are represented as

$$\frac{i_{n\_d}(s)}{u_{n\_d\_vsc}(s)} = \frac{i_{n\_q}(s)}{u_{n\_q\_vsc}(s)} = \frac{i_n(s)}{u_{n\_vsc}(s)} = G_i(s) = \frac{1}{Ls + r} \tag{3.18}$$

As expressed in Equation (3.18), the open loop system has a stable pole at *-r/L*, which can be cancelled by the PI controller. The close loop function for *h* harmonics current controller can be calculated as

$$B_h = \frac{1}{\tau_h S + 1} \tag{3.19}$$

Where τ_h is the desired spend of the response time to the setting point that can be selected, additionally, Kp_h and Ki_h are the proportional and integral constants of the *h* harmonic PI controller, respectively. The value of Kp_h and Ki_h can be calculated as

$$\frac{Ki_h}{Kp_h} = \frac{r}{l} \tag{3.20}$$

$$\frac{Kp_h}{L} = \frac{1}{\tau_h} \tag{3.21}$$

3.4 Simulation results

In this section, the two simulation models are based on the control systems that were proposed in Section 3.3.2 and 3.3.3. were simulated in the PSCAD/EMTDC environment to verify the hybrid converter performance and harmonic current cancellation effects. Fig. 3-7 shows the flow chart of the simulation test, and this

section shows the hybrid converter operation results of two control strategies and the performance of the harmonics current controller based on the SRF controller.

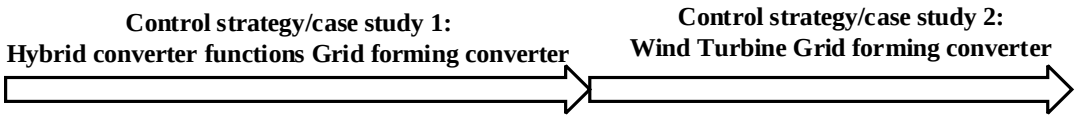

Fig. 3-7 Simulation tests

The offshore wind farm uses the average model to simulate. And the hybrid converter components, including the diode rectifier and VSC converter use the detailed model. These PSCAD models are displayed in Appendix A Hybrid Converter Based on the Diode rectifier and VSC Converter. The timestep of those testing is 20 *us*.

3.4.1 Case study on hybrid converter functions as grid forming converter

Table 3-1 Parameter of the hybrid HVDC system

Parameters		Nominal Value
Wind farm Aggregated model	Power rating	200 MW
	Transformer voltage ratio	0.69 kV / 33 kV
Onshore converter station	DC voltage rating	320 kV
	Capacitance	600 μF
6P-DR Of Offshore Hybrid converter	Power Rating P_{T6PDR}	200 MW
	Transformer voltage ratio	33 kV / 67 kV
	Inductance	0.15 p.u.
	Resistance	0.0015 p.u.
2-Level VSC Of Offshore Hybrid Converter	Power Rating	200 MW
	Transformer voltage ratio	33 kV / 67 kV
	Inductance	0.15 p.u.
	Resistance	0.0015 p.u.

The PSCAD model parameters are listed in Table 3-1, and the PSCAD model that uses the proposed control system is illustrated in Fig. 3-4.

The onshore station enabled the control system at 0 s, which provides the overall DC-link voltage to the hybrid HVDC system. Then, the offshore station and OWF started to establish the AC voltage and frequency. Fig. 3-8 shows the hybrid converter performance under the proposed control system. At 0 s, the onshore converter station regulates the overall DC voltage at 320 kV (1 p.u.) to provide initial energy for the hybrid converter to operate. At 1 s, the AC voltage controller of the hybrid converter and OWF were enabled, which provides an AC voltage at the desired value of 33 kV (1 p.u.) at the PCC point, as shown in Fig. 3-8 (a). The active power was generated by OWF from 0 to 200 MW (1 p.u.) during 1.0–1.5 s.

Due to the series connection configuration, the 6P-DR and VSC components of the hybrid converter work in the offshore converter station and share the HVDC DC-link voltage (Edc_{hvdc}), as shown in Fig. 3-8 (b). Additionally, the transmitted power by the 6P-DR and VSC (P_{dr} and P_{vsc}) is proportional to its DC-link voltage (Edc_{dr} and Edc_{vsc}). The transmitted power of the hybrid converter components is presented in Fig. 3-8 (c).

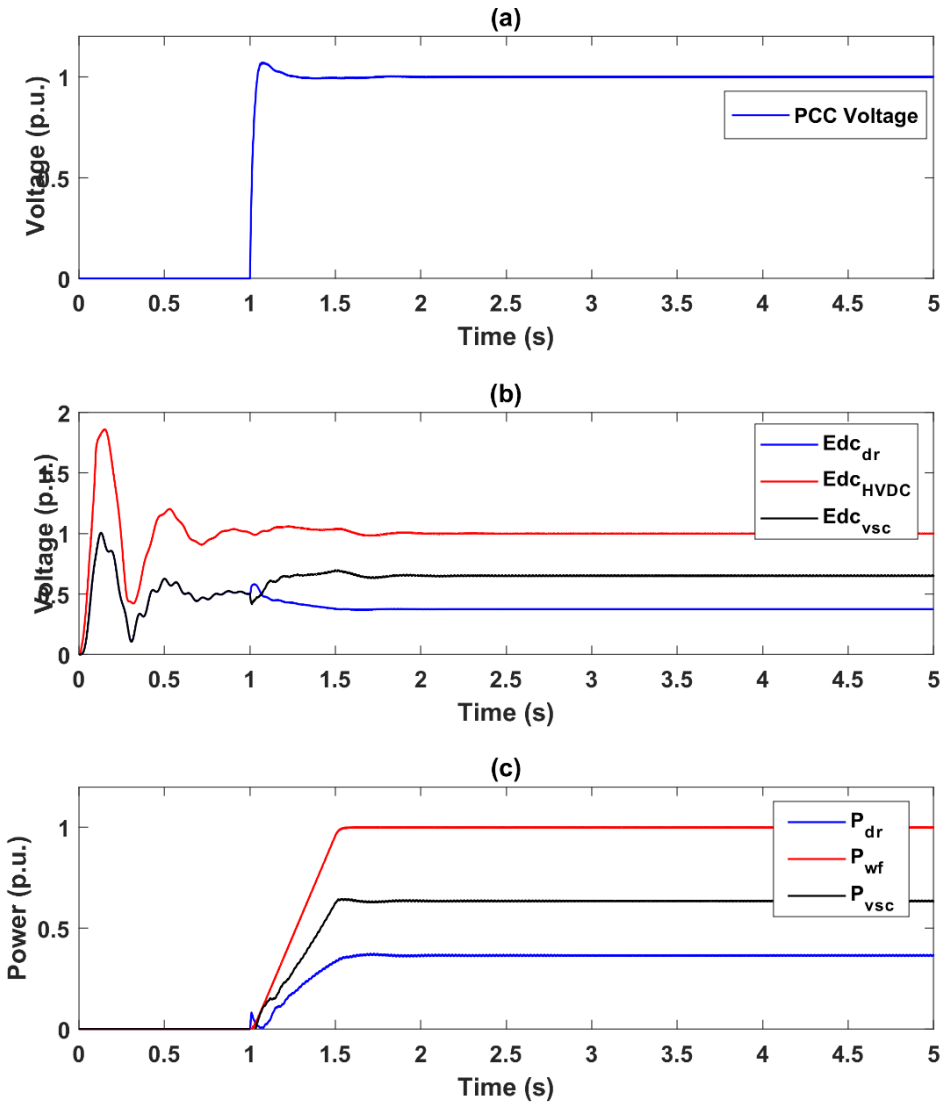

Fig. 3-8 Performance of the hybrid converter functions as the grid-forming converter

Fig. 3-9 presents the AC voltage behaviour of the VSC converter of the hybrid converter that steps the AC voltage based on control commands. The PCC voltage (V_{pcc}) was regulated at 33 kV (1 p.u.) at the beginning, and the AC voltage reference was dropped to 0.96 p.u. at 3 s, then climbed to 1.1 p.u., and finally back to 1 p.u. at 7 s.

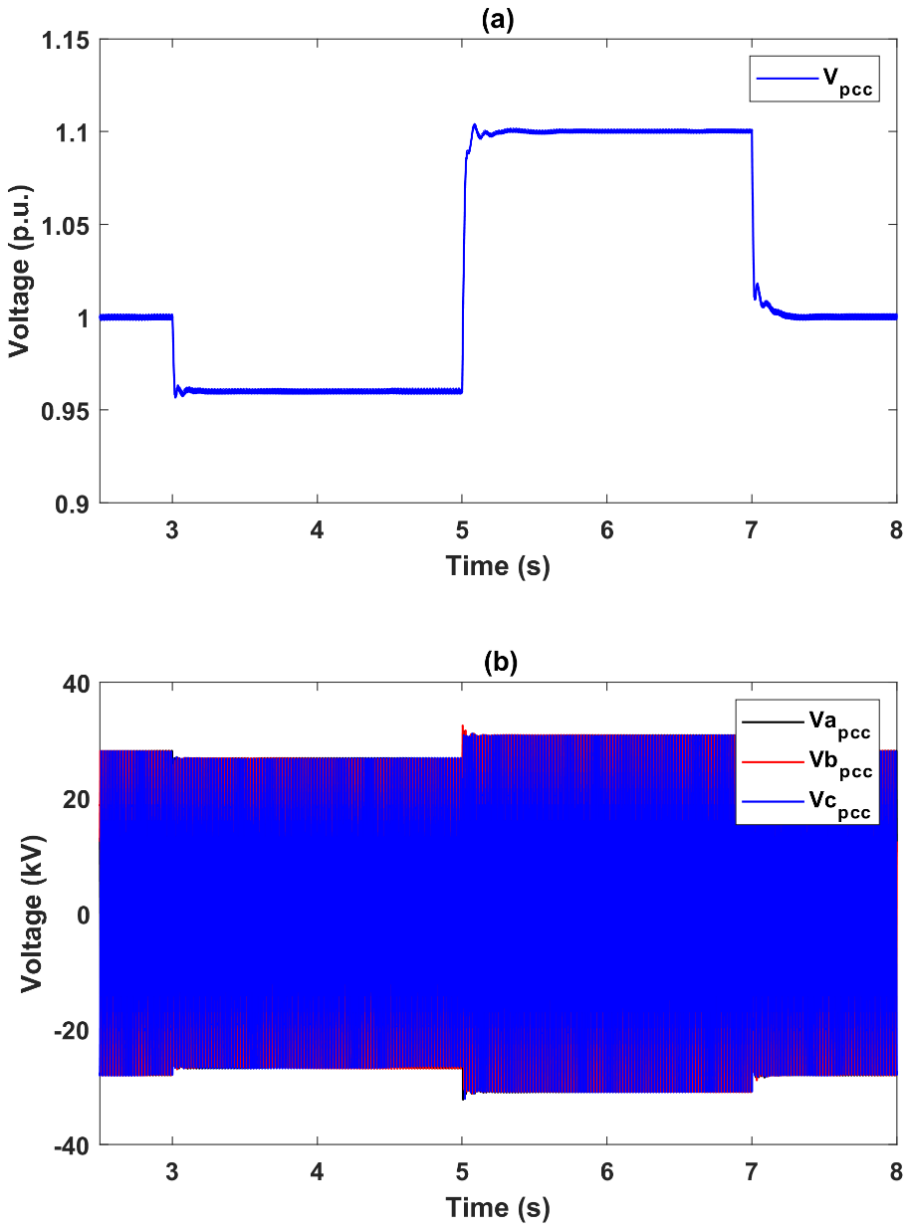

Fig. 3-9 Performance of AC voltage control

The results of the harmonic compensation control loop are illustrated in Fig. 3-10 that shows the PCC current waveforms for the same period. The PCC current without harmonic compensation is shown in Fig. 3-10 (a), and the compensated PCC current is shown in Fig. 3-10 (b) and (c). To test the performance of harmonics current compensation SRF-controller. Fig. 3-10 (b) shows the shape of the PCC current when the 5^{th} and 7^{th} harmonic compensation controllers are working. Fig. 3-10 (c) presents the PCC current when all relevant harmonic compensation controllers (5^{th}, 7^{th}, 11^{th},

and 13th) are enabled. The PCC current waveforms have a high harmonic content without the harmonic current compensation controller. When the harmonic compensation operates, the PCC current appears harmonic-free.

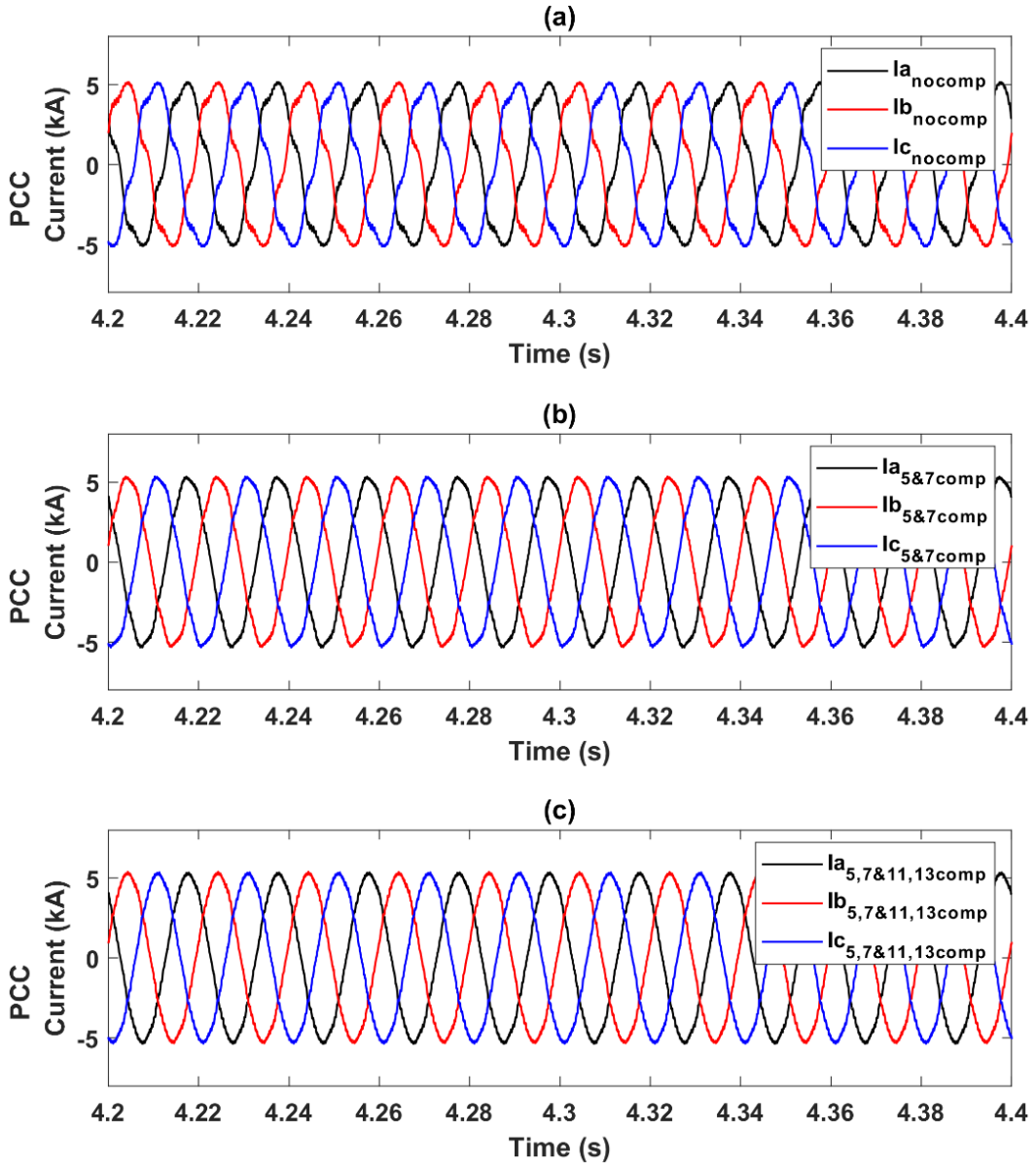

Fig. 3-10 Current at PCC point: (a) PCC current – no harmonic compensation; (b) PCC current – 5th and 7th harmonics compensated; (c) PCC current – 5th, 7th, 11th, and 13th harmonics compensated.

To confirm the result of the harmonics compensation controller, Fig. 3-11 shows the harmonic spectrum of the PCC phase current, which is calculated by using the fast

Fourier transform. The simulation results verify that the 5^{th},7^{th}, 11^{th}, and 13^{th} harmonic currents were suppressed by the harmonic compensation controller. The total harmonic distortion (THD) is labelled on the left of the figure.

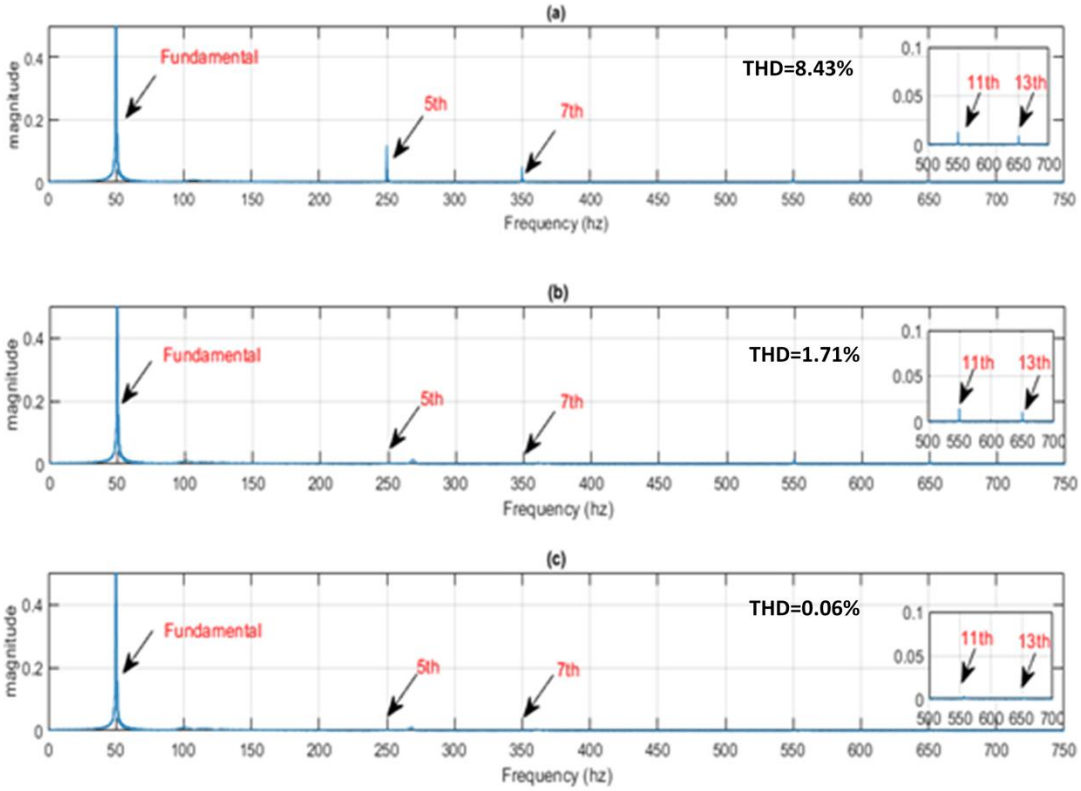

Fig. 3-11 Current frequency spectrum: (a) No harmonics compensation; (b) 5^{th} and 7^{th} harmonics compensation; (c) 5^{th}, 7^{th}, 11^{th}, and 13^{th} harmonics compensation.

To verify the response of the hybrid converter VSC to changing harmonic contents in the PCC currents, OWF is simulated in a power step that increases the power flowing through to the hybrid converter 6P-DR and affects the magnitude of the circulating harmonic currents.

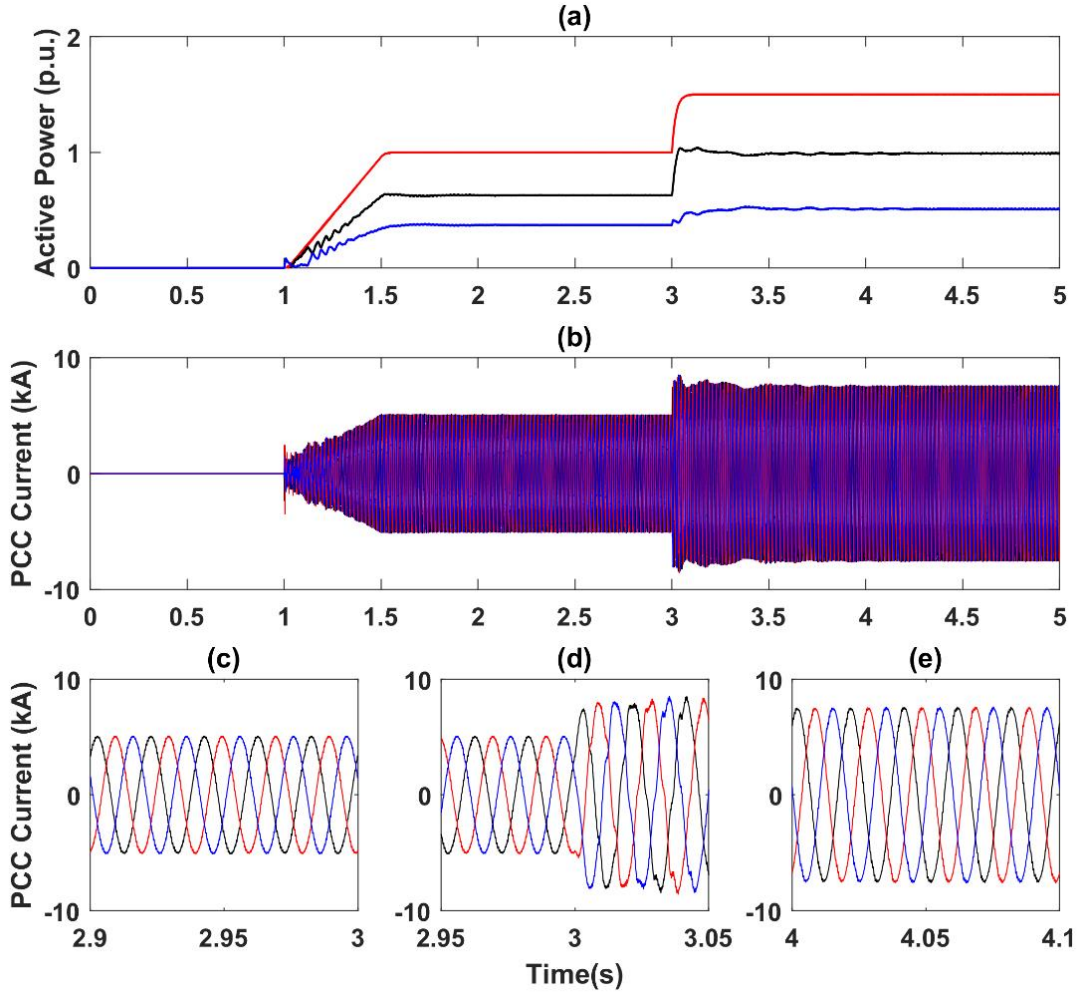

Fig. 3-12 Performance of the hybrid converter during a power step (a) Transmitted power through the different components of the offshore hybrid converter; (b) current at the PCC point; (c) PCC current during 2.7–3.0 s; (d) PCC current during 2.9–3.2 s; (e) PCC current during 3.2–3.5 s

As seen in Fig. 3-12, OWF generated 1 p.u. active power to an onshore grid at the beginning of the simulation, and then the generated power increased to 1.5 p.u. at 3 s, as displayed in Fig. 3-12 (a). The PCC current increased, causing larger harmonic currents that temporarily increased the total harmonic distortion on PCC currents. The increase in harmonic distortion triggered corrective action by the VSC of the hybrid converter, which in turn increased its compensation harmonic currents. Fig. 3-12 (b)

shows that the PCC current became harmonic-free after this period. Fig. 3-12 (c) shows the PCC current before the power increased, at the change point, and after the power increased.

3.4.2 Case study on OF-WTs functions as grid forming converter

The parameters of the PSCAD model are listed in Table 3-2, and the PSCAD model for the proposed control system is illustrated in Fig. 3-5.

Table 3-2 Parameter of hybrid HVDC system

Parameters		Nominal Value
Wind farm Aggregated model	Power rating	200 MW
	Transformer voltage ratio	0.69 kV / 33 kV
Onshore converter station	DC voltage rating	320 kV
	Capacitance	600 μF
6P-DR Of Offshore Hybrid converter	Power Rating P_{T6PDR}	200 MW
	Transformer voltage ratio	33 kV / 67 kV
	Inductance	0.15 p.u.
	Resistance	0.0015 p.u.
2-Level VSC Of Offshore Hybrid Converter	Power Rating	200 MW
	Transformer voltage ratio	33 kV / 67 kV
	Inductance	0.15 p.u.
	Resistance	0.0015 p.u.

Fig. 3-13 shows the simulation results on the hybrid converter operating at different WT input power steps. The VSC controls the DC link voltage as 160 kV (1 p.u) due to the series connection of the hybrid converter station. The two components of the hybrid converter are proportional to its DC link voltage. Fig. 3-13 (a) shows that the active power of the hybrid converter transmits equal demand active power because the hybrid converter is controlled in the same share in the hybrid HVDC system.

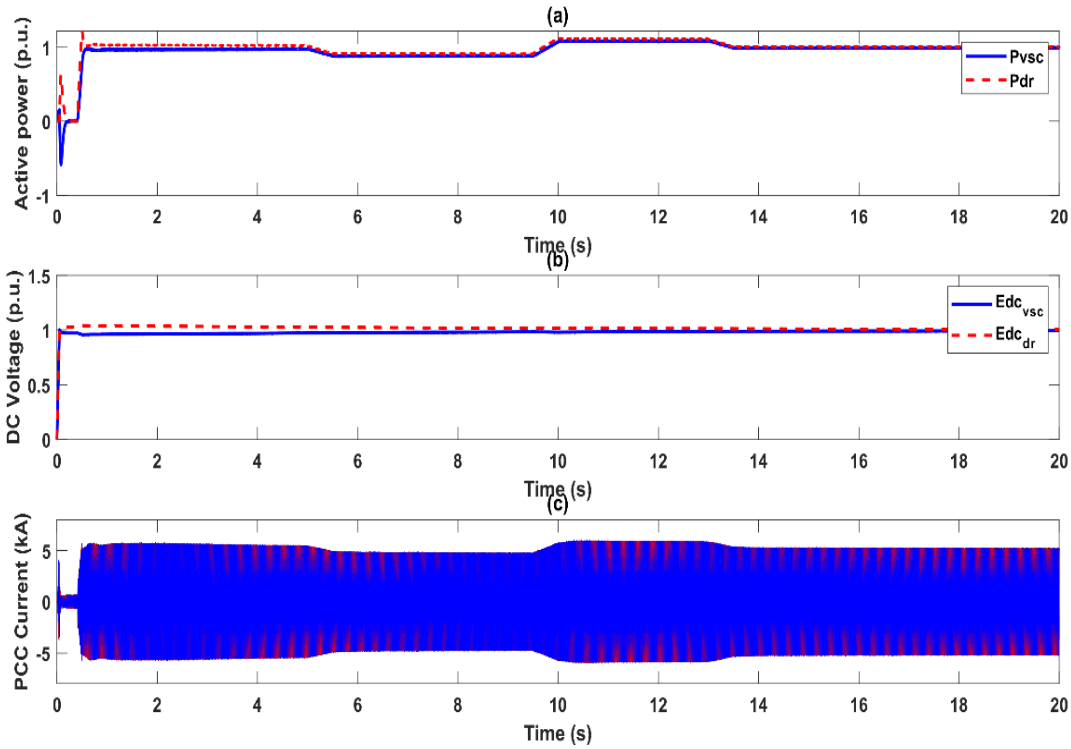

Fig. 3-13 Performance of the hybrid converter when WT functions as a grid-forming converter: (a) Transmitted active power of hybrid converter components, (b) DC-link voltage of hybrid converter components, (c) current at the PCC point

Fig. 3-14 presents the PCC current at the same time to verify the harmonic current controller effects. Fig. 3-14 (a) shows the PCC current when the harmonic compensation is enabled, and its current waveforms show that the signal is free of harmonics. Fig. 3-14 (b) shows the PCC current when the harmonic current compensation is disabled; the current waveforms display high harmonic contents.

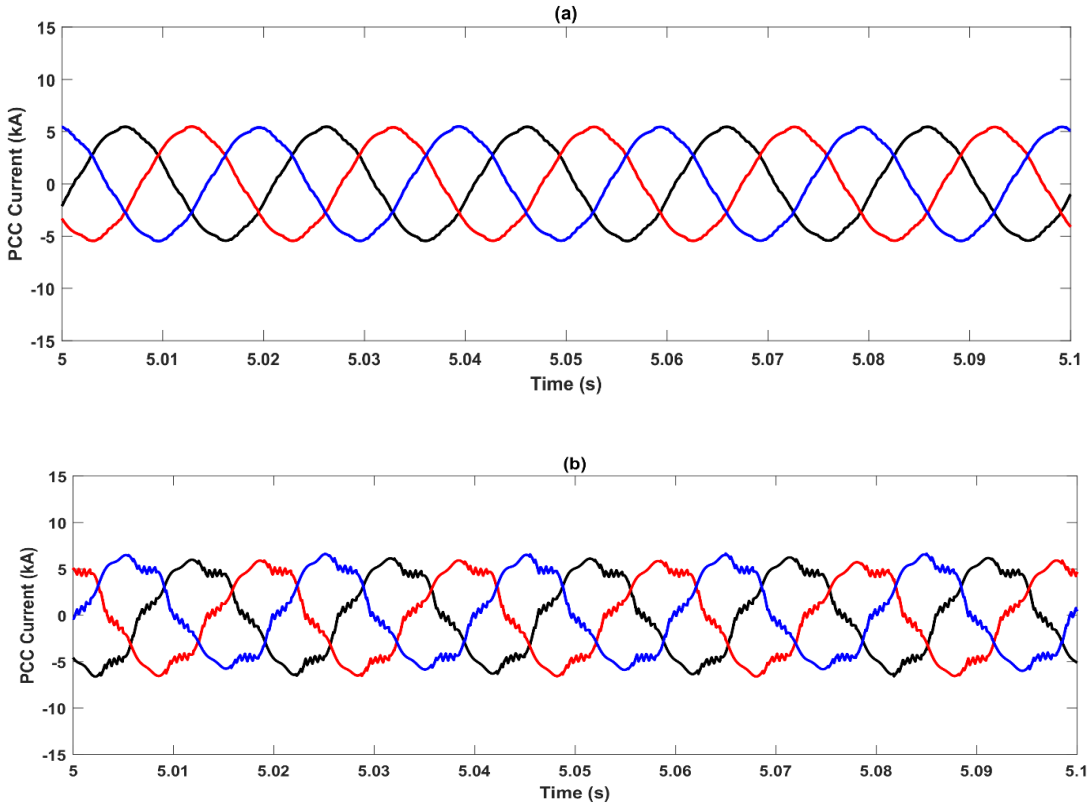

Fig. 3-14 Current waveform at PCC point: (a) PCC current – harmonics compensation operated, (b) PCC current – harmonics compensation disabled

3.5 Summary

This chapter introduced a hybrid converter topology that is based on a series connection between the 6P-DR and VSC. In this configuration, the controllable VSC controller plays an important role in the hybrid converter, including the fundamental voltage and harmonic compensation controls. Two control strategies are described in this chapter: using the hybrid converter as a grid-forming converter and using GSC-WTs as a grid-forming converter. The corresponding control systems were also described in this chapter. An easy-to-tune harmonic compensation controller based on the SRF technique was used in the hybrid converter to cancel the harmonic components produced by the 6P-DR. Simulation results in PSCAD/EMTDC verified

the two control strategies and performance of the harmonic compensation controller.

The hybrid converter topology can combine the highlights of two converter types. In this configuration, the diode rectifier provides a lost cost, small power losses and a small footprint, while the VSC converter gives a control ability to hybrid converter to provide an ancillary service to the offshore side. To address the potential issues provided by diode rectifier like uncontrollable features and harmonic current components, Chapter 4 introduces an advanced power electronic devices Vienna rectifier in the hybrid converter application and will describe the topology, control system and backup services.

Chapter 4 Low Harmonics Hybrid Converter Based on a Vienna Rectifier and VSC Converter Used for Offshore Wind Energy Conversion with backup capability

4.1 Introduction

Chapter 3 discusses and analyzes an enhanced hybrid converter with a 6P-DR and VSC, which is based on the original hybrid converter featuring a 12P-DR and VSC. The improved hybrid converter clarifies the control strategies for offshore wind farms in order to avoid complex transformers and control systems at the offshore site. The proposed hybrid converter used in offshore converter stations offers lower investment and operating costs compared to the existing solutions, which is a cost-effective option for future offshore wind farm connections.

This chapter will discuss the use of the Vienna rectifier as part of the hybrid converter to replace the 6P-DR. The Vienna rectifier was described in Chapter 2. This proposed hybrid converter topology consists of a Vienna rectifier in series with a VSC, which further improves the control capability of the hybrid converter compared to the existing hybrid converter. The Vienna rectifier offers cost advantages over the VSC and MMC due to its reduced number of IGBTs, resulting in lower investment costs. Furthermore, the Vienna rectifier's low harmonic characteristics not only contribute to cost savings in the offshore converter station but also reduce the footprint size by eliminating the need for filters. Additionally, it is worth noting that the VSC can assist the hybrid converter in enhancing current quality. By modifying its control system, the VSC can function as a built-in active power filter, eliminating the need for an external filter, particularly in situations where the IGBTs in the Vienna rectifier fail or are taken

out of service.

The following section presents the control strategy for the hybrid converter. Grid forming control will be applied in the wind farm, and two control modes for the hybrid converter will be introduced: normal operation mode and backup auxiliary mode. The performance of the hybrid converter will be evaluated through simulation studies in PSCAD, covering both steady-state and dynamic response analysis. Furthermore, two additional simulations will be set up to compare the effects of the backup auxiliary mode. At the end, the sizing of the hybrid converter is discussed based on the pervious test analysis and compared to the current converter station.

4.2 Proposed hybrid HVDC system and control system

Fig. 4-1 shows the HVDC system composed of a hybrid converter that is based on a Vienna rectifier and a VSC converter. The onshore converter station uses the VSC converter to regulate the overall DC link voltage of the overall HVDC system. The hybrid converter station uses the hybrid converter, the AC side of the hybrid converter connects with OWF at the PCC point, and the DC side connects with the onshore converter station.

As mentioned previously, the Vienna rectifier series connects with the VSC converter to establish the power flow and meet the demands of the onshore grid via a DC cable. The objectives of the proposed hybrid converter are to provide low harmonics, low cost, and high reliability at offshore converter stations. In addition, the backup ancillary mode provided by the VSC of the hybrid converter can handle the performance if the IGBTs of the Vienna rectifier stop switching because of a fault.

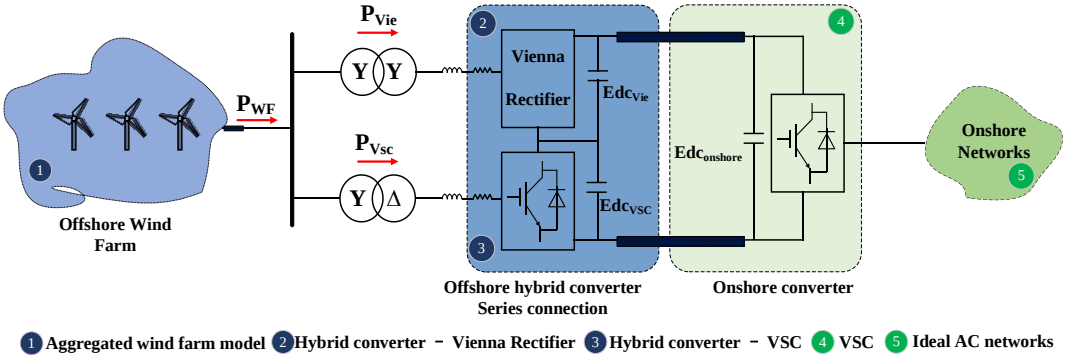

Fig. 4-1 Proposed HVDC system based on hybrid converter

4.2.1 The Operation Mechanism of Vienna Rectifier

a) Basic structure

As reviewed in Chapter 2, the Vienna rectifier has three types of topologies: original Type, I-Type, and T-Type [38]. Fig. 4-2 shows the original type of circuit diagram and equivalent circuit diagram, which can be assumed as a three-phase, three-level, non-regenerative converter. For one phase, only one switching device connects with diodes, which reduces power losses. These three types of Vienna rectifier can be regarded as a diode bridge that connects with switching devices at the middle point.

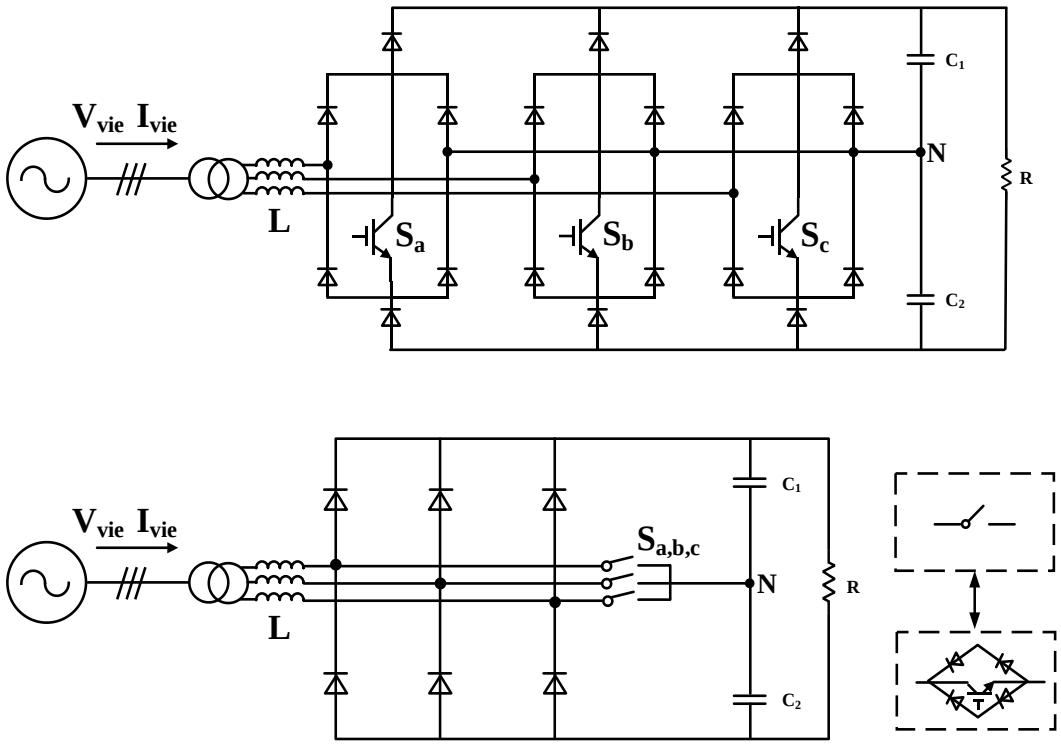

Fig. 4-2 Vienna Rectifier circuit topology and its equivalent circuit

The average diagram of the Vienna rectifier is shown in Fig. 4-3, including the AC-side and DC-side average models. On the AC side, the AC systems are expressed as e_a, e_b, and e_c. The average modelling of the Vienna rectifier system is presented next.

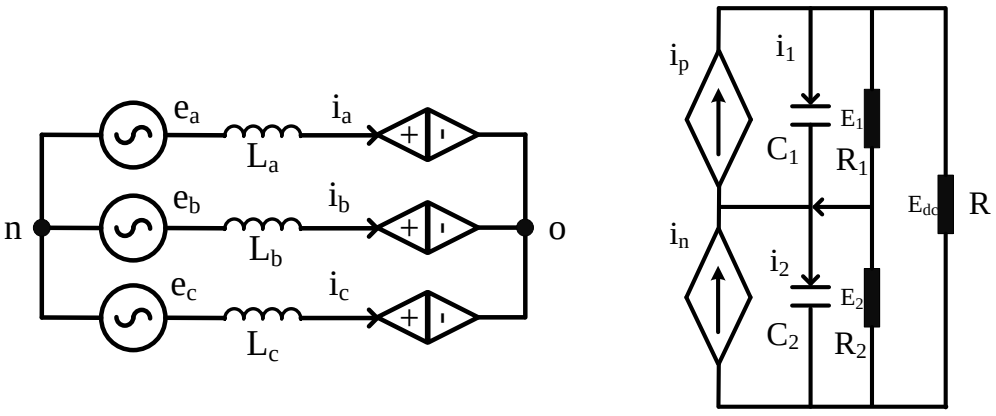

(a) (b)

Fig. 4-3 The average model of Vienna rectifier: (a) AC side, (b) DC side

Applying the Kirchhoff Voltage Law equation [75] in Fig. 4-3 (a), the equation are:

$$\begin{cases} e_a - L\dfrac{i_a}{dt} = \dfrac{E_{dc}}{2} \cdot V_{aref} = u_{ao} + u_{on} \\ e_b - L\dfrac{i_b}{dt} = \dfrac{E_{dc}}{2} \cdot V_{bref} = u_{bo} + u_{on} \\ e_c - L\dfrac{i_c}{dt} = \dfrac{E_{dc}}{2} \cdot V_{cref} = u_{co} + u_{on} \end{cases} \quad (4.1)$$

$$\begin{cases} e_a = Vm\cos\theta \\ e_b = Vm\cos(\theta - \dfrac{2\pi}{3}) \\ e_b = Vm\cos(\theta + \dfrac{2\pi}{3}) \end{cases} \quad (4.2)$$

Where u_{on} is the voltage at common mode and u_{ao}, u_{bo}, and u_{co} are the Vienna rectifier terminal voltages. Equation (4.2) defines the grid phase voltages e_a, e_b, and e_c, which are balanced. V_m and Θ represent the amplitude and phase angles of the grid voltage. Because this type of rectifier is current forced commutated, the voltage poles of rectifiers u_a, u_b, and u_c are defined not only by the controlled switching state but also by the polarity of the AC phase current of the relevant instance.

In the average DC-side model, E_{dc} as the output voltage and ΔE as the voltage unbalance are defined as the sum and difference of the output voltage on the capacitors E_1 and E_2, respectively. The voltage unbalanced factor k [75] can be expressed as

$$E_{dc} = E_1 + E_2 \quad (4.3)$$

$$\Delta E = E_1 - E_2 \quad (4.4)$$

$$k = \left(\frac{E_1 - E_2}{E_1 + E_2}\right) \quad (4.5)$$

The switching voltage after transformation can be obtained as:

$$\begin{cases} u_{ao} = \frac{E_{dc}}{2}[sgn(i_a) + \frac{\Delta E}{E_{dc}}](1 - S_a) \\ u_{bo} = \frac{E_{dc}}{2}[sgn(i_b) + \frac{\Delta E}{E_{dc}}](1 - S_b) \\ u_{co} = \frac{E_{dc}}{2}[sgn(i_c) + \frac{\Delta E}{E_{dc}}](1 - S_c) \end{cases} \quad (4.6)$$

sgn () is the sign function, and the switching function S_x is defined as:

$$sgn(i_x) = \begin{cases} 1 \ if i_x \geq 0 \\ -1 \ if i_x < 0 \end{cases} \quad (4.7)$$

$$S_x = \begin{cases} 1 \ if S_x \text{ is turn on} \\ 0 \ if S_x \text{ is turn off} \end{cases} \quad (4.8)$$

Based on the above equation,

$$\begin{cases} (V_{a\_ref} + u_o) = [sgn(i_a) + k](1 - S_a) \\ (V_{b\_ref} + u_o) = [sgn(i_b) + k](1 - S_b) \\ (V_{c\_ref} + u_o) = [sgn(i_c) + k](1 - S_c) \end{cases} \quad (4.9)$$

Where V_{abc_ref} is the sinusoidal component, and u_o is the zero-sequence component. In addition, the relationship between u_{on} and u_o can be calculated as

$$u_0 = -u_{on}\frac{2}{E_{dc}} \quad (4.10)$$

Fig. 4-3 (b) shows the average model at the DC side, i_p and i_n represents the upper and lower diode currents. According to Kirchhoff Current Law (KCL), the state model and the current trough diode are shown below.

$$\begin{cases} i_1 = C_1 \dfrac{dE_1}{dt} = i_p - (\dfrac{E_{dc}}{R} + \dfrac{E_1}{R_1}) \\ i_2 = C_2 \dfrac{dE_2}{dt} = i_n - (\dfrac{E_{dc}}{R} + \dfrac{E_2}{R_2}) \end{cases} \tag{4.11}$$

$$\begin{cases} i_p = i_{Dap} + i_{Dbp} + i_{Dcp} \\ i_n = i_{Dan} + i_{Dbn} + i_{Dcn} \end{cases} \tag{4.12}$$

$$i_{Dxp} = \begin{cases} (1 - S_x) i_x & (i_x \geq 0) \\ 0 & (i_x < 0) \end{cases} \tag{4.13}$$

$$i_{Dxn} = \begin{cases} 0 & (i_x \geq 0) \\ -(1 - S_x) i_x & (i_x < 0) \end{cases} \tag{4.14}$$

Combine the Equation (4.9),(4.13) and (4.14), so,

$$\begin{cases} i_p = i_{Dap} + i_{Dbp} + i_{Dcp} = \sum\limits_{x=a,b,c} \dfrac{1}{2}[1 + sgn(i_x)](1 - S_x) i_x \\ i_n = i_{Dan} + i_{Dbn} + i_{Dcn} = \sum\limits_{x=a,b,c} \dfrac{1}{2}[1 - sgn(i_x)](1 - S_x)(-i_x) \end{cases} \tag{4.15}$$

In addition, the voltage unbalance ΔE is obtained as Equation (4.16) for neutral-point voltage.

$$C \frac{d\Delta V}{dt} = i_p - i_n + I_o = \sum_{x=a,b,c} \frac{i_x}{k + sgn(i_x)} (V_{x\_ref} + u_o) \tag{4.16}$$

Where I_o is the current difference between the R_1 and R_2.

Due to the unity power factor, which is a Vienna rectifier advantage, this study uses the Vienna rectifier as part of the hybrid converter in the offshore converter station. The instantaneous input current can be expressed as

$$\begin{cases} i_a = I_m cos\theta \\ i_b = I_m \cos(\theta - \frac{2\pi}{3}) \\ i_b = I_m \cos(\theta + \frac{2\pi}{3}) \end{cases} \quad (4.17)$$

b) Control system and PWM modulation

As a three-phase converter, the Vienna rectifier uses the rotating reference frame synchronized to the input AC voltage (AC grid or infinite bus) by a phase-locked-loop (PLL) [76]. In a steady state, the voltages and currents are DC signals in the d-q reference frame. The phase voltage and current are expressed as

$$v_{abc} = Ri_{abc} + L\frac{di_{abc}}{dt} + v_{vie\_conv} \quad (4.18)$$

Where v_{dc} and i_{abc} are AC voltage and currents, respectively; v_{vie_conv} is the Vienna rectifier converter voltage; and R and L are the resistance and input inductance between the converter and AC side, respectively. The voltage equation in the d-q synchronous reference frame is:

$$v_{d\_conv} = v_{vie\_d} - Ri_{vie\_d} - L\frac{di_{vie\_d}}{dt} + \omega_g L i_{vie\_q} \quad (4.19)$$

$$v_{q\_conv} = v_{vie\_q} - Ri_{vie\_q} - L\frac{di_{vie\_q}}{dt} - \omega_g L i_{vie\_d} \quad (4.20)$$

Where the v_{vie_d}, v_{vie_q}, i_{vie_d} and i_{vie_q} are the d-q components of the Vienna rectifier voltage and current, and ω_g is the frequency of the offshore grid. In this configuration, the active power and reactive power are controlled by i_d and i_q, the direct and quadrature components, respectively. For a unity power factor, the i_q reference is set to 0 in the q-axis control, and the DC voltage is regulated by varying the i_d in the d-axis control[37, 75]. The overall control system is shown in Fig. 4-4. The equation

corresponding to the DC side is expressed as

$$I_{dc} = C\frac{dV_{dc}}{dt} + I_L \tag{4.21}$$

The power exchanged between the AC and DC sides is

$$P = \frac{3}{2}(v_d i_d + v_q i_q) = V_{dc} I_{dc} \tag{4.22}$$

The controllers are simple PI. Combining the PI controllers, the equation is

$$R(s) = K_p + \frac{K_i}{s} = K_p(\frac{1 + T_i s}{T_i s}) \tag{4.23}$$

From Fig. 4-4. and equations (4.19) and (4.20), the Vienna rectifier d and q components of the converter voltages are cross-coupled. The system input reference can be split into two components: one obtained by the converter, while the other one is a feedforward term to eliminate cross-coupling. When the compensation terms are used for decoupling, the system input from the converter can be written as

$$v'_{d\_conv} = (i_d - i_{dref})(K_p + \frac{K_i}{s}) + \omega_g L i_{vie\_q} + V_{vie\_d} \tag{4.24}$$

$$v'_{q\_conv} = (i_q - i_{qref})(K_p + \frac{K_i}{s}) - \omega_g L i_{vie\_q} + V_{vie\_q} \tag{4.25}$$

As shown in Fig. 4-4., the cross-compensation part is applied in the inner current loop in the Vienna control system to cancel the cross-coupling terms. In addition, the control system can control the d-axis and q-axis independently. In q-axis control, the q current reference $i^*_{vie\_q}$ is set to 0 to ensure the Vienna rectifier operates as a unity power factor converter. Therefore, the d-axis control is used for further analysis. According to Equation (4.24), using the Laplace transformation, the equation can be written as

$$si_d(s) = (-\frac{R}{L})i_d(s) + (\frac{1}{L})v_{d\_conv}(s) \tag{4.26}$$

$$i_d(s) = (\frac{1}{sL + R})V_{d\_conv(s)} \tag{4.27}$$

The transfer function is,

$$G(s) = (\frac{1}{R})(\frac{1}{1 + s\tau}) \tag{4.28}$$

Where the time constant τ=L ／R, the DC voltage controller as an outer loop used in the d-axis loop to control the DC voltage between the DC-link capacitance of the Vienna rectifier station in the hybrid converter. The control signals through the PI controller can be expressed as:

$$i_{dref}(s) = (v_{dc\_vieref}(s) - v_{dc\_vie}(s))(K_p + \frac{K_i}{s}) \tag{4.29}$$

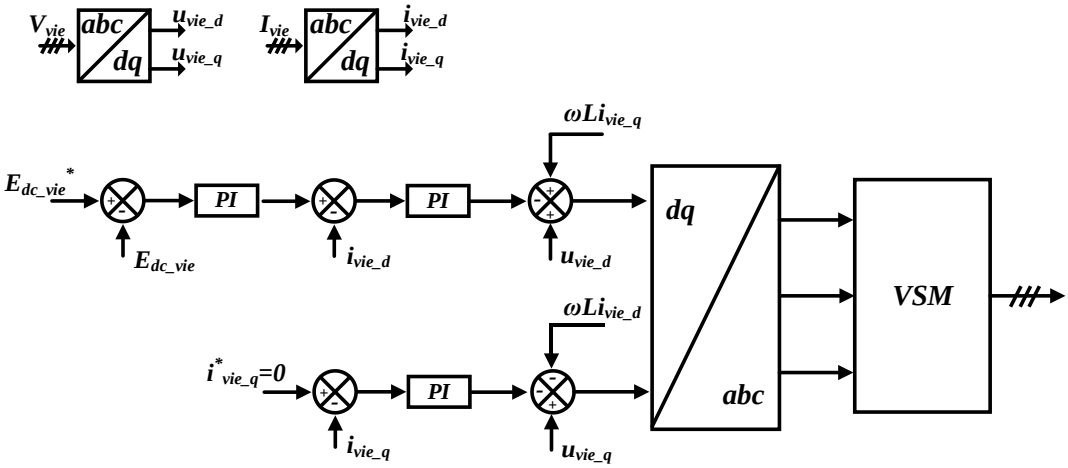

Fig. 4-4 Control system of Vienna rectifier

Additionally, the Vienna rectifier is used as a unity power factor converter, and it has limited capability has limited capability for a reactive power factor is ±30°. Without the limitation, the duty cycle of the PWM modulation can be expressed as:

$$DC_x = \begin{cases} 1 - abs(m_x) & \text{if } sgn(i_x) = sgn(m_x) \\ 1 & \text{if } \mathrm{sgn}(i_x) \neq sgn(m_x) \end{cases} \quad (4.30)$$

Where $x = a,b,c$ that represents phase A,B,C, the modulation index m_x equal to $2v_{conv\_x}/E_{dc}$ is the ratio between the converter voltage and half DC link voltage. i_x is the output current and *sgn ()* is the sign function. For example, if the signs of current and voltage is a different direction, the output voltage is clamped to the neutral point and vice versa.

c) Simulation results of Vienna rectifier connected with load

To explain the performance of the Vienna rectifier, PSCAD simulation results show the Vienna rectifier connected with a pure resistive load, as illustrated in Fig. 4-5. The parameters of the AC system, Vienna rectifier, and load are given in Table 4-1. Table 4-1 System parameters

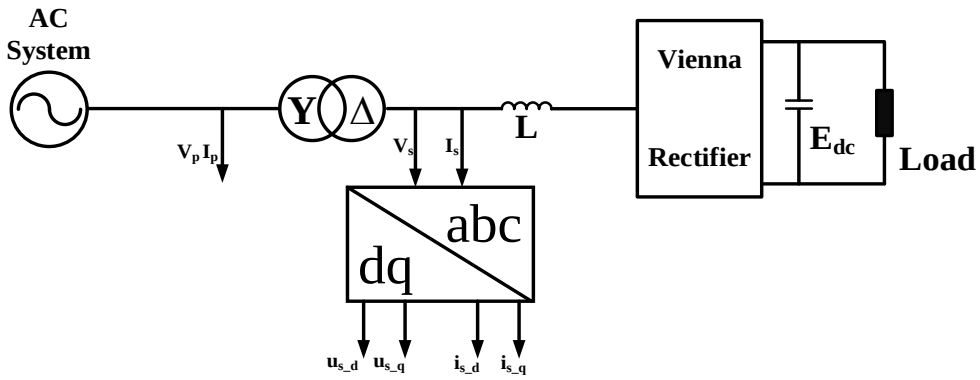

Fig. 4-5 Diagram of Vienna rectifier connects with load

Table 4-1 System parameters

Parameters		Nominal value
AC System	Voltage magnitude	67 kV
	Frequency	50 Hz
Y/D Transformer	Voltage Ratio	67 kV/67 kV
	Leakage Reactance	0.1 p.u.
Vienna Rectifier	Capacitance	600 μF
	Inductance	5.2 mH
Load	Pure Resistance	100 Ω

For a Vienna rectifier design to the control DC voltage and *iq* current, Fig. 4-6 shows the performance, including the DC link voltage of load and q current to verify the control system effects. The red line of the figure is the reference value, and the blue line is the measured value. The DC link voltage is controlled at 100 kV (1 p.u.), and the q current is controlled at 0 to provide a unity power factor.

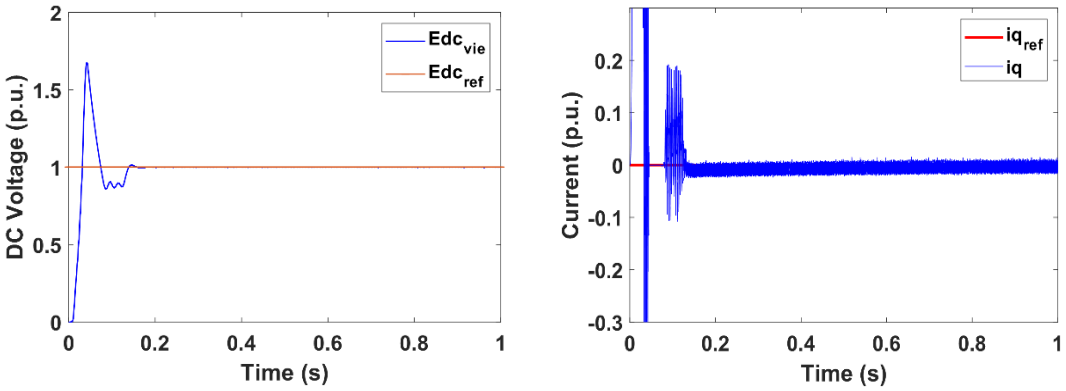

(a) (b)

Fig. 4-6 Performance of Vienna rectifier connects with load: (a) DC link voltage, (b) i_q current

Fig. 4-7 displays the current and voltage at the primary and secondary sides of the transformer. Due to the characteristics of the Vienna rectifier, the current has few harmonics. In addition, the voltage and current in one cycle are illustrated in Fig. 4-8.

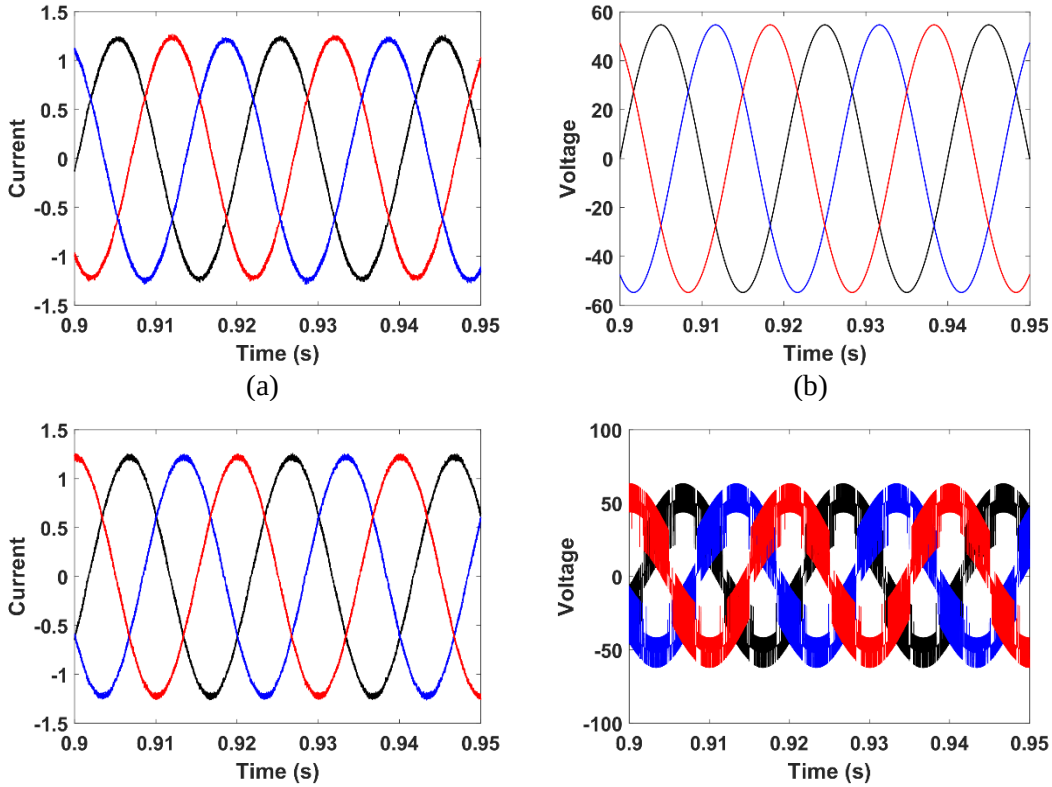

Fig. 4-7 Current at primary side and secondary side of transformer: (a) Current at primary side, (b) Voltage at primary side, (c) Current at secondary side, (d) Voltage at secondary side

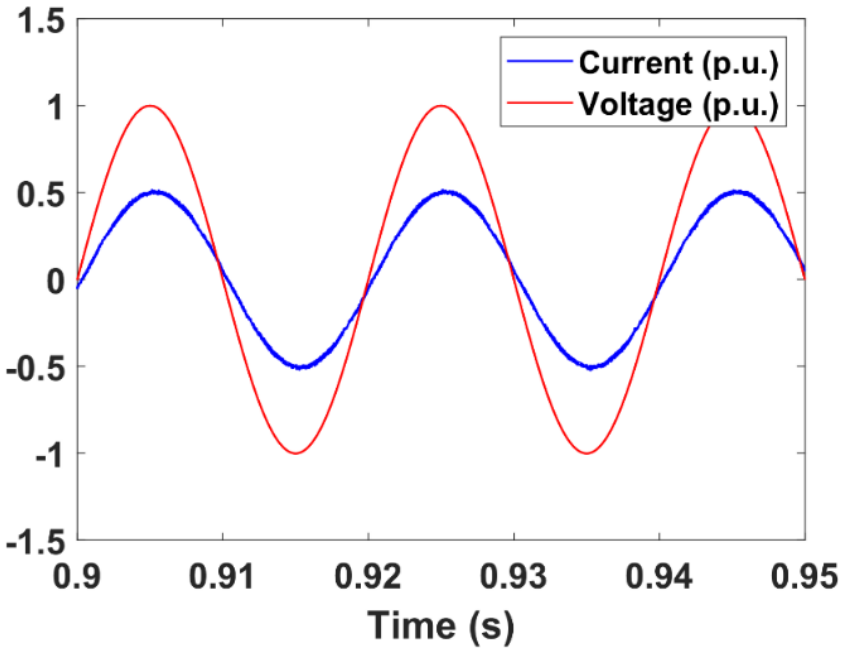

Fig. 4-8 Voltage and current of Vienna rectifier

4.2.2 The Operation Mechanism of VSC converter

Fig. 4-9 shows the hybrid converter topology based on the Vienna rectifier and VSC converter. According to the previous discussion, the Vienna rectifier control system is designed to control the DC voltage and q current (i_q) in the hybrid topology converter. The VSC converter of the hybrid converter has the ability to control the power magnitude at the PCC point to support an offshore HVDC system.

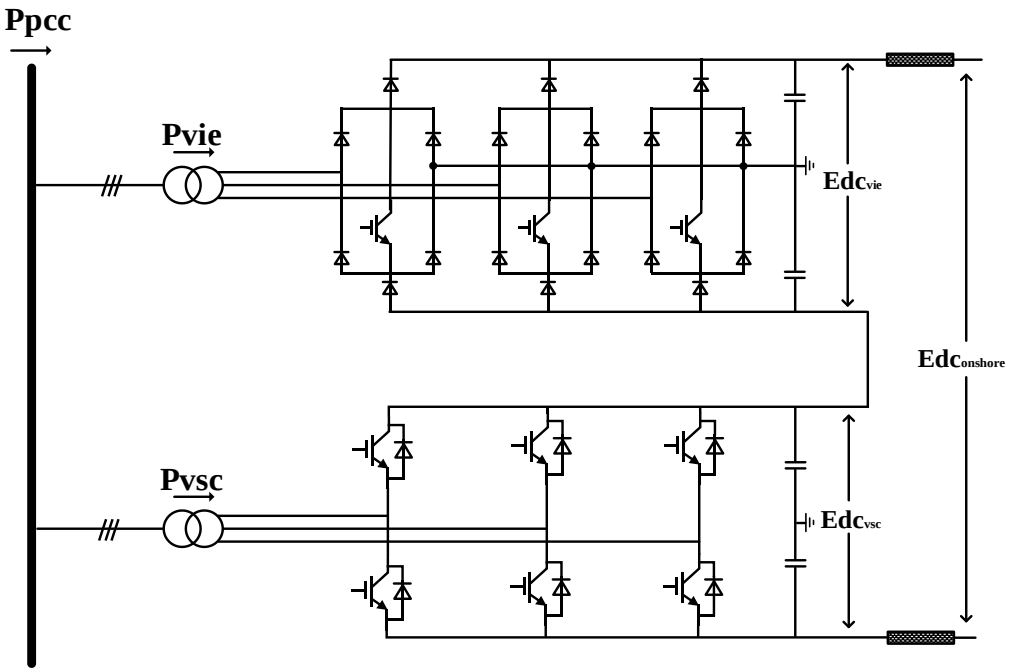

Fig. 4-9 Hybrid converter based on Vienna rectifier and VSC converter

a) First harmonics control system

Fig. 4-10 displays the control system of the hybrid VSC converter, which includes the inner current control loop and outer power control loop. The inner current controller is widely used in VSC control to provide a fast response and ensure that the converter does not operate in an overload state. In the current loop, the cross-coupling term in the inner current relationship is:

$$v_{sd} = u_d - \omega L i_q + v_d \tag{4.31}$$

$$v_{sq} = u_q - \omega L i_d + v_q \tag{4.32}$$

The converter side in the *dq* frame can be calculated as:

$$\frac{di_{sd}}{dt} = -i_{sd}\frac{R}{L} + \omega i_{sq} + \frac{1}{L}(v_{sd} - v_{cd}) \tag{4.33}$$

$$\frac{di_{sq}}{dt} = -i_{sq}\frac{R}{L} + \omega i_{sd} + \frac{1}{L}(v_{sd} - v_{cd}) \tag{4.34}$$

Combined the above equation, then:

$$\frac{d}{dt}\begin{bmatrix} isd \\ isq \end{bmatrix} = \begin{bmatrix} \frac{-R}{L} & 0 \\ 0 & \frac{-R}{L} \end{bmatrix}\begin{bmatrix} i_{sd} \\ i_{sq} \end{bmatrix} + \begin{bmatrix} \frac{1}{L} & 0 \\ 0 & \frac{1}{L} \end{bmatrix}\begin{bmatrix} u_d \\ u_q \end{bmatrix} \tag{4.35}$$

Where u_d and u_q are obtained by the PI controller of the inner current control loop and can regulate the *dq* current as defined below:

$$u_d = K_p(i^*_d - i_d) + K_i \int (i_d - i_d)dt \tag{4.36}$$

$$u_q = K_p(i^*_q - i_q) + K_i \int (i_q - i_q)dt \tag{4.37}$$

Where K_p and K_i are the proportional and integral gains of current controller.

A Laplace transmission of the inner control loop's relationship, the function results as follows:

$$G(s) = \frac{\frac{K_p}{L}\left(s + \frac{K_i}{K_p}\right)}{s^2 + \frac{(R + K_p)}{L}s + \frac{K_i}{L}} \tag{4.38}$$

According to equation (4.38), the proportional and integral gain can be calculated as follows:

$$K_p = 2\zeta\omega L - R \tag{4.39}$$

$$K_i = \omega^2 L \tag{4.40}$$

Where ω is the frequency, and ζ is the damping factor. The inner current loop is illustrated in the Fig. 4-10

The reference value controlled by the inner current control loop is applied by the outer control loop. The principal outer controllers are the power controller, DC voltage controller, and AC voltage controller. The choice of the outer controller depends on the application. In the hybrid converter, the VSC converter uses the power controller to control the PCC power magnitude if the hybrid converter operation is in the normal mode. If the Vienna rectifier of the hybrid converter has a fault caused by faulty IGBTs, the VSC uses the DC voltage controller to regulate the DC voltage.

The power equation of the VSC controller based on *dq* current can be calculated as

$$p(t) = \frac{3}{2}[vd(t)id(t) + vq(t)iq(t)] \tag{4.41}$$

$$p(t) = \frac{3}{2}[-vd(t)iq(t) + vq(t)id(t)] \tag{4.42}$$

The u_d and u_q are the *dq* voltage at the PCC point; u_q equals zero if the system is in a balanced steady state operation, and the reference value of *dq* current is

$$i^*_d = \frac{2P^*}{3v_d} \tag{4.43}$$

$$i^*_q = -\frac{2Q^*}{3v_d} \tag{4.44}$$

When the outer controller is selected to DC voltage controller, the id current fed to the inner current loop depends on the error in the comparison of the reference value and measured value. The relationship in mathematics is as follows:

$$i^*_d = K_p(E^*_{dc} - E_{dc}) + K_i(E^*_{dc} - E_{dc})dt \quad (4.45)$$

The diagram of the outer controller is shown in Fig. 4-10.

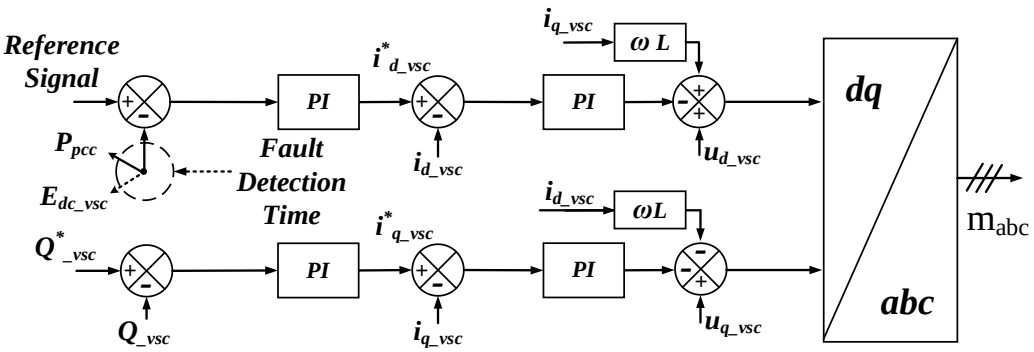

Fig. 4-10 Control system of hybrid-VSC converter

b) Harmonics compensation control system

The harmonic current compensation controller is the key component when the backup ancillary mode operates because harmonic currents are produced by a Vienna rectifier switching fault. Using the same technique as in a hybrid converter where the 6P-DR series connects with the VSC, the SRF technique is used to detect the harmonic current and cancel out it at the PCC point.

The SRF technique rotates times dq synchronous frame at an expected frequency that is equal to the selected harmonic current [77, 78]. Fig. 4-11 shows the harmonic current compensation controller diagram using the SRF technique. The h represents the rotation frequency. The selected harmonic current is detected as a DC signal and the rest of the harmonics are AC signals. The LPF aims to cancel all disturbances from the non-detected harmonic AC signal components. Then, the filtered signals are able to be compared and tuned by the PI controller. Finally, the tuned signal feeds to *dq* to the *abc* transformer rotated by a selected frequency.

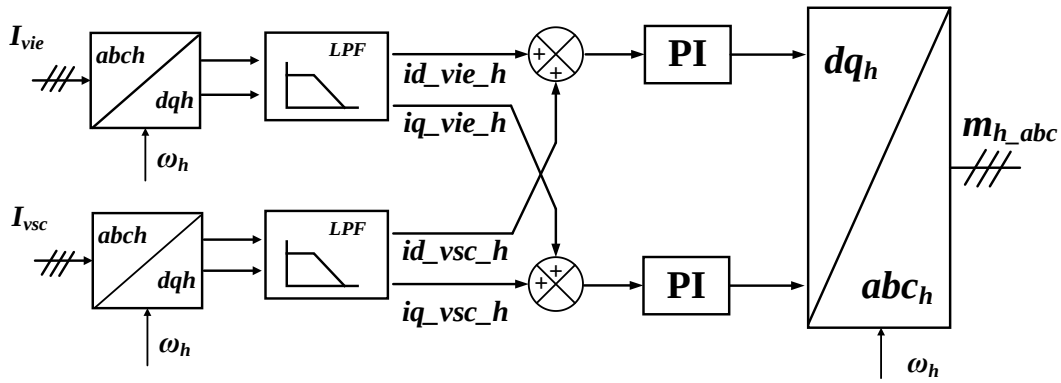

Fig. 4-11 Harmonics compensation controller used SRF-Technique

4.3 The operation modes for hybrid-HVDC system

4.3.1 Normal operation Mode

Fig. 4-12 shows the overall control system of an offshore hybrid converter station. As described before, because the Vienna rectifier has good performance with low harmonic currents and good controllability, the Vienna rectifier controls its DC link voltage. In the meantime, the VSC of the hybrid control system controls the power magnitude at the PCC point to support offshore wind farms. The offshore wind farm model uses an aggregated model operated as a grid-forming converter to support the AC voltage and generate power to the PCC point, which is controlled by a distributed frequency PLL controller.

2 ***Hybrid converter – Vienna Rectifier control system***

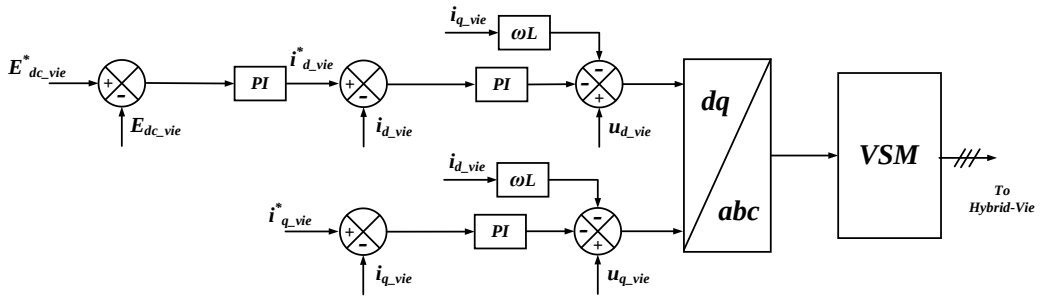

3 ***Hybrid converter – VSC control system and its back-up controller***

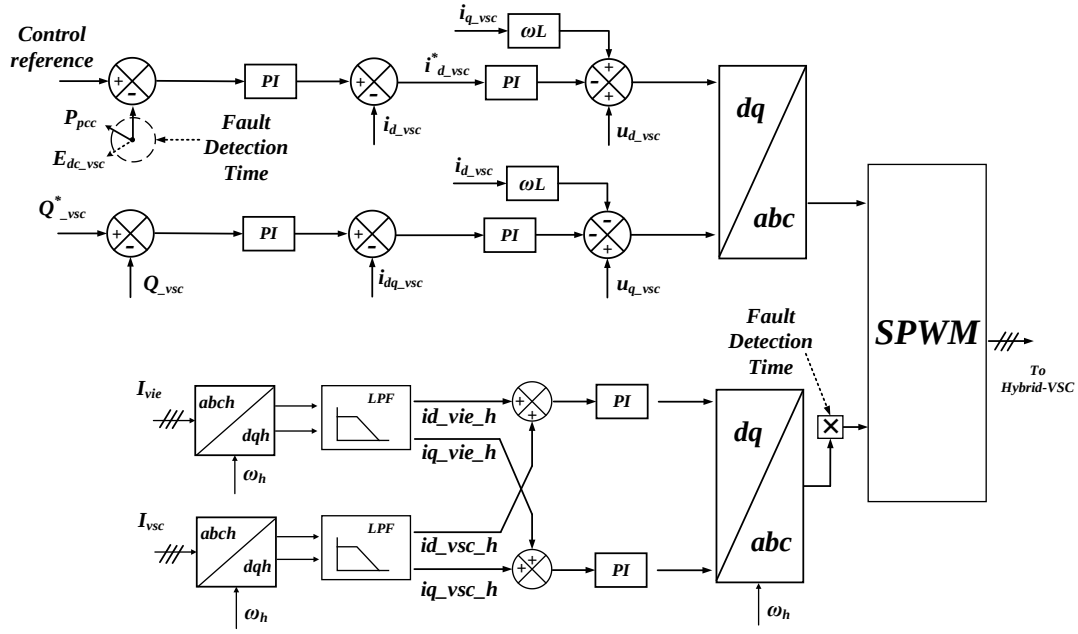

Fig. 4-12 Overall control system diagram of hybrid converter

The onshore converter station uses the VSC converter to control the DC link voltage of the overall HVDC system, Edc_{hvdc}. The Vienna rectifier controls its DC link voltage, $Edc_{vie.}$ Additionally, the VSC DC link voltage Edc_{vsc} is the rest of the overall DC link voltage. The relationship between the offshore station and the onshore converter station is:

$$Edc_{vie} + Edc_{vsc} = Edc_{hvdc} \tag{4.46}$$

The Vienna rectifier functions as a three phase, three level booster converter, and the behaviour is the same as a VSC converter. The Vienna rectifier and VSC converter can be assumed as controlled voltage sources. Fig. 4-13 shows the equivalent circuit of the DC side. The Vienna rectifier series connects with VSC and connects to the onshore source. The DC current (I_{dc}) flows in the mesh. The transmitted power of each component is given below:

$$P_{pcc} = P_{vie} + P_{vsc} \tag{4.47}$$

$$P_{vie} = Edc_{vie} \times I_{dc} \tag{4.48}$$

$$P_{vsc} = Edc_{vsc} \times I_{dc} \tag{4.49}$$

Combining the above equations, the relationship between the active power and DC current and voltage is calculated as below:

$$\begin{aligned} P_{pcc} &= Edc_{vie} I_{dc} + Edc_{vsc} I_{dc} \\ &= (Edc_{vie} + Edc_{vsc}) I_{dc} \\ &= (Edc_{vie} + (Edc_{hvdc} - Edc_{vsc}) I_{dc} \end{aligned} \tag{4.50}$$

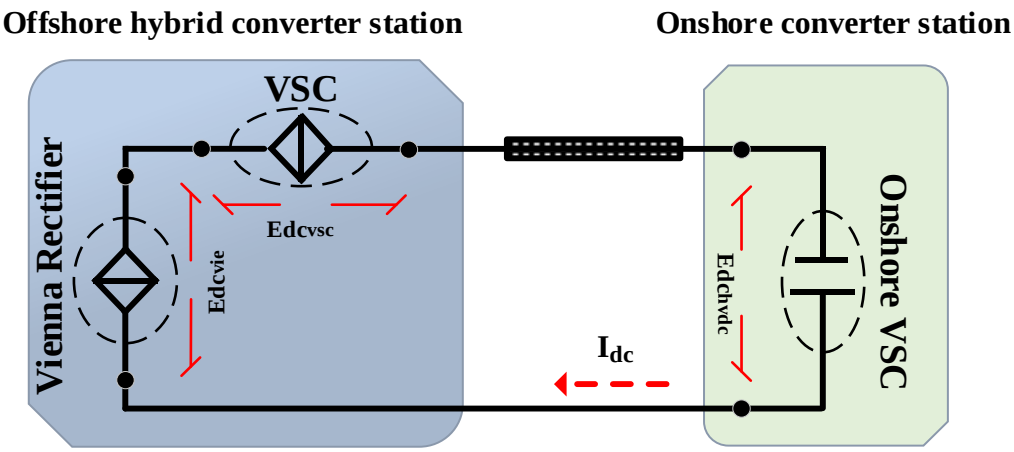

Fig. 4-13 Equivalent DC side circuit of the HVDC link based on the Offshore hybrid converter

In this configuration, the transmitted power by the hybrid converter components is proportional to its DC link voltage. The Vienna rectifier is responsible for the DC voltage control to assign the transmitted power from OWF. In addition, the VSC of the hybrid converter controls the magnitude of power at the PCC point and can provide backup ancillary services if the IGBTs of the Vienna rectifier are faulty.

4.3.2 Backup auxiliary Mode

To improve the reliability of the proposed HVDC system, the hybrid converter based on the Vienna rectifier and VSC has a built-in backup ancillary services mode, which is used to handle situations when IGBTs of the Vienna rectifier are faulty. In this situation, the non-IGBT Vienna rectifier will be operated as 6P-DR and be unable to provide control. To meet this situation, the VSC of the hybrid converter will change the control target from PCC power magnitude to the DC link voltage of VSC, which plays the same role as a Vienna rectifier in the normal operation mode for regulating the DC voltage. The VSC command changes not only affect the Vienna rectifier but also maintain the system stability during faults.

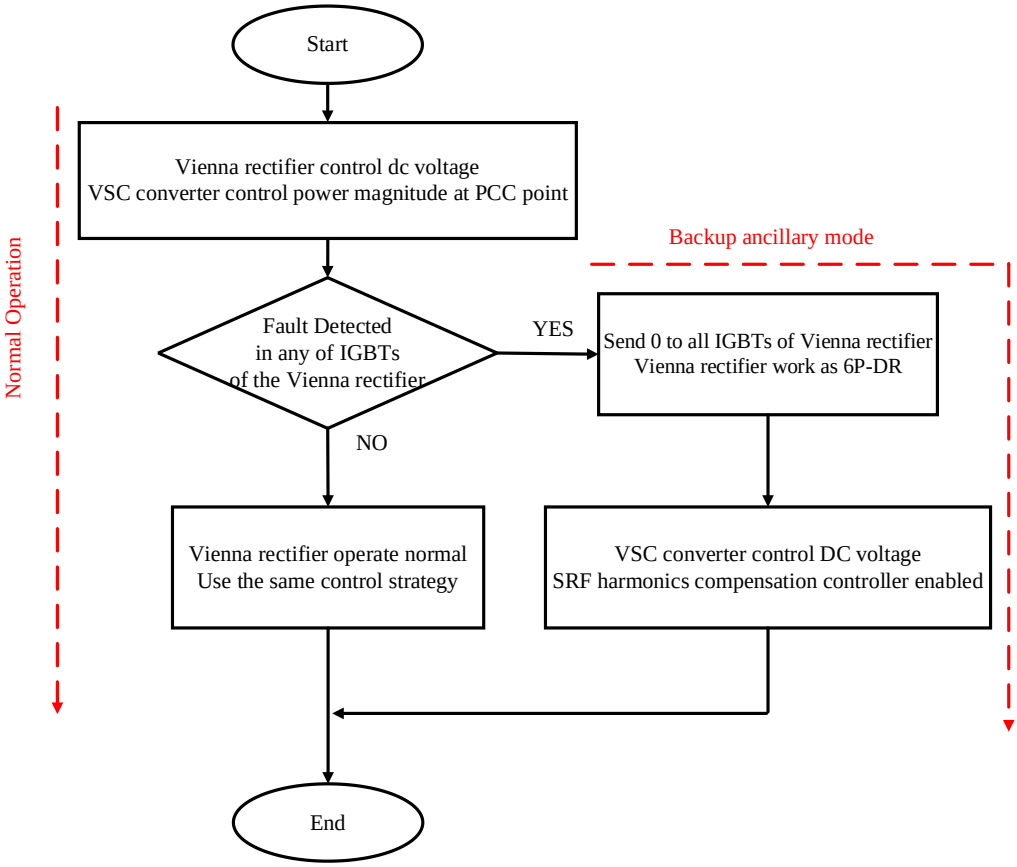

Fig. 4-14 Flow chart of hybrid converter operation

Fig. 4-14 shows the flow chart of operation, including the normal operation mode and backup ancillary mode. When the system operates in a normal mode, the Vienna rectifier controls the DC voltage, and VSC controls the power magnitude and disables the harmonic compensation controller. When any IGBT of the Vienna rectifier is faulty, the 0 signal will be sent to all IGBT ports to maintain the IGBT in an open state. At the same time, the VSC converter no longer needs to control the power magnitude. The DC voltage assignment depends on the VSC of the hybrid converter. This action not only maintains the power-DC voltage ratio but also regulates the hybrid HVDC system's operation stability.

In addition to DC voltage regulation, the VSC of the hybrid converter needs to function as an active power filter because the non-IGBT Vienna rectifier will operate as 6P-DR. The SRF technique is used to detect the harmonic current produced by non-

IGBT Vienna rectifier, which is then suppressed by VSC.

The backup ancillary mode aims to ensure that the hybrid HVDC system operates in a stable manner and that the PCC current maintains the expected sinewave over the transmission devices' lifetimes. This backup ancillary mode prevents the complete offshore system from being shut down in the event of an internal error in the converter.

4.4 Simulation results

The proposed hybrid HVDC system shown in Fig. 4-1 was built in the PSCAD/EMTDC environment to test the system performance for different test cases, e.g., the basic performance, input active power steps, DC voltage control, and operation in basic ancillary mode. Based on the analysis of the above test results, a novel converter configuration was proposed and simulated to explore the sizing of the hybrid converter. Finally, the controllability, cost, footprint and filter size comparisons of offshore converter stations are discussed based on public data.

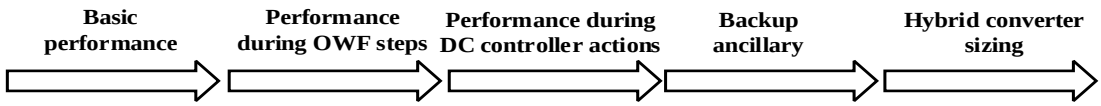

Fig. 4-15 Simulation tests

The offshore wind farm uses the aggregated wind model with an initial DC voltage source. The hybrid converter components, including the Vienna rectifier and VSC converter use the detailed model. These PSCAD models are displayed in Appendix B. The timestep of those tests is 20 *us*.

4.4.1 Basic performance

The control systems shown in Fig. 4-12 are used for testing the performance of

the hybrid converter used in offshore HVDC system under the PSCAD environment. Table 4-2 shows the system parameters used for offshore hybrid converter system. In addition, Table 4-3 displays the control action during the simulation process.

Table 4-2 system parameters of the hybrid HVDC system

Parameters		Nominal Value
Wind farm Aggregated model	Power rating	400 MW
	Transformer voltage ratio	0.69 kV / 66 kV
Onshore converter station	DC voltage rating	640 kV
Vienna rectifier Of Offshore Hybrid Converter	Power rating P_{Tvie}	200 MW
	DC voltage rating	320 kV
	Transformer voltage ratio	66 kV / 230 kV
	Inductance L_{vie}	0.15 p.u.
	Resistance R_{vie}	0.0015 p.u.
2-Level VSC Of Offshore Hybrid Converter	Power rating P_{Tvsc}	200 MW
	DC voltage rating	320 kV
	Transformer voltage ratio	66 kV / 230 kV
	Inductance L_{vsc}	0.15 p.u.
	Resistance R_{vsc}	0.0015 p.u.

Table 4-3 Control actions of simulation

Time	Event
0 – 10s	Vienna Rectifier controls its DC link voltage as 0.5 p.u.
10 – 10.5s	OWF input active power decreased from 1.0 p.u. to 0.9 p.u.
14 – 14.5s	OWF input active power increased from 0.9 p.u. to 1.1 p.u.
18 – 18.5s	OWF input active power decreased from 1.1 p.u. to 1.0 p.u.
22 – 22.1s	Vienna Rectifier controls its DC link voltage increased from 0.5 p.u. to 0.525 p.u.
26 – 26.1s	Vienna Rectifier controls its DC link voltage decreased from 0.525 p.u. to 0.50 p.u.
30 – 30.1s	Vienna Rectifier controls its DC link voltage decreased from 0.5 p.u. to 0.475 p.u.
34 – 34.1s	Vienna Rectifier controls its DC link voltage increased from 0.475 p.u. to 0.5 p.u.

Fig. 4-16 shows the active power, DC link and current of the hybrid converter. The Vienna rectifier controls its DC link voltage at 320 kV (0.5 p.u of HVDC system DC link voltage)., and OWF input active power is 400 MW (1 p.u.) until 10s. Then, the OWF control output active power at a different level from 10 s to 20 s period to test the performance when the power change and the DC voltage is controlled to test different magnitudes used to test the DC voltage controller from 20 s to 35 s. Finally, the system control strategies go back to the initial settings. Fig. 4-16 (a) and (b) show the hybrid converter's active power and AC voltage. The voltage and current at the PCC point are illustrated in Fig. 4-16 (c) and (d). The current flowing into the hybrid-

VSC and hybrid Vienna rectifier are displayed in Fig. 4-16 (e) and (f), respectively.

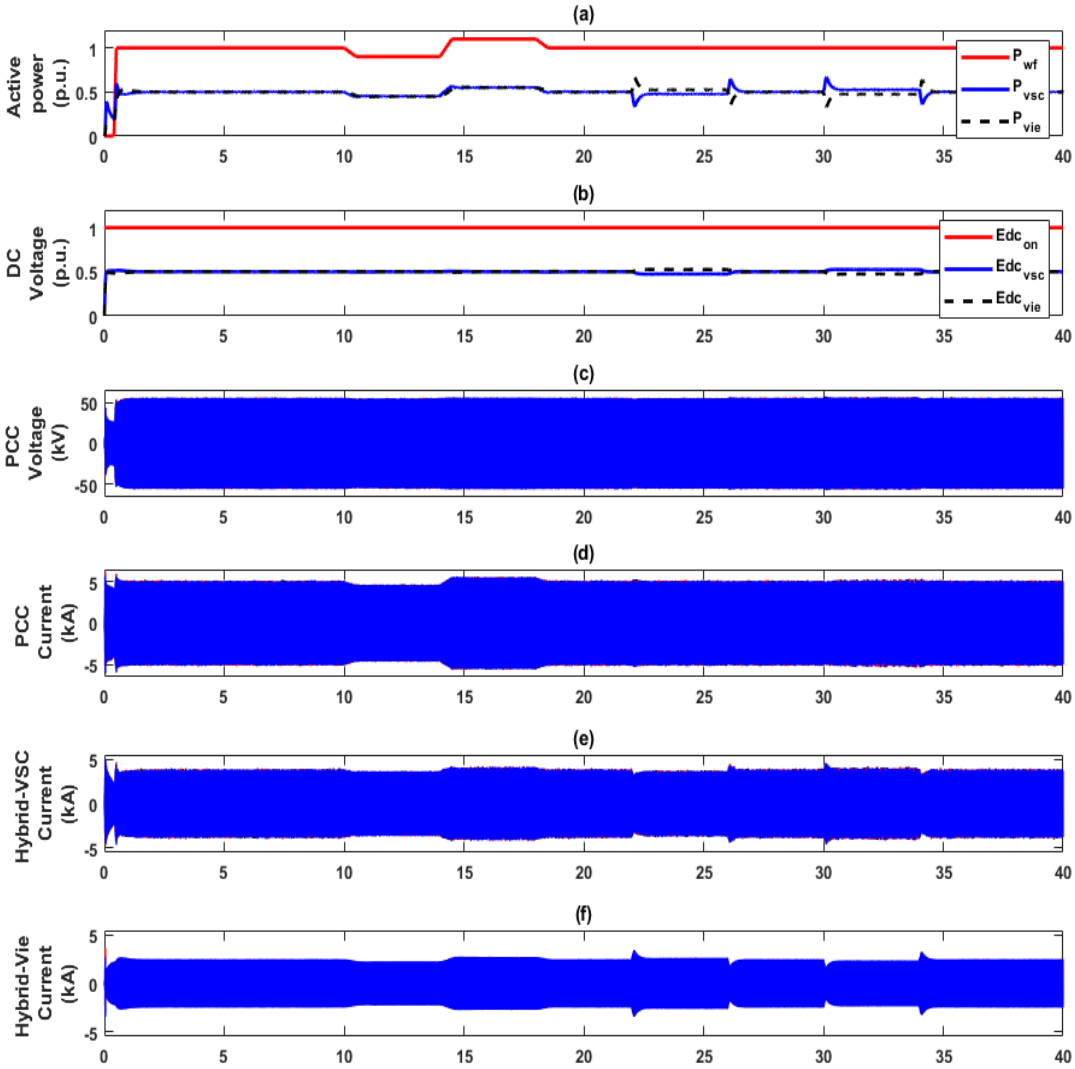

Fig. 4-16 Performance of proposed hybrid HVDC system: (a). Active power of hybrid converter components, (b) DC link voltage, (c) Current at PCC point, (d) Current at VSC of hybrid converter, (e) Current at Vienna rectifier of hybrid converter

Fig. 4-17 displays the simulation results at the beginning, from 0s to 10s. Fig. 4-17 (a) and Fig. 4-17 (b) show the active power and DC voltage of system components, respectively. The DC link voltage of the onshore DC network is 640 kV (1 p.u.), the DC link voltage of the Vienne rectifier is 0.5 p.u. and the DC link voltage of VSC is 0.5 p.u., which means the two power electronics components of the hybrid converter

are each controlled to occupy half of the onshore DC network. Due to the series connection in the hybrid converter, the hybrid converter components transmitted active power is proportional to the ratio of their DC link voltage on the basis of the onshore DC network. In Fig. 4-17 (a), the OWF input active power is 400 MW (1 p.u.), while the Vienna rectifier and VSC converter delivered 0.5 p.u. respectively, from OWF to the onshore DC network. The current at the PCC point is illustrated in detail in Fig. 4-17 (c) to prove the low harmonics at the offshore PCC point.

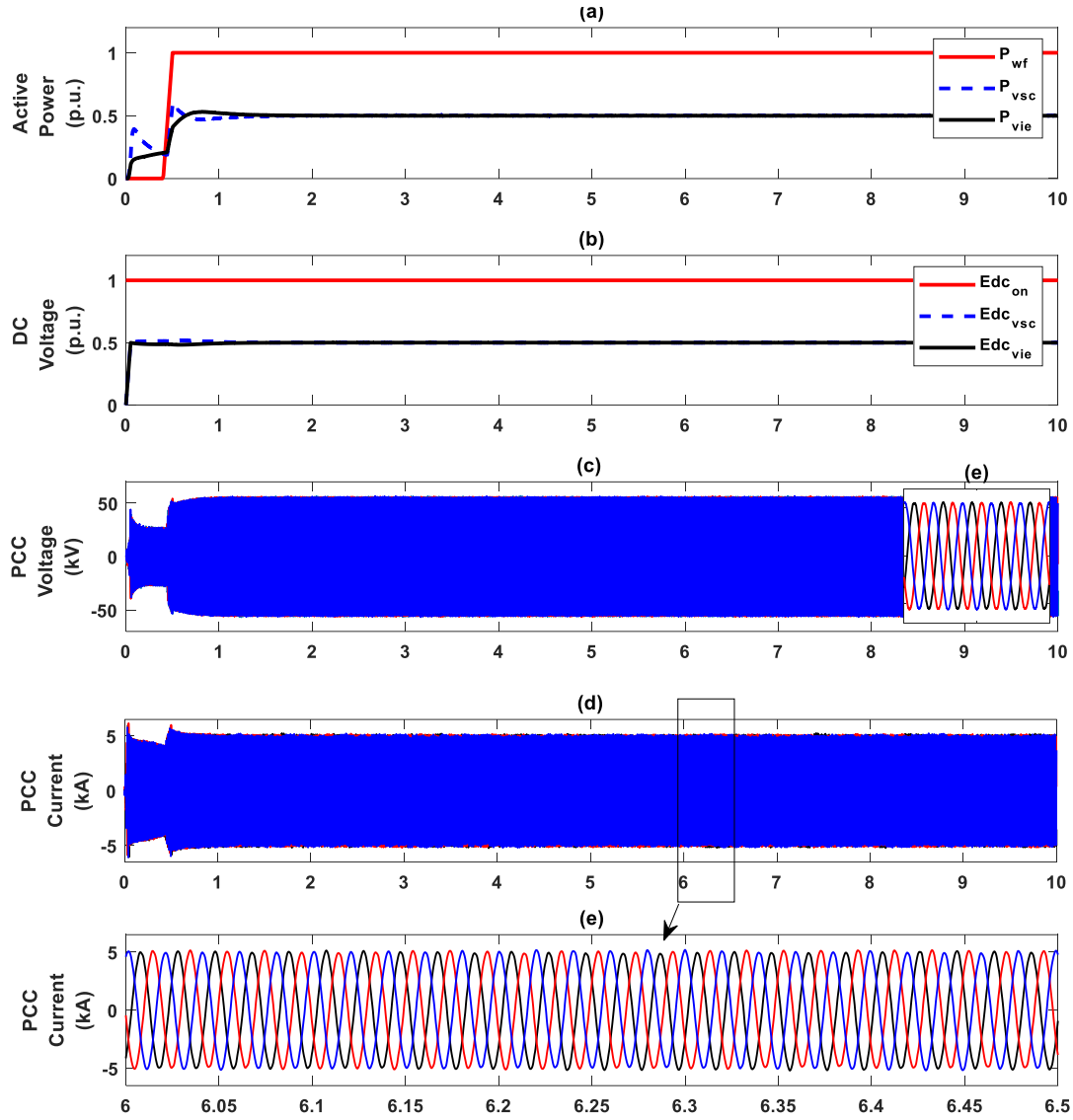

Fig. 4-17 Simulation results from 0s to 10s (a). Active power of hybrid converter components and offshore wind farm during 10s, (b). DC link voltage of hybrid converter components during 10s. (c) Current at PCC point during 0.4s

Fig. 4-18 provides the individual harmonics analysis of the PCC phase current. It shows that the harmonic components remain at a low level, and the total harmonics distortion is only 0.92%.

Fig. 4-19 shows the harmonic analysis of PCC voltage and the THD of PCC voltage is 1.14%.

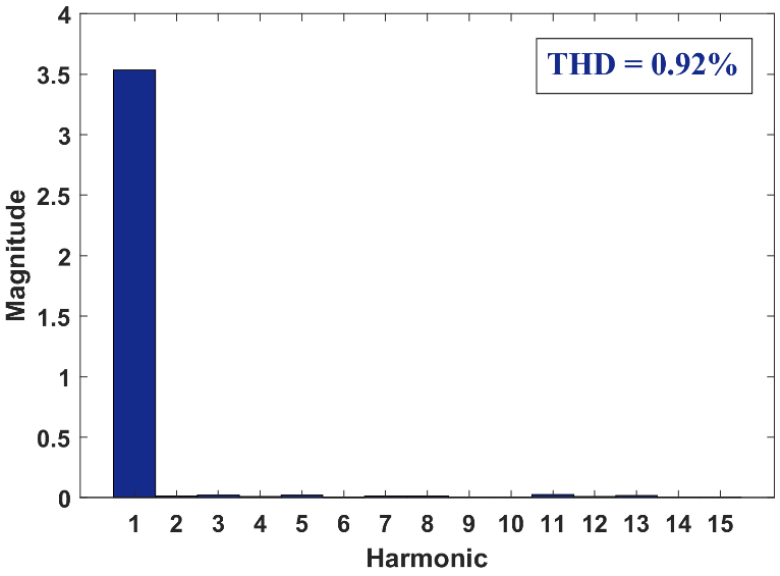

Fig. 4-18 PCC current harmonics analysis

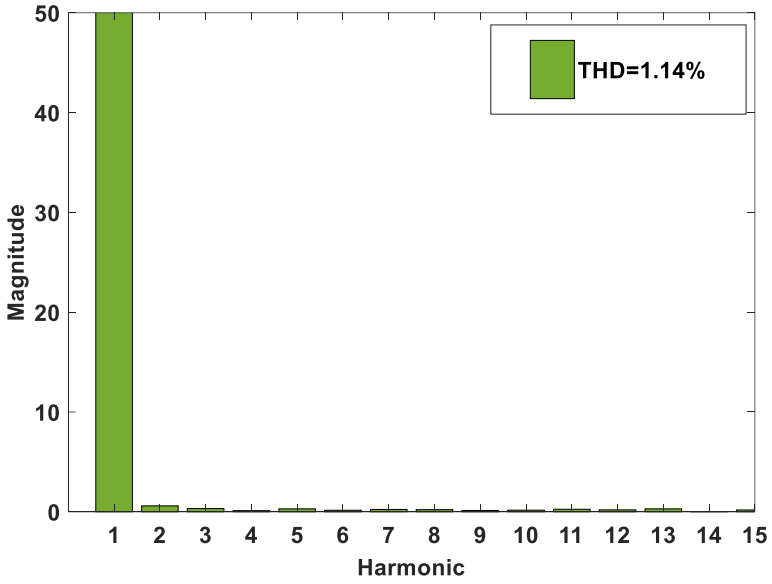

Fig. 4-19 Harmonic analysis of PCC voltage

4.4.2 Hybrid HVDC system during the OWF input active power step

In order to investigate whether the hybrid converter can operate with different power outputs from the offshore wind farm, the wind farm model is controlled to output different active powers. Fig. 4-20 shows the results from 10s to 20s, during this period, the wind farm will deliver different powers to test the operation of the hybrid converter. Fig. 4-20 (a) shows the power transmitted by the wind farm and the hybrid converter, in combination with their DC voltage, as shown in Fig. 4-20 (b).

The output OWF active power drops from 1 p.u. to 0.9 p.u. at 10 s, then increases from 0.2 p.u. to 1.1 p.u. at 14 s, and finally decreases to 1 p.u. at 18 s. It can be seen from Fig. 4-20 (b), that the DC link voltage of the hybrid converter remains constant at its initial setting during the OWF input power steps.

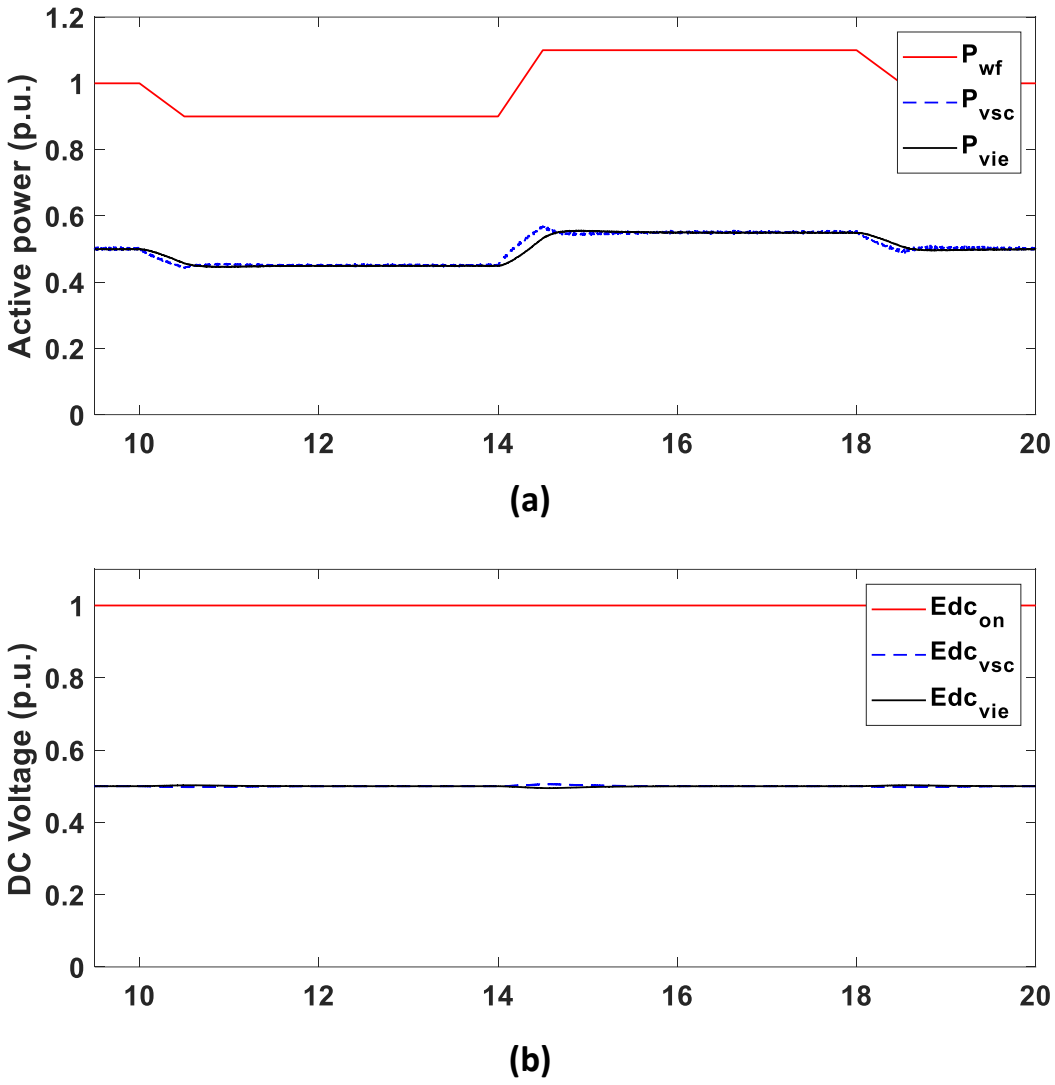

Fig. 4-20 Transmitted power and DC voltage of wind farm and hybrid converter when wind farm power changes

In addition to detecting that the DC voltage is being maintained at the initial setting, the waveform of the PCC current is also an area of concern, particularly the waveform during the periods of changing output power from the wind farm. The following three diagrams show the waveforms of the PCC current as the power changes and partially magnify the waveforms before and after the power change. As mentioned earlier, the output power of the OWF decreases from p.u. to 0.9 p.u. at 10s.

Fig. 4-21 shows the results of the data from 9.5s to 11.5s, during which the OWF power decreases. Fig. 4-21 (b) and (c) show the PCC current waveform from 9.5s to 9.8s and 11.2 to 11.5s, respectively.

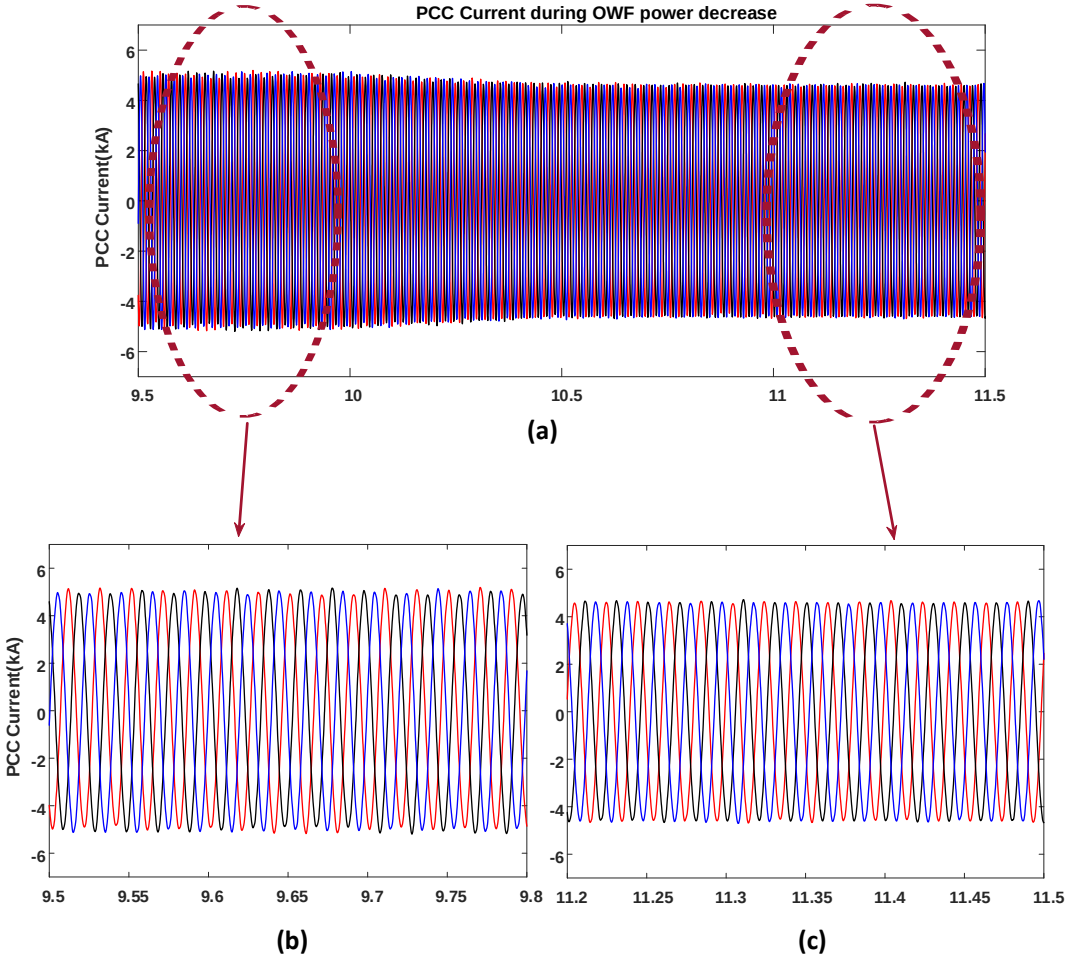

Fig. 4-21 PCC current waveform during OWF output power decrease from 1 p.u. to 0.9 p.u.

At 14s, OWF output power increases from 0.9 p.u. to 1.1 p.u. Fig. 4-22 (a) shows the PCC waveform from 13.5s to 15.5s, and Fig. 4-22 (b) and (c) show the PCC current waveform from 13.2s to 13.5s and 15.2 to 15.5s, respectively.

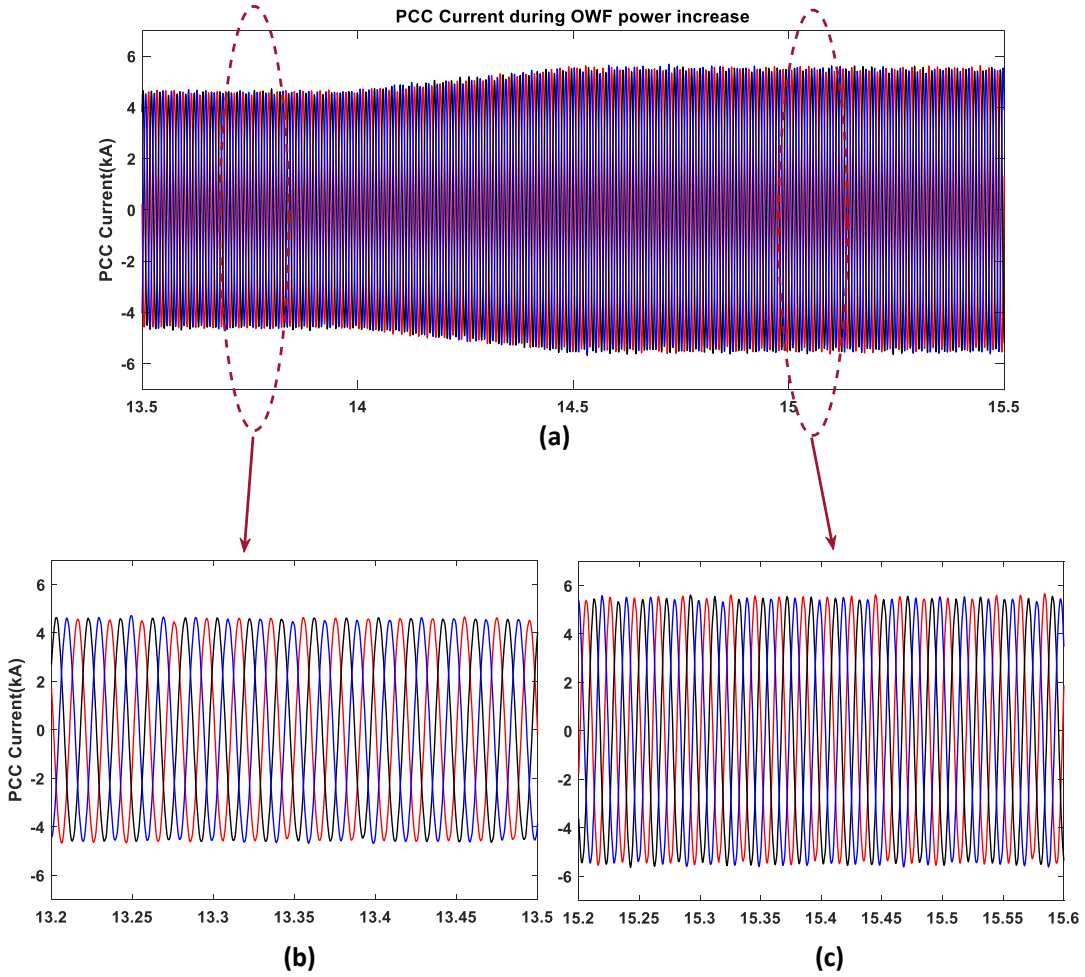

Fig. 4-22 PCC current waveform during OWF output power increase from 0.9 p.u. to 1.1 p.u.

OWF output active power is controlled to initial setting 1 p.u. at 14s, Fig. 4-23 displays a simulation result from 17.5s to 19.5s.

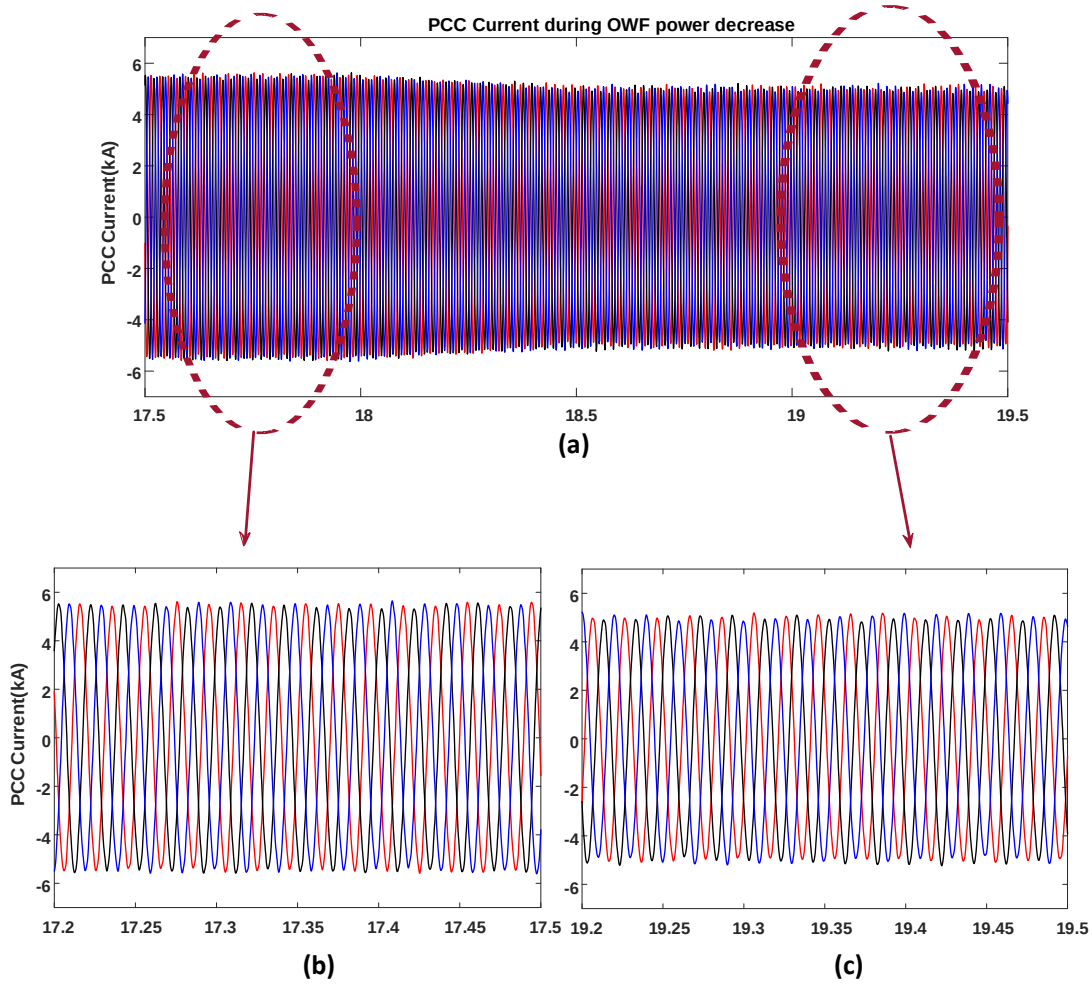

Fig. 4-23 PCC current waveform during OWF output power decrease from 1.1 p.u. to 1 p.u.

The DC voltage control of the hybrid converter is maintained at the initial setting by controlling the different power outputs of the wind farm. Because the characteristic part of the hybrid converter transmits power proportional to the DC voltage, the Vienna rectifier and VSC consistently share power at a 50% ratio from offshore to onshore during power increases and decreases. The PCC current waveform also maintains the expected sine waveform without significant harmonic currents as the wind farm power changes.

4.4.3 Transmitted active power exchanged by the DC voltage control

As discussed in section 4.3.1, due to the characteristics of the series connection type hybrid converter, the onshore converter station maintains the system DC-link voltage as constant. DC-link voltage ratio of hybrid converter components determines the transmitted power of hybrid converter components. Fig. 4-24 shows simulation results from 20s to 40s. During this period, the DC voltage controller of the Vienna rectifier controls its DC-link voltage change to observe the transmitted power from offshore to onshore.

In the initial setup, the onshore converter station controls the system DC-link voltage as 1 p.u. The Vienna rectifier controls its DC-link voltage at 0.5 p.u. and the DC-link voltage of the VSC converter is 0.5 p.u. Thus, each component of the hybrid converter, Vienna rectifier and VSC converter is responsible for 50% of power transmission from offshore to onshore. At 22s, the Vienna rectifier controls its DC-link voltage from 0.5 p.u. to 0.525 p.u., then decreases from 0.525 p.u. to 0.5 p.u. at 26s. This is to test the performance of the hybrid converter when the Vienna rectifier DC voltage controller is commanded to increase the DC voltage. Also, in order to test the performance when a decrease command was received, in the 30s the Vienna rectifier controls its DC link voltage decreased from 0.5 p.u. to 0.475 p.u., and at 34s, the DC voltage is controlled to 0.5 p.u. As shown in Fig. 4-24 (a), the power transferred by the hybrid converter is proportional to the DC voltage, and the system can operate stably during this part of the test. In addition, the DC-link voltage of the hybrid converter is displayed in Fig. 4-24 (b).

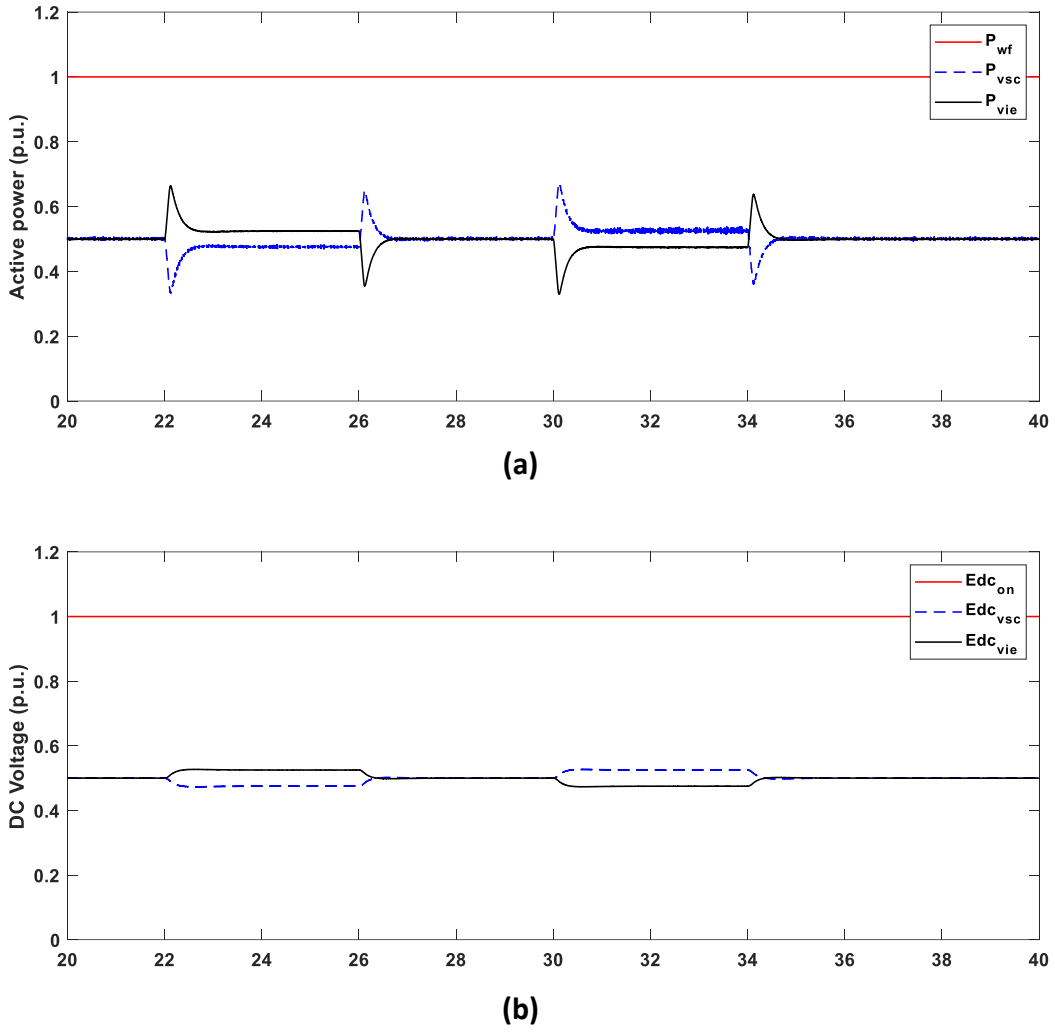

Fig. 4-24 Transmitted power and DC voltage of wind farm and hybrid converter from 20s to 40s

The currents at the PCC point, VSC and Vienna rectifier are illustrated in Fig. 4-25, which shows the waveform when the Vienna rectifier controls its DC-link voltage increases from 0.5 p.u. to 0.525 p.u.. The input current flowing into the Vienna rectifier will increase as the DC-link voltage of the Vienna rectifier increases; in contrast, the input current to VSC will decrease as the VSC DC-link voltage drops. The PCC current will remain the same after the control command. In summary, Fig. 4-25 presents the current as the Vienna rectifier controls its DC-link voltage increase.

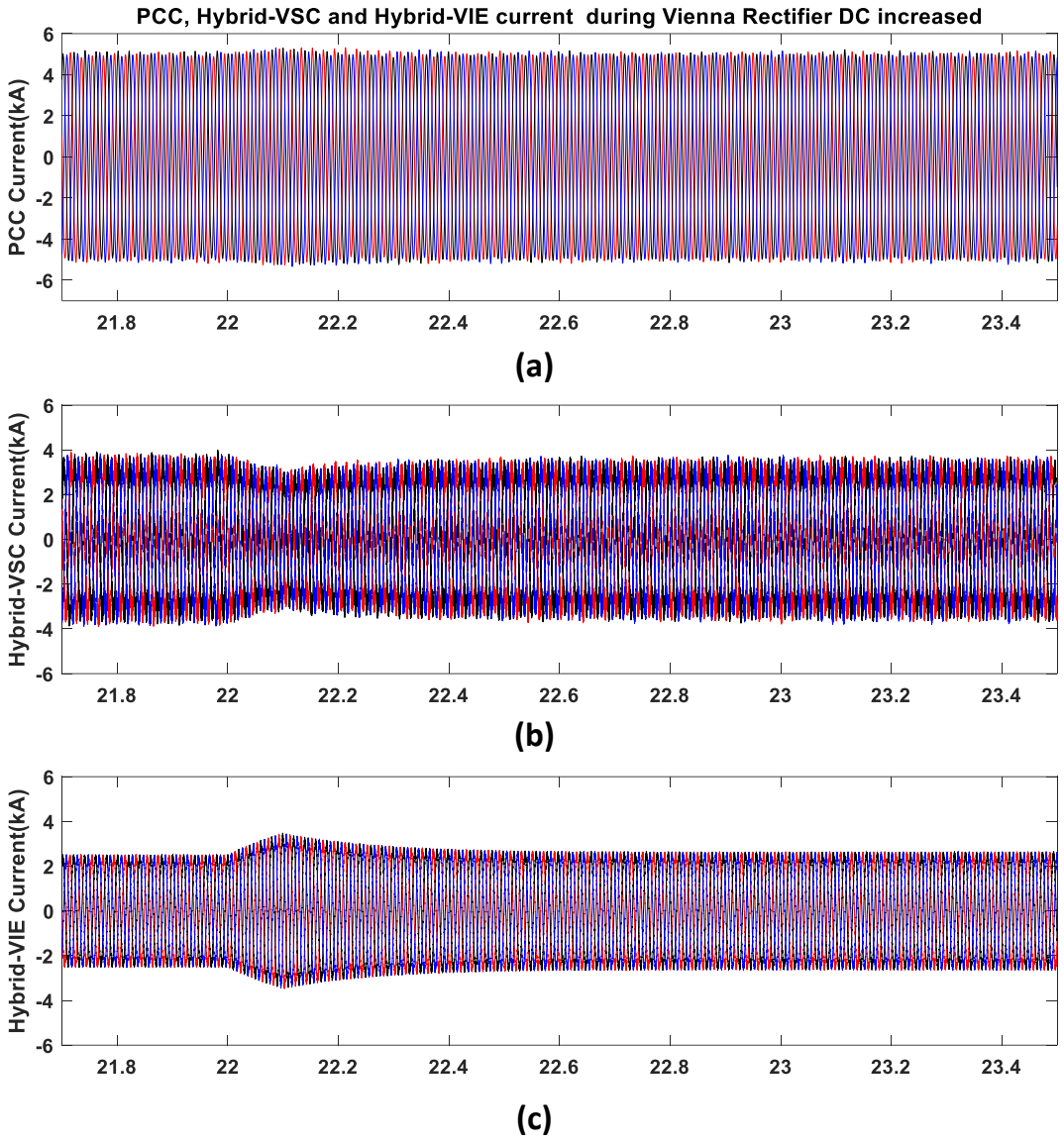

Fig. 4-25 PCC current and hybrid converter components current during Vienna rectifier DC increased

Similar to the figure above, Fig. 4-26 (a), (b) and (c) shows the PCC current, VSC input current and Vienna rectifier input current, respectively. The purpose of this is to test the current when the Vienna rectifier controls its DC-link voltage drop. As the Vienna rectifier DC-link voltage decreases, the current flow into the Vienna rectifier has decreased. The current flow into the VSC converter increases as its DC-link

voltage increases. The current at the PCC point remains the same magnitude.

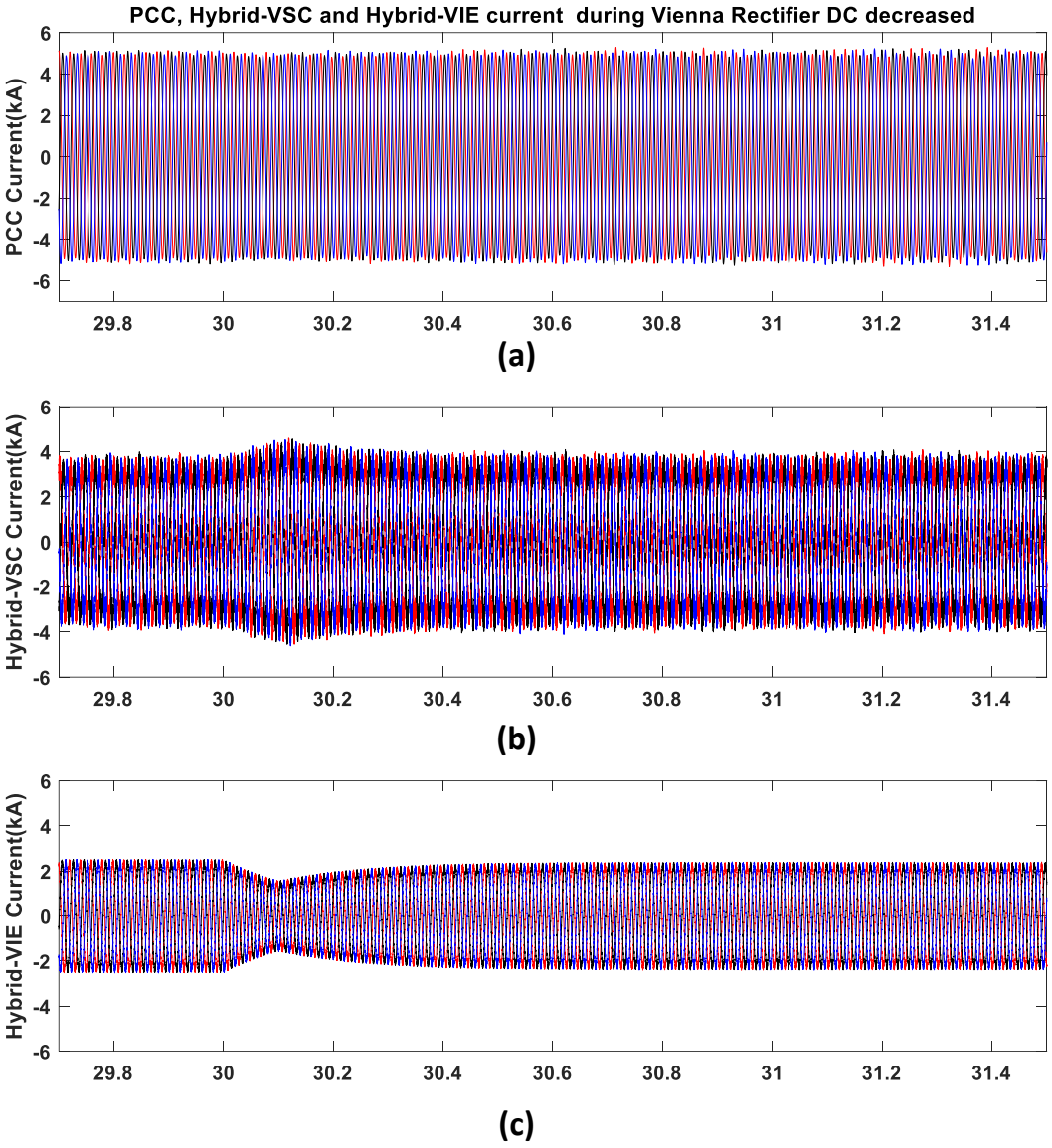

Fig. 4-26 PCC current and hybrid converter components current during Vienna rectifier DC decreased

Due to the characteristics of the series structure, the hybrid converter can determine how much power is transmitted by each component by controlling the voltage of its components. In the set control strategy, Vienna controls its own DC-link voltage to determine the proportion of power to be transmitted. With this characteristic,

the question regarding the size of the hybrid converter can be discussed, i.e. how to use the large size of the Vienna rectifier to transmit power together with the small size of the VSC. Under this assumption, the Vienna rectifier will increase its own DC-link voltage to control the power transmitted by the Vienna rectifier.

4.4.4 Hybrid HVDC system operated in the backup ancillary mode

This section presents two test case simulation results to compare the performance of the hybrid converter with and without backup ancillary mode. For both test cases, the Vienna rectifier controls its DC link voltage as 0.5 p.u., and the VSC of the hybrid converter controls the power magnitude at the PCC point at the beginning. At 5s, the IGBTs of the Vienna rectifier are simulated as faulty, and the VSC converter controls the DC link voltage rather than the power magnitude. The difference between the two test cases is the backup ancillary mode, Fig. 4-27 shows that the hybrid converter station does not enable backup ancillary mode at 5s, and the SRF harmonic compensation controller will not work for harmonics cancellation. As a comparison, Fig. 4-28 displays a simulation result that the hybrid converter enables the back ancillary mode, and the SRF harmonic compensation controller will be used to reduce the harmonic current.

Fig. 4-27 shows the performance of the hybrid converter when the Vienna rectifier's IGBTs are faulty, and the backup ancillary mode is not enabled. DC-link voltage and transmitted power are presented in Fig. 4-27 (a) and Fig. 4-27 (b). As the control system of the VSC converter controls the DC-link voltage at 5s, the DC-link voltage and transmitted power do not collapse due to the failure of the Vienna rectifier. Fig. 4-27 (c) display the PCC current, and to compare the difference in PCC current waveform before and after the Vienna rectifier's fault, Fig. 4-27 (d) and (e) show the PCC current at 4.5s to 4.6s and 7.0s to 7.1s respectively. Without backup auxiliary

mode activation, harmonics currents appear in the PCC current, as can be seen from Fig. 4-27 (e). In addition, an FFT analysis of the current in Fig. 4-27 (e) has been produced, and the results are shown in the blue bar in Fig. 4-29.

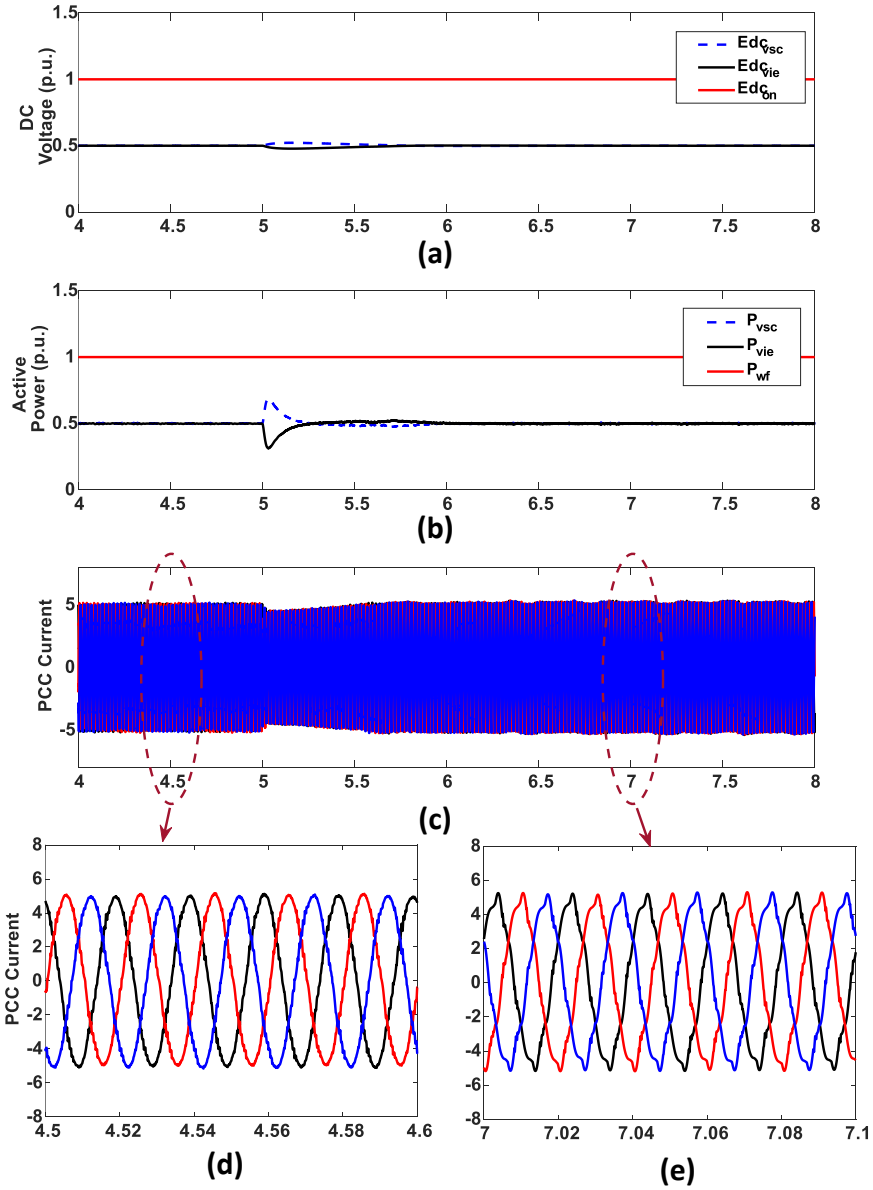

Fig. 4-27 Performance of hybrid converter during mode change action without harmonics compensation control

The performance of the hybrid converter with the backup ancillary mode is illustrated in Fig. 4-28. The harmonics compensation controller is working with a VSC converter control command change. When the backup ancillary mode is enabled, the harmonic current produced by the non-IGBTs Vienna rectifier is suppressed by a built-in active power filter, which is from the VSC of the hybrid converter operating in the backup ancillary control mode, SRF harmonics compensation controller is activated.

Fig. 4-28 (a) and (b) show DC-link voltage and transmitted power, respectively, and PCC current is shown in Fig. 4-28 (c). By contrast to the simulation result shown in Fig. 4-27, the harmonics current compensation controller operates to eliminate harmonic currents, although the VSC converter changes the control target. The current waveforms before and after the harmonics controller is activated are also shown in Fig. 4-28 (d) and (e), respectively, in order to facilitate a comparison of the PCC current waveform. In addition, Fig. 4-28 (e) is also analyzed by FFT and its result is shown as the orange bar in Fig. 4-29.

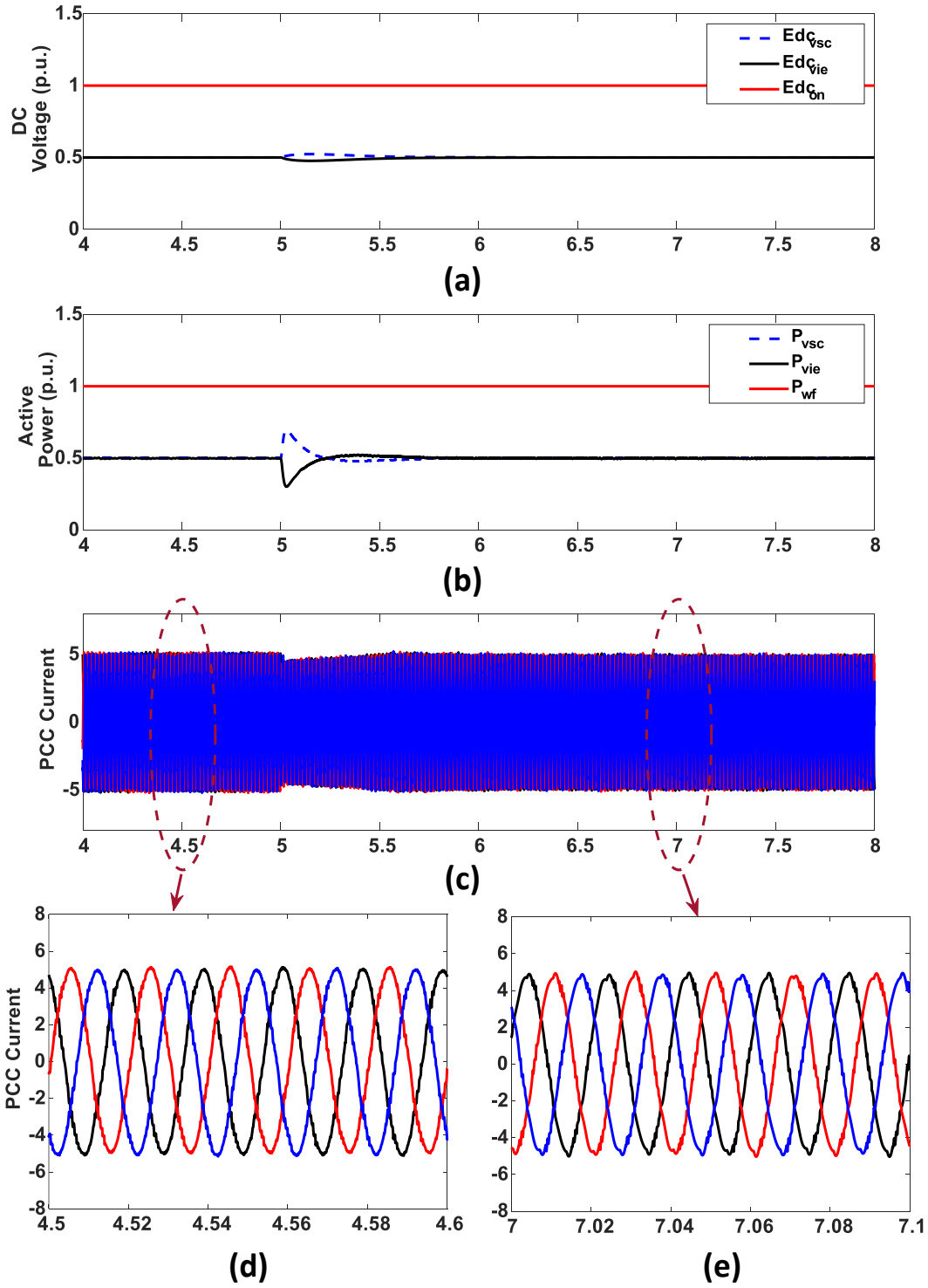

Fig. 4-28 Performance of hybrid converter during mode change action with harmonics compensation control

The two simulation results are analyzed separately for individual harmonics

analysis, and the comparison result is presented in Fig. 4-29. The blue bar diagram shows the analysis results of PCC current without the backup ancillary mode; the orange bar diagram shows the analysis PCC current analysis with the backup ancillary mode. It is clear that the 5^{th}, 7^{th}, 11^{th} and 13^{th} harmonic current decreases when the backup ancillary mode is enabled. In addition, the THD for the two simulation results is 6.1% and 1.8%, respectively. There is a 4.3% drop when the mode starts.

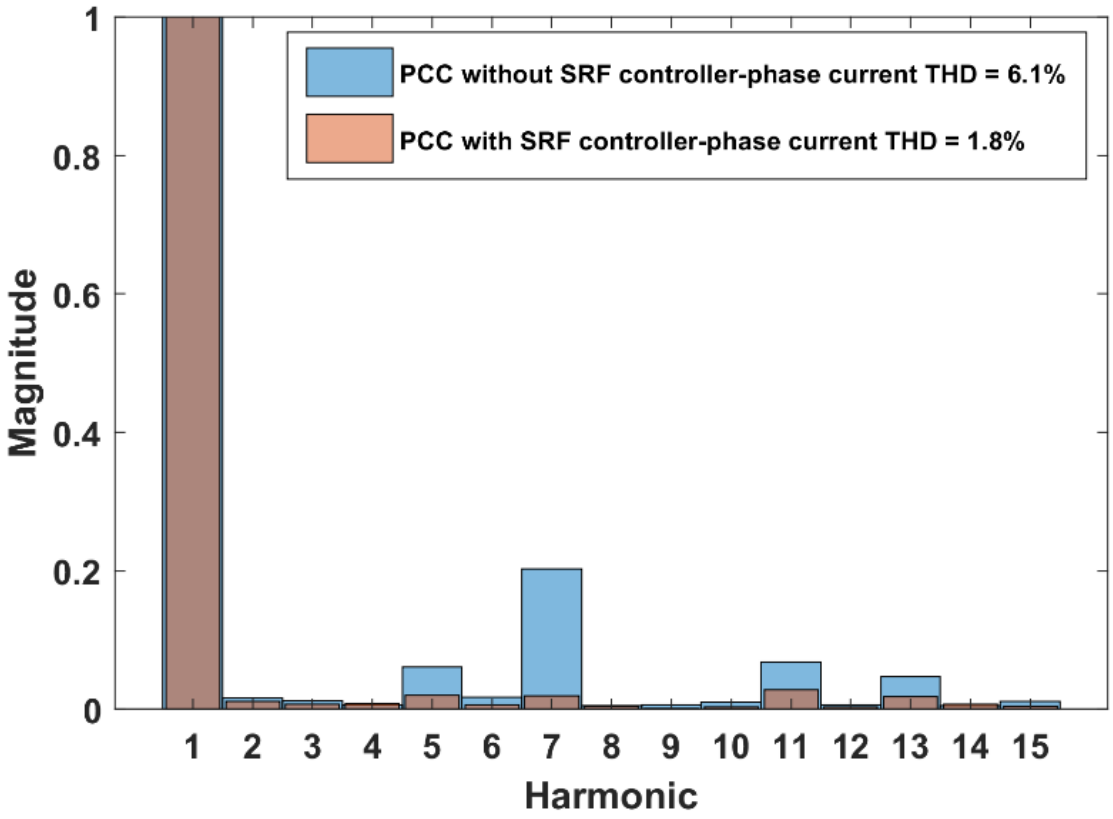

Fig. 4-29 Comparison of the harmonics analysis of PCC phase current without harmonic compensation controller and PCC phase current with harmonic compensation controller

4.4.5 The size of the hybrid converter

The analysis of the results of the previous simulation shows that the hybrid converter can be controlled in relation to the amount of power transferred by the DC voltage converter of the Vienna rectifier. This section discusses the power transfer

ratio of the hybrid converter in terms of the sizing of the hybrid converter. It aims to explore a potential solution that utilizes a reduced-size VSC converter series connected with an increased-size Vienna rectifier.

Table 4-4 Parameters of offshore HVDC system based on new size hybrid converter

Parameters		Nominal Value
Wind farm Aggregated model	Power rating	400 MW
	Transformer voltage ratio	0.69 kV / 66 kV
Onshore converter station	DC voltage rating	640 kV
Vienna rectifier Of Offshore Hybrid Converter	Power rating P_{Tvie}	267 MW
	DC voltage rating	427 kV
	Transformer voltage ratio	66 kV / 230 kV
	Inductance L_{vie}	0.15 p.u.
	Resistance R_{vie}	0.0015 p.u.
2-Level VSC Of Offshore Hybrid Converter	Power rating P_{Tvsc}	143 MW
	DC voltage rating	213 kV
	Transformer voltage ratio	66 kV / 230 kV
	Inductance L_{vsc}	0.15 p.u.
	Resistance R_{vsc}	0.0015 p.u.

Table 4-4 shows the parameters used for this test. The offshore wind farm generates 400 MW, and the transformer ratio of the wind farm, Vienna rectifier side and VSC side remain the same as in the previous test. The difference is that the rated power of the transformer connected to the Vienna rectifier is 267 MW, while for the VSC is 143 MW. As a result, the inductance and resistance values connecting the hybrid converter component are different from the previous simulation test.

The Vienna rectifier is designed to regulate its DC voltage to 0.67 p.u. (427 kV) of the entire HVDC system DC voltage. Consequently, the VSC will maintain a DC voltage of 0.33 p.u. (213 kV) in accordance with this control target. As a result, the power generated by offshore wind farm will be divided between the Vienna rectifier

and the VSC, with the former carrying 0.67 p.u. (267 MW) and latter carrying 0.33 p.u. (133 MW) of the total power.

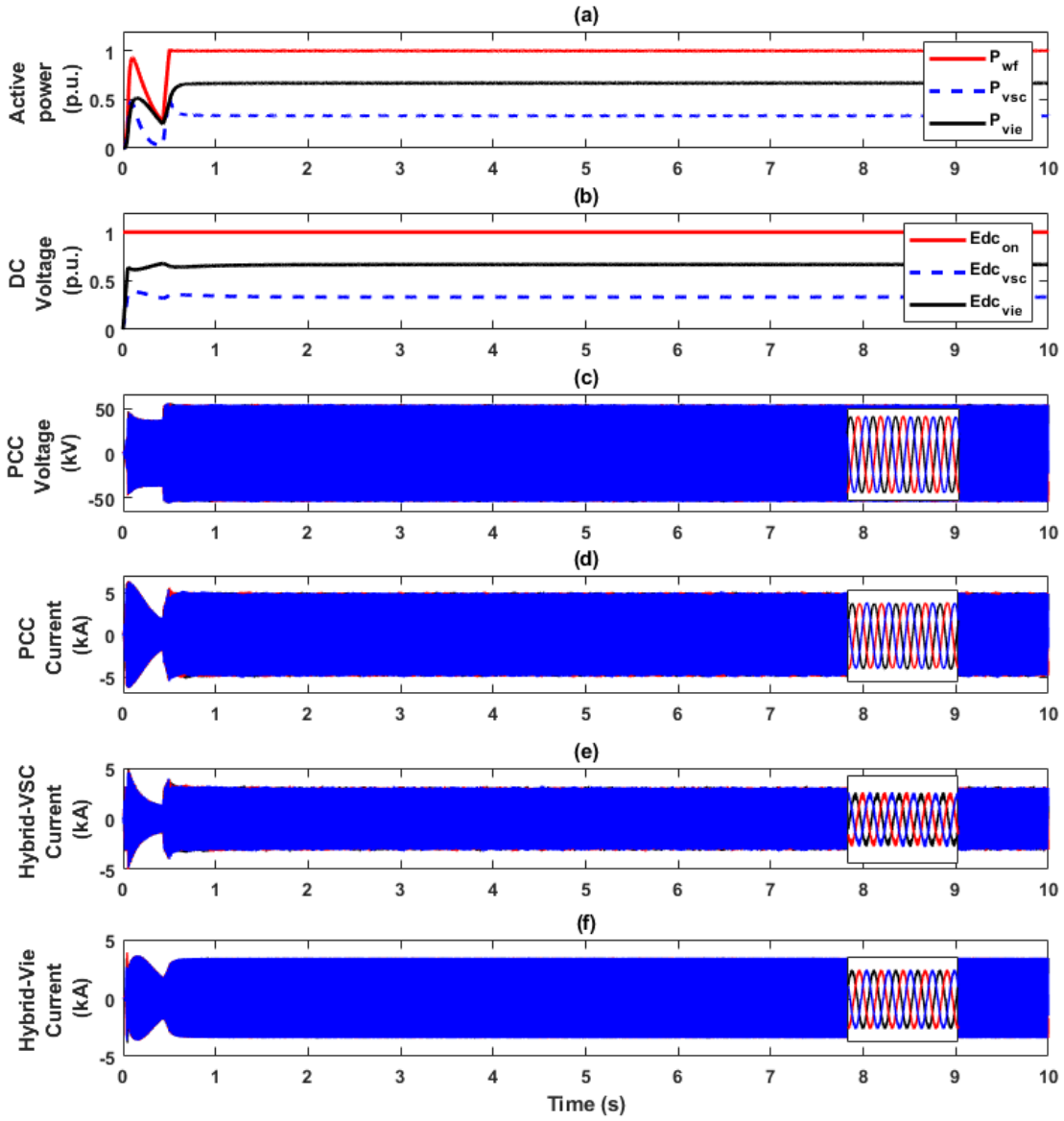

Fig. 4-30 Simulation results of the new configured hybrid converter's size: (a) Active power, (b) DC Voltage, (c) PCC voltage, (d) PCC current, (e) Current flowing into Vienna rectifier, (f) Current flowing into VSC converter

Fig. 4-30 shows the simulation results of the hybrid converter's new configuration. Fig. 4-30 (a) and (b) present the power and voltage profiles of the hybrid converter components, respectively. The voltage of the Vienna rectifier is regulated at

0.67 p.u., and the power is proportional to this voltage. Fig. 4-30 (c) and (d) display the voltage and current at the PCC point. With an additional zoomed detail diagram, the results show the expected voltage and current waveform. The currents at the VSC and Vienna rectifier are depicted in Fig. 4-30 (e) and (f), respectively, along with their corresponding enlarged detail diagrams.

This experiment demonstrates that the hybrid converter can be effectively integrated with a small VSC and a large Vienna converter. The proposed configuration allows a wide variety of power and DC voltage rations between the Vienna rectifier and the series VSC converter. User can select an appropriate ratio based in their requirements, including the amount of bi-directional power flow for black start capability voltage control, level of harmonic current suppression and DC voltage level allowed for the IGBT switches. As an example, the simulation presented in this paper shows the performance of a 50% - 50% and 67% - 33% power/DC voltage ratio between the Vienna rectifier and the VSC. This combination not only reduces the initial investment costs but also minimizes the offshore footprint, thereby offering significant benefits.

4.4.6 Cost and Sizing Analysis of the Proposed Hybrid Converter

European Network of Transmission System Operators of Electricity (Entso-e) [79] published a report regarding offshore transmission technology, including the offshore technology, HVDC projects around Europe and converter costing information. The cost of a 500 MW VSC converter is about 75 – 92 million Euros. The weight of a 400 MW VSC platform is 3500 tonnes, which costs 32 – 38 million Euros if installed as Topside. Thus, the cost and weight of 1 MW is 0.15M€/MW and 8.75 tonnes/MW [80]. Compared to HVDC based on the VSC converter, the cost and weight of the DR-HVDC system can potentially be decreased by 30% and 80%, respectively[81, 82].

The hybrid converter based on 12 PDR and VSC reduces costs by around 17.6% and weight by 28.1% [66]. The proposed hybrid converter based on the Vienna rectifier and VSC reduces around 10% of the converter cost and 25.1% of the weight. The diode rectifier converter station has the lowest cost and weight, but the largest AC filter needs to be installed at the offshore side, which increases the investment cost and footprint at the offshore side. In addition, the diode rectifier converter is an uncontrollable device, which relies on wind turbines. DR-HVDC has significant advantages and disadvantages.

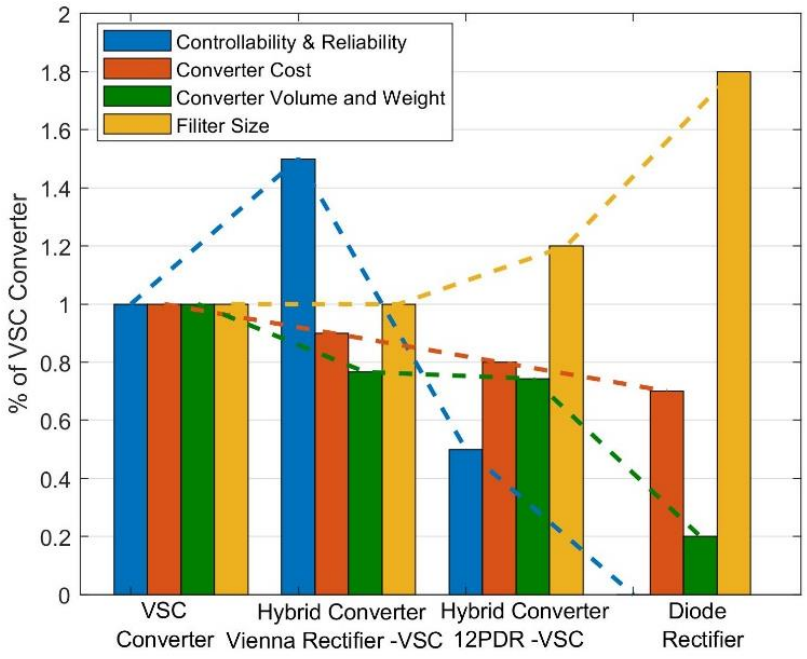

Fig. 4-31 Converter station comparison

HVDC systems based on hybrid converters have extended control capabilities and smaller filters compared to diode rectifier converter stations. With the Vienna rectifier included in hybrid converters, hybrid converters have more control options. Therefore, offshore converter stations do not require filter stations or complex transformers, which can reduce costs and footprint. In comparison to VSC converters, hybrid converters have a lower cost and a smaller footprint. Additionally, switching losses are

lower due to the reduction in IGBTs.

4.5 Summary

This chapter proposed a hybrid converter topology based on a Vienna rectifier and VSC to be used in offshore HVDC systems. The proposed hybrid converter provides low-cost, low-harmonics, low-complexity and high-reliability operations for offshore HVDC systems. In addition, the proposed converter has the capacity to maintain a controlled and harmonic-free performance in the event of a Vienna rectifier switching failure. In this configuration, the VSC of the hybrid converter functions as an active power filter during non-IGBT Vienna rectifier operation. The performance of the hybrid converter was simulated with PSCAD/EMTDC to verify the system operations in steady state and dynamic conditions. In addition, the backup ancillary mode was verified. Therefore, according to the testing results analysis, the hybrid converter's size is discussed in this chapter, which uses the larger Vienna rectifier and smaller VSC in series connections. In the end, the hybrid converter based on the Vienna rectifier and VSC converter shows the advantages of controllability cost, footprint and AC filter size in the converter station.

Moreover, the hybrid converter eliminates the need for a filter on the offshore side. This is due to the Hybrid Vienna-VSC converter's use of an SRF-based harmonic current compensation controller as a backup, which can cancel harmonic components if a failure occurs in the VSC converter's switching devices. The SRF-based harmonic current compensation controller provides a solution that is not only easy to tune but also resilient to frequency variations. However, its limitation lies in the slow response time of the low pass filter used in the SRF-based harmonic current compensation technology, especially when the hybrid converter operates in backup auxiliary mode. Chapter 5 discusses the details and provides a method to improve the SRF technique.

Chapter 5 Fast detection and control techniques for harmonic mitigation in Hybrid Converters

5.1 Introduction

The above chapters introduced two kinds of hybrid converters: a 6P-DR series connected with a two-level VSC and a Vienna rectifier series connected with a 2-Level VSC. The advantages of the hybrid converter arise from the combined advantages of the two converter topologies. For example, the 6P-DR-VSC hybrid converter added the robustness, simplicity and efficiency of an uncontrollable rectifier. The Vienna rectifier brings low harmonic currents, simplicity and high efficiency. Additionally, the backup ancillary mode is built into the Vienna rectifier-VSC hybrid converter.

The VSC converter of the hybrid converter brings the controllability and harmonic current compensation to the characteristics of the hybrid converter. Due to the harmonic current produced by 6P-DR, the VSC converter includes the capability to work as an active power filter to clear harmonic pollution at the PCC. This functionality is needed in the Vienna rectifier-VSC hybrid converter when the IGBTs of the Vienna rectifier are faulty and the system operates as an uncontrolled 6P-DR.

Several techniques are used for detecting and compensating harmonics in active power filters, such as the harmonic control loop based on the proportional resonant controller or the synchronous reference frame controller based on the PI controller (SRF-PI). These techniques have been used by some authors in the hybrid converter control systems to provide harmonic cancellation at the PCC. The PR controller-based harmonic compensation can provide a fast response to set-point changes but has a complex tuning process and is very sensitive to grid frequency variations. Although

the SRF-PI technique has an easy-tuning and robust control system, a slow set-point response is the shortcoming of its technique because of the small bandwidth low pass filters within the SRF-PI control architecture.

In this chapter, a robust and fast-acting controller, the Two Degrees of Freedom Internal Model controller (2DF-IMC) is introduced and used to replace the PI controller in the SRF harmonic approach to control the VSC of the hybrid converter as an active power filter. The most relevant feature of the 2DF-IMC controller is its capability to detect and control harmonics without relying on low-pass filters. This allows the proposed controller to provide a much faster overall THD reduction in offshore AC currents. When the Vienna rectifier-VSC hybrid converter mode switches, the 2DF-IMC controller provides a faster response compensation in harmonics at the PCC.

5.2 Synchronous reference frame (SRF) technique used for harmonic current detection.

5.2.1 Harmonics compensation controller based on SRF-PR controller

The Proportional resonant–based controller (PR controller) is used in estimated harmonic in active power filter applications. PR controllers are able to follow the target harmonic reference to their respective resonant frequencies with zero steady-state error by applying an infinite gain at the desired resonant frequency. In conventional hybrid converters, the reference [59] uses the PR controller to cancel out the harmonic current at the PCC point, which uses the VSC of the hybrid converter to function as an active power filter via the harmonic compensation control loop based on a PR controller.

The use of the SRF-PR controller provides a fast response for set-point changes

in harmonic compensation. In contrast, attaining adequate controller tuning and stability is difficult for the PR controllers and increases the complexity of controller tuning. Additionally, the controller resonant frequency should be tuned to the reference frequency because of the narrow infinite gain band. On the other hand, non-ideal PR controllers are able to use second-order generalized integrators that provide a wider resonant band but have an increased penalty of tracking errors [83].

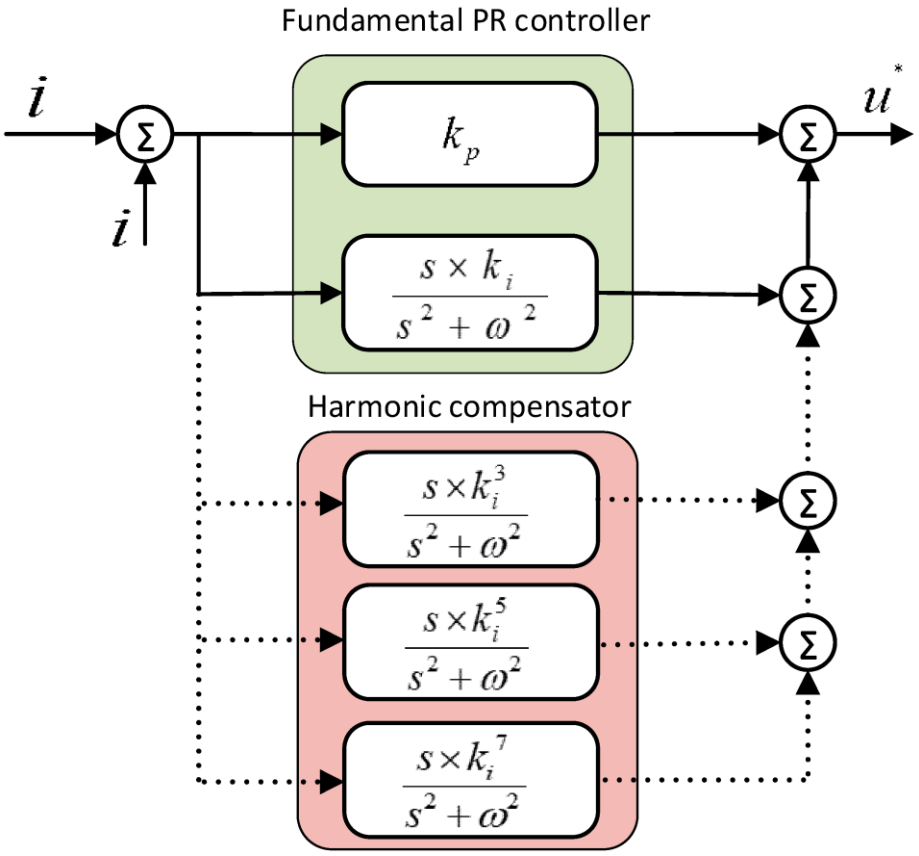

Fig. 5-1 Harmonics control technique base on PR-Controller [84]

5.2.2 Harmonics compensation controller based on SRF-PI controller

Fig. 5-2 shows the diagram of the SRF technique using a PI controller and low pass filter. This harmonic compensation controller is used in the hybrid converter is

proposed in this thesis. This technique relies on several *dq* frames rotating at the angular frequency (ω_h) and sequence of the harmonics to be compensated. The compensation process is illustrated

, which displays the 5th and 7th harmonic currents to show the compensation process; the red and blue bars represent the 5th harmonic and 7th harmonics, respectively. The output of a given rotating *dq* frame an AC component (the sum of all frequency components of the signal that are not rotating at the same speed as the *dq* frame) and a DC component (the DC representation of the frequency component rotating at the same speed and sequence of the rotating *dq* frame). The low pass filter after the *dq* transformation aims to remove the AC components and obtain the expected *dq* components of the harmonic signals, which are then provided as inputs to a PI controller inside the given harmonic currents compensation control loop. For example, in the 5th harmonic current compensation control loop, the 5th harmonics (red bars) and 7th harmonics (blue bars) measurements from the non-linear load pass through the low pass filter to obtain the expected 5th harmonic current *dq* values, which are then used by the PI controller as reference. The same process is applied in other harmonic compensation loops. After the PI controller produces a *dq* control signal, such signal is converted back to an *abc* value using the inverse *dq* transformation rotating at the angular frequency and sequence of the given harmonic. This process results in the VSC producing a harmonic current output that cancels out the given harmonic produced by the nonlinear load when provided to the PCC point.

SRF-PI provides an easy-to-tune process for harmonic current compensation with stable controls and no tracking errors. Additionally, SRFs enable individual harmonic currents to be controlled as DC signals with the PI controllers. Despite the above advantages, the slow response times are the disadvantages of SRF-PI harmonic current compensation controllers. The low pass filter in the controller architecture causes the

slow response time and also increases the computational workload.

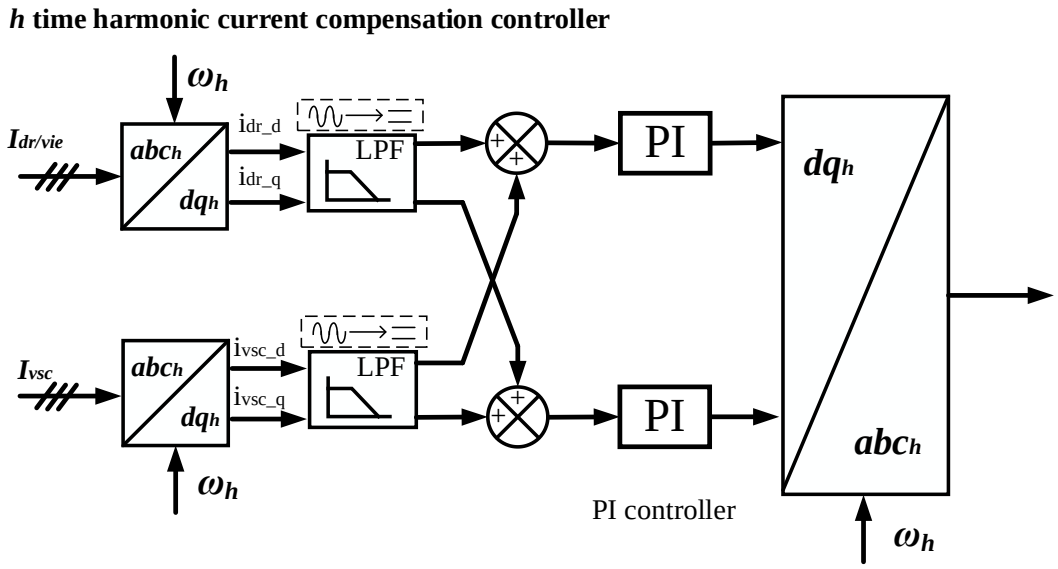

Fig. 5-2 SRF technique based on PI-Controller

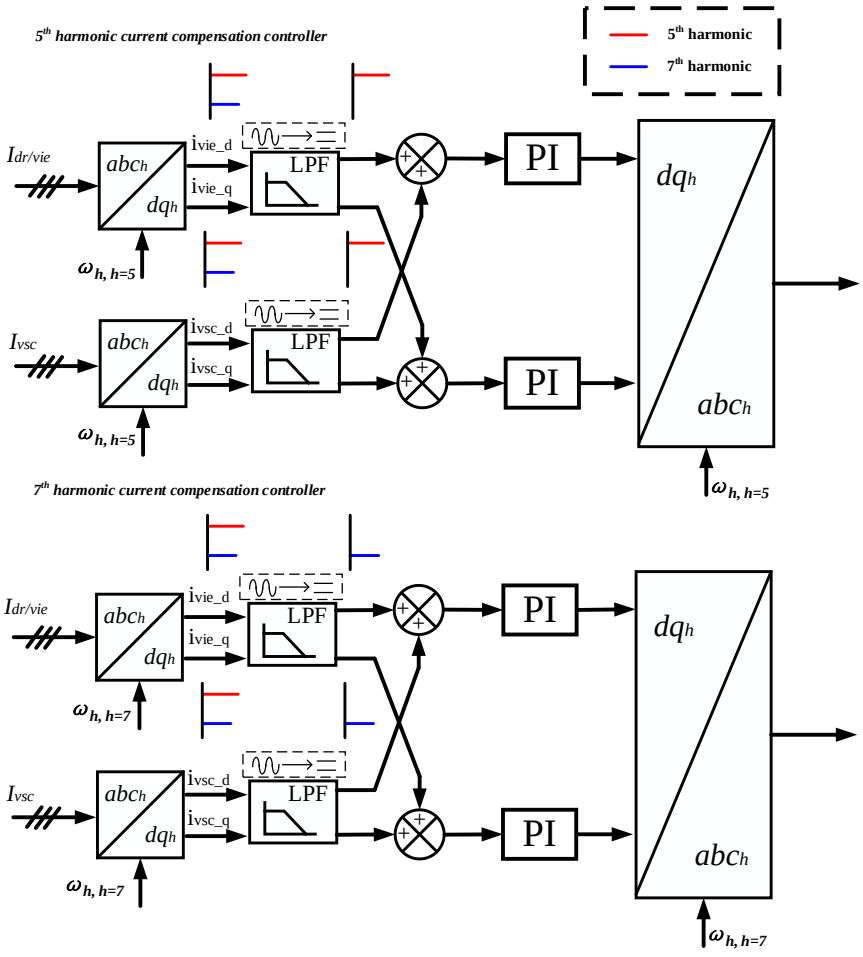

Fig. 5-3 Compensation process used SRF-PI controller

5.3 SRF technique using 2DF-IMC controllers for harmonic compensation.

To address delays produced by the low-pass filters in the SRF-PI controllers, the two-degrees-of-freedom internal match controller (2DF-IMC) is proposed to replace the PI controller within the controller process, as presented Fig. 5-4. The 2DF-IMC controller can detect and control harmonics without the need of low pass filters in the control architecture. By removing the low pass filter, the 2DF-IMC of each separate harmonic current compensation loop will track the harmonics of the set-point at the same time without the delay caused by the filter.

The 2DF-IMC technique uses an internal model of the plant to define controller constants. 2DF-IMC controllers have been successfully used in power electronic converters to increase close-loop robustness. The increased robustness of the 2DF-IMC controller can be explained by its controller structure, which, by using a second degree of control freedom, adds an artificial damping term to the plant's transfer function. By doing so, the plant transfer function acquires a fixed parameter that the controller can replicate accurately in its internal model. This leads to the definition of controller constants that remain effective in providing stable control even when the parameters of the plant change or when such parameters are not accurately depicted in the controller's internal model.

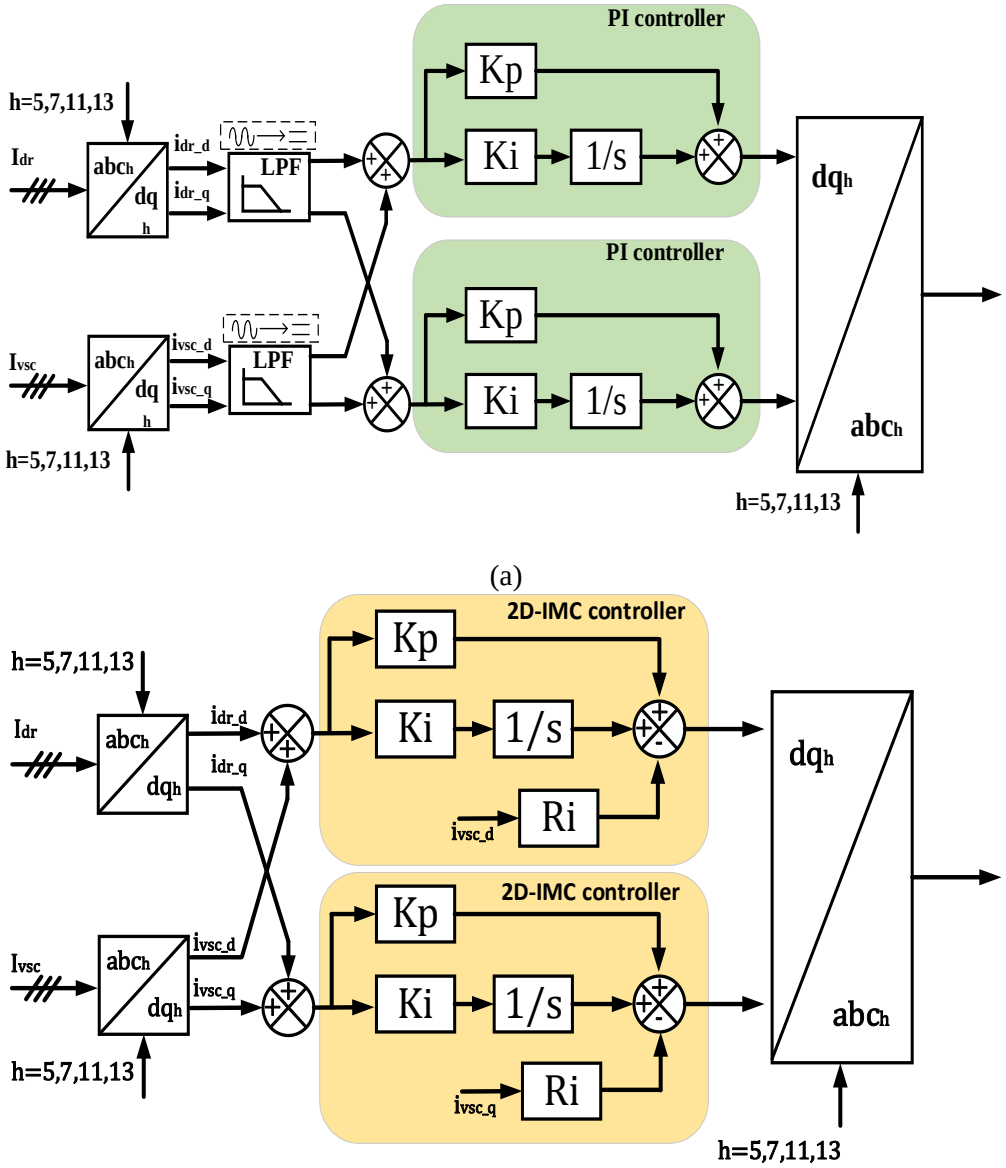

Fig. 5-4 Harmonic current compensation controller (a) tuned by PI controller, (b) tuned by 2DF-IMC controller

Another advantage of the 2DF-IMC is the increased disturbance rejection capabilities that the artificial damping adds to the plant dynamics. If the value of the artificial damping parameters is selected correctly, a closed-loop 2DF-IMC controller can reject disturbances (i.e. exogenous signals added to the input of the plant that deviate the output from the desired value) as fast as its close-loop set-point dynamics.

Fig. 5-5 shows the basic structure of the 2DF-IMC controller, where $G(s)$ is the

plant to control, $M(s)$ is the augmented plant with an artificial inner feedback loop (the second degree of control freedom) of value R, $M'(s)$is the plant model and $L(s) = \left(\alpha/(s+\alpha)\right)^z$is low pass filter designed to make the controller a proper function. The order of the filter, z, is chosen according to the order of $G(s)$ and α can be interpreted as the closed loop bandwidth of the control system.

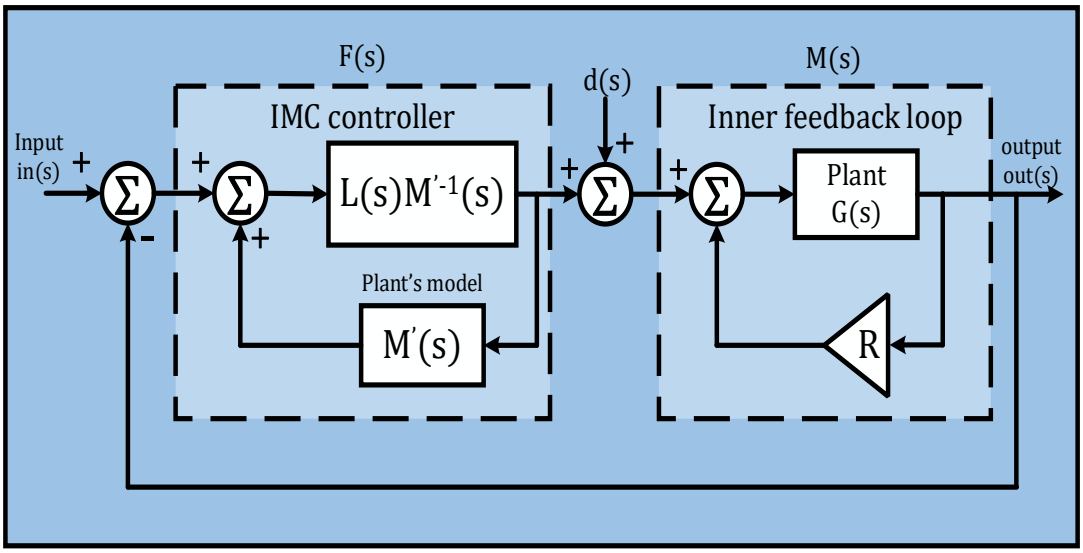

Fig. 5-5 Diagram structure of IMC controller

The active damping feature of the 2DF-IMC controllers can be used by multiple-SRF harmonic detection and control algorithms to remove the low-pass filters in their harmonic detection stages, leading to a significant increase in the speed of response of the controllers. This is explained in detail in the following section.

The *d* and *q* outputs of an SFR rotating at the angular speed and sequence of a "*n*" current harmonic are hybrid signals consisting of DC and AC components. The DC components can be used to define the magnitude and angle of the *n* harmonic, whereas the AC signal is the representation of the rest of the harmonics in the measured current.

$$i_{n\_d} = \underbrace{\Gamma_n i_n \cos(\beta_n)}_{\text{DC component}} + \underbrace{\sum_{k=1,k\neq n}^{\infty} \Gamma_k i_k \cos(-\Gamma_k[(\Gamma_n n - \Gamma_k k)(\omega_s t)] + \beta_k)}_{\text{AC component}}$$

$$i_{n\_q} = \underbrace{i_n \, sin(\beta_n)}_{\text{DC component}} + \underbrace{\sum_{k=1,k\neq n}^{\infty} i_k \, sin(-\Gamma_k[(\Gamma_n n - \Gamma_k k)(\omega_s t)] + \beta_k)}_{\text{AC component}} \tag{5.1}$$

The DC and AC components are labelled in Equation (5.1). i_{n_d} and i_{n_q} are the n harmonic dq signals. β_n is the phase shift of the n harmonic, i_n is the magnitude of the n harmonic, i_k is the magnitude of the k harmonic current, ω_s is the synchronous frequency in radians, t is the time, β_k is the phase shift of the k harmonic, and $\Gamma_k = \text{sign}[sin(2\pi k/3)]$ represents the sequence of the k harmonic and is reflected in Equation (5.1) as an algebraic sign.

The modulator signal fed to the VSC by a filter-less SRF is a hybrid waveform composed of 2 parts: a) a useful control action that is the DC dynamics of the fundamental and harmonic dq current loops combination, b) constant harmonic disturbances that are the product of using the filter-less SRF, which are meaningless for control purposes. It is evident that the only useful information of Equation (5.1) for control purposes is the DC components of the signal. This explains the use of the low pass filter in the typical SRF-based harmonic controllers. However, if the filter it is not applied and the signal is provided directly to a PI controller, then the output of the controller will be, because of the principle of superposition, the effective control action (the DC output) plus a periodic waveform that is meaningless for control purposes and acts as a "AC disturbance" added to the input of the plant. This AC disturbance can be fully rejected with 0 steady-state error when using 2DF-IMC. The reason for this is that a n constant AC harmonic disturbance, produced by any given 2DF-IMC controller of the system, is reflected as a constant DC signal disturbance in the 2DF-IMC dedicated to the control of the n harmonic. Specifically, it will be reflected as a DC disturbance signal of magnitude $H_{n\_AC} \, cos(\beta_n - \phi_{n\_AC})$ for the d control loop and a DC disturbance signal of magnitude $H_{n\_AC} \, sin(\beta_n - \phi_{n\_AC})$ for the q control loop.

Because the 2DF-IMC is specifically built to reject step-like and constant DC disturbances, it is an ideal choice for compensating AC disturbances generated by the other 2DF-IMC controllers with the same robustness and speed of response of its set-point tracking feature, as they will be reflected as a DC disturbance signal. For this reason, arrays of 2DF-IMCs specifically designed to compensate for individual harmonics will jointly compensate for AC disturbances generated by one another as fast as they track a set point change. Fig. 5-4 shows the schematic of the 2DF-IMC along with the SRF.

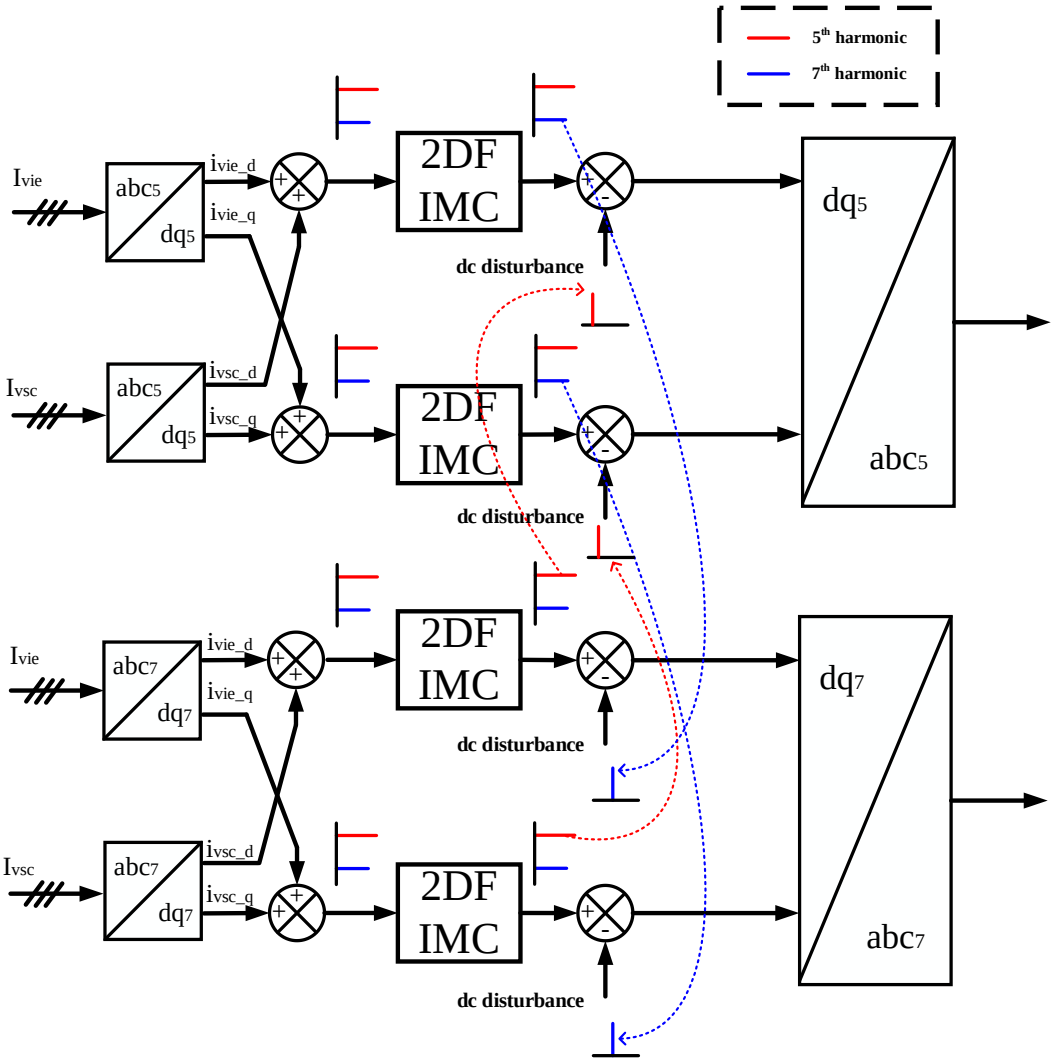

Fig. 5-6 Compensation process used 2DF-IMC controller

As described in section 3.3.4, The equations defining the dynamics of the *dq* fundamental and harmonic currents between VSC and the AC grid are:

$$v_{n\_d\_inv} = ri_{n\_d} + ldi_{n\_d}/dt - \omega_s li_{n\_q} - v_d \qquad (5.2)$$
$$v_{n\_q\_inv} = ri_{n\_q} + ldi_{n\_q}/dt + \omega_s li_{n\_d} - v_q$$

Where r and l are, respectively, the equivalent resistance and inductance between the VSC and the AC grid, i_{n_d} and i_{n_q} are the average *dq* current components of the n harmonic, $v_{n\_d\_inv}$ and $v_{n\_q\_inv}$ are the *dq* components of the n harmonic of the average voltages generated by the VSC, and v_d and v_q are the *dq* voltage components of the offshore AC grid.

The transfer functions between the *dq* VSC harmonic currents and the *dq* VSC harmonic voltages can be represented by the same equation if the cross-coupling terms ($\omega_s l i_{n_q}$and $\omega_s l i_{n\_d}$), and the grid voltage components (v_d and v_q) from Equation (5.2) are considered disturbances, not present during the calculation of the *dq* current control but instead being numerically compensated by a feedforward loop. Hence, the VSC current-to-voltage relationships in the *dq* frame are given:

$$\frac{i_{n\_d}(s)}{v_{n\_d\_inv}(s)} = \frac{i_{n\_q}(s)}{v_{n\_q\_inv}(s)} = \frac{i_n(s)}{v_{n\_inv}(s)} = G_i(s) = \frac{1}{ls + r} \tag{5.3}$$

The inner feedback loop is implemented in the plant by making the input signal to the plant equal to

$$M_i(s) = 1/(R_i + ls + r) \tag{5.4}$$

The inner feedback loop is implemented in the plant by making the input signal to the plant equal to

$$v_{n\_inv}(s) = v_{n\_inv}'(s) - i_n(s)R_i \tag{5.5}$$

Under this scenario, the 2DF-IMC control constants are

$$Kp_i = \alpha_i l \quad Ki_i = (r + R_i)\alpha_i \tag{5.6}$$

Where α_i is the bandwidth of the closed loop system and is selected based on the response speed of the controllers. If the gain of R_i is selected to match the pole of $M_i(s)$ with the pole of $F_i(s)$ on the transfer function from the disturbance $d_i(s)$ to the output of the plant, then $R_i$is required to have the value of

$$R_i = \alpha_i l - r \tag{5.7}$$

With the value of R_i specified by Equation (5.7), the relationship between the output voltage and disturbances $v_{n\_inv}(s)/d_{n\_i}(s)$ becomes

$$v_{\_inv}(s)/d_i(s) = s/(l(\alpha_i + s)^2) \quad (5.8)$$

As seen in Equation (5.8), the disturbances $d_i(s)$ are rejected by the plant and the controller with the same time constant, which in turn depends on α_i.

5.4 Simulation results

As shown in Fig. 5-7, the 2DF-IMC will replace the PI controller in the SRF harmonic compensation processing, and then the performance result will be presented, and the response time is compared with the SRF-PI speed of response. In this test, the hybrid converter based on the Vienna rectifier and VSC converter is used, as shown in Appendix C, and the harmonics controller based on 2DF-IMC in the PSCAD model is shown in Appendix C.7 2DF-IMC SRF Harmonic Controller. The simulation time step is 20 *us.*

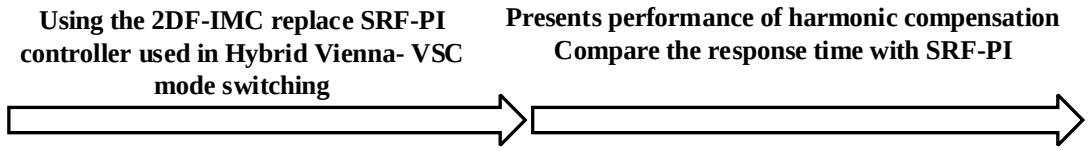

Fig. 5-7 Simulation test

In order to test the features of 2DF-IMC, the PSCAD model used the Vienna-VSC hybrid converter model. In this model, the auxiliary mode is prepared to provide harmonic compensation when the IGBTs of the Vienna rectifier are faulty. The test model sets the IGBTs of the Vienna rectifier switching fault at 5 s, then the Vienna rectifier functions as a non-IGBT Vienna rectifier and runs at 3 s. Finally, the harmonic current compensation controller is enabled.

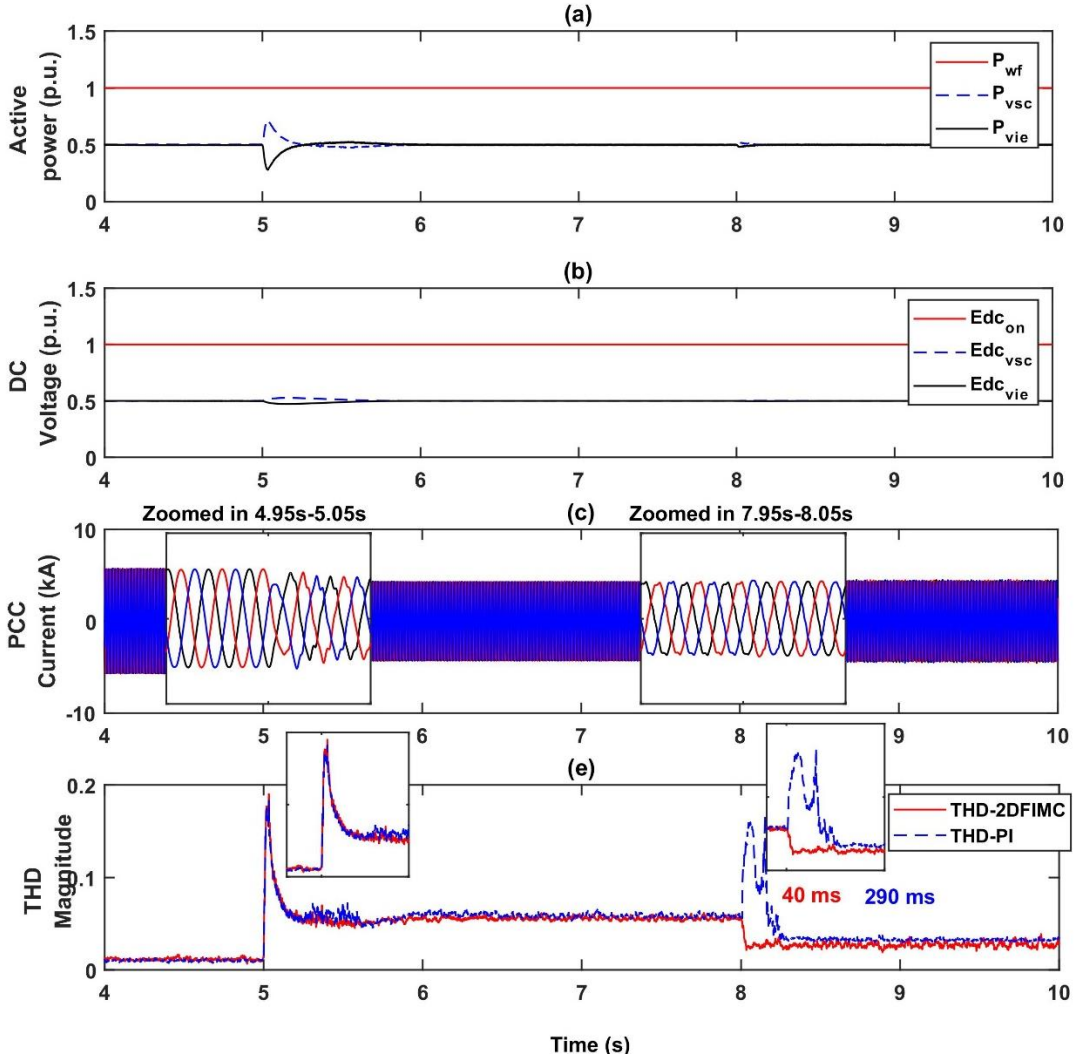

Fig. 5-8 Performance of hybrid HVDC system operated from normal control mode to backup ancillary mode (a) Active power of hybrid converter components, (b) DC link voltage of hybrid converter components, (c) PCC current during the Vienna rectifier operated as 6P-DR (4.95s - 5.05s), (d) PCC current during backup ancillary mode enabled, (e) THD of PCC current during the Vienna rectifier operated as 6P-DR (4.95s - 5.05s), (f) THD of PCC current during backup ancillary mode enabled

Fig. 5-8 shows the performance as the hybrid converter switches from the normal mode to the backup ancillary mode. Fig. 5-8 (a) and (b) show the basic performance active power and DC voltage, respectively. Fig. 5-8 (c) shows the PCC current waveform from 4.95 s to 5.05 s, which is the switching point from the normal mode to

the non-IGBT Vienna rectifier function mode. Fig. 5-8 (d) provides the second switching point when the hybrid converter enables the backup ancillary mode using the 2DF-IMC harmonic current compensation controller.

Fig. 5-8 (d) and (e) show the THD value during the running time to present the response speed of the harmonics compensation controller. For comparison, the compensation result used by the 2DF-IMC controller is compared to the result of the conventional PI controller. The red line represents the trend of THD results using 2DF-IMC, while the blue line is the trend of THD results using the conventional PI controller. With this presentation of the results in the time domain, the compensation response time is 40 ms when using the 2DF-IMC controller and 290 ms when using the PI controller. The response time of harmonic compensation is improved when the low pass filter influence is eliminated using the 2DF-IMC.

5.5 Summary

This chapter proposed a fast harmonic current compensation controller, which is applied in the 2DF-IMC controller based on the fundamental SRF-PI controller. In addition, the harmonic compensation controller used by 2DF-IMC was tested in a Vienna rectifier – VSC hybrid converter PSCAD model. The typical controllers used in harmonic filtering were also introduced in this chapter to show the advantages and disadvantages. The use of 2DF-IMC improves the conventional PI controller to provide a fast response to set-point without a tracking error. In this configuration, the 2DF-IMC removes the low-pass filter effect. This increases the closed-loop response time of the system without filter stages and provides a more attractive option for the deployment of hybrid offshore systems.

Chapter 6 Conclusion and future work

6.1 Conclusions

This thesis focuses on the modelling, design and operation of a hybrid converter used in offshore HVDC system, where a hybrid converter is used in series connect with other power electronic converters on the offshore side and the VSC converter is used at onshore.

In this thesis, an improved hybrid converter topology that consists of a 6-pulse diode rectifier and a voltage source converter is proposed. The improved converter topology reduces the complexity of the existing hybrid converter that is based on 12 pulse diode rectifier that is normally caused by its three winding three phase transformer, which in turn reduces the cost and footprint of the system. Also, two control strategies related to the improved hybrid converter have been proposed, one using a hybrid converter functions as the grid forming converter to provide stabilized voltage and frequency, and the other using a wind turbine as the grid forming converter. Notwithstanding, the 5^{th} and 7^{th} harmonic currents increase at PCC because of the reduced number of rectifier diodes. Here, the VSC converter of the hybrid converter not only controls the AC voltage and/or DC voltage but also controls the harmonic current compensation to cancel the 5^{th}, 7^{th}, 11^{th} and 13^{th} harmonic current at PCC. The SRF technique, based on the PI controller was introduced in the hybrid converter control system for individual harmonic current compensation with an easy-to-tune process and zero steady-state error.

According to the findings of the previous study, the wind turbine converter functions as the grid-forming converter, and the novel hybrid converter based on an advanced Vienna rectifier and VSC converter has been proposed. Due to the low

harmonic characteristics of the Vienna rectifier, the novel hybrid converter exhibits the low harmonic feature at PCC. Meanwhile, the proposed novel hybrid converter has a lower cost and higher reliability compared to the existing solutions. In this configuration, the hybrid converter inherently has lower harmonics without using any other active power filter requirements in normal operation conditions. In addition, the backup ancillary capability is ready to engage in case of the switches of the Vienna rectifier fail. When any IGBTs of the Vienna rectifier are faulty, the VSC converter of the hybrid converter will perform as an active power filter via SRF technique based on PI controller. With this control strategy, the built-in active power filter is able to regulate the proposed control demand and desired PCC current quality. Finally, the proposed configuration allows a wider variety of power and DC voltage rations between the Vienna rectifier and the series VSC converter. User can select an appropriate ratio based in their requirements, including the amount of bi-directional power flow for black start capability voltage control, harmonic current suppression and DC voltage level allowed for the IGBT switches. Furthermore, compared to the existing DR station, the proposed novel hybrid converter does not require an additional large footprint size filter at the offshore side. On the other hand, compared to VSC converters, hybrid converters have a lower cost and a smaller footprint. Additionally, switching losses are lower due to the reduction in IGBTs.

Although the SRF technique based on the PI controller provides a simple tune process for harmonics compensation, its response is slow because of the low pass filter used in its control structure. To increase the harmonic compensation response, especially in the times of mode changing in the hybrid converter based on the Vienne rectifier and VSC, the 2DF-IMC controller is proposed to cancel out the harmonic current at the PCC point in the hybrid converter application. This harmonics compensation controller results in a much faster overall THD reduction. The reason

for this feature is that the 2DF-IMC controller has a strong disturbance rejection capability, and the low pass filter is removed from the harmonics compensation control loop. The proposed 2DF-IMC controller provides a fast response time to setpoint, an easy-to-tune process without steady-state error.

All test models were built in the PSCAD/EMTDC environment to test the performance of proposed hybrid converters used in offshore HVDC systems. The PSCAD models are shown in Appendix. The simulation results indicate adequate and stable performance for the proposed solutions, like the hybrid converter modelling and design of the harmonic compensation controller discussion, which paves the way to considering hybrid converters in future offshore HVDC systems.

6.2 Suggestions for future work

Based on the findings and conclusions of the accomplished work, potential areas of future work have been identified and are presented in the following sub-sections, which can further enhance the security and reliability of hybrid converters. Here are the potential areas that can be improved in the hybrid converter. The suggestion includes:

6.2.1 Small signal modelling for the stability analysis of the proposed hybrid converter

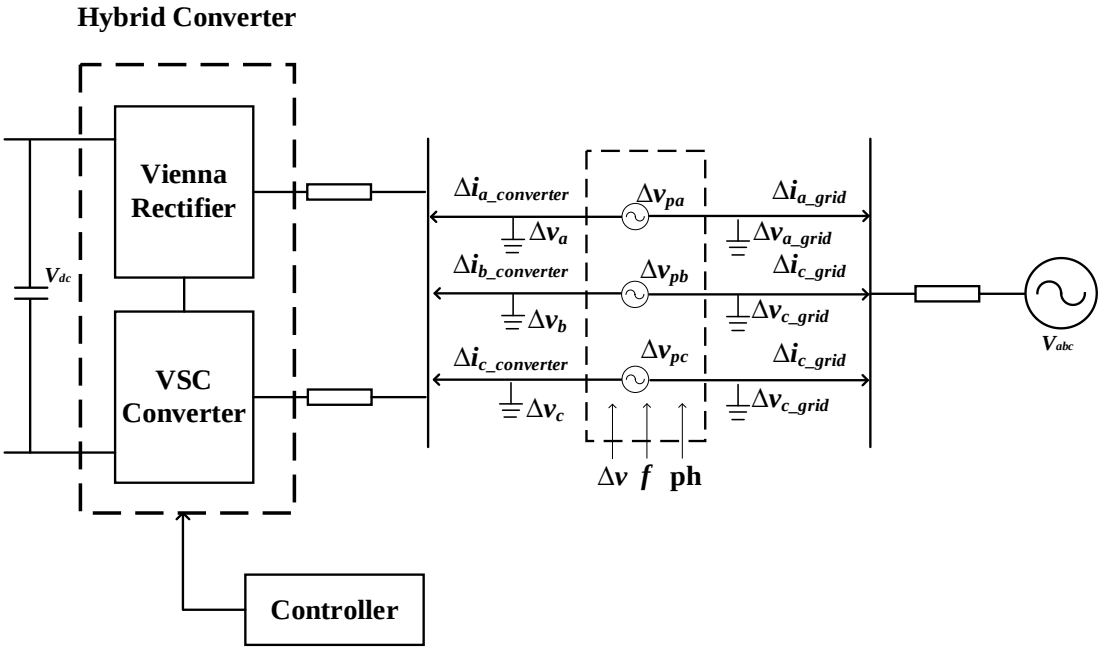

Fig. 6-1 A suggested frequency scan method used for small signal analysis

For a hybrid converter, small signal analysis has the potential to provide valuable insights in terms of stability analysis, converter design, controller interactions, and parameter sensitivity. To perform small signal analysis, it is necessary to understand the mathematical model of the proposed hybrid converter and develop circuit

equations or equivalent circuit models based on its topology and component characteristics. Additionally, the converter needs to be linearized, which typically involves defining the model around a specific operating point to represent it as a linear transfer function.

When performing simulations, particularly in the case of time domain simulations using tools such as Simulink or PSCAD. An injection point needs to be determined, which can involve applying a perturbation voltage or current to the system. And the interested frequency range and frequency step also need to be determined. The admittance and impedance can be calculated by recording voltage and current when the disturbance is injected during the simulation. The admittance plot and impedance plot can be generated for analysis. Another thing that needs to be suggested is the analysis frame, the *dq* frame, the Alpha/beta frame, and the PN0 frame, which can be considered [85, 86].

By injecting the perturbation voltage, frequency and phase to capture the voltage and current following into the converter and calculating the admittance and impedance of the converter. On the other hand, the voltage and current flowing into the grid are also captured, and the relative admittance and impedance are calculated. In addition, the Nyquist plot is also generated to analyse the system stability, which is to note the frequency of interest.

For a hybrid converter, frequency scans can be conducted at various operational modes to compare impedance plots under different conditions. For example, compared to the hybrid converter based on Vienna rectifier and VSC converter when it runs in normal control mode or backup ancillary mode.

6.2.2 Improving Technology Readiness Levels of the Proposed Hybrid

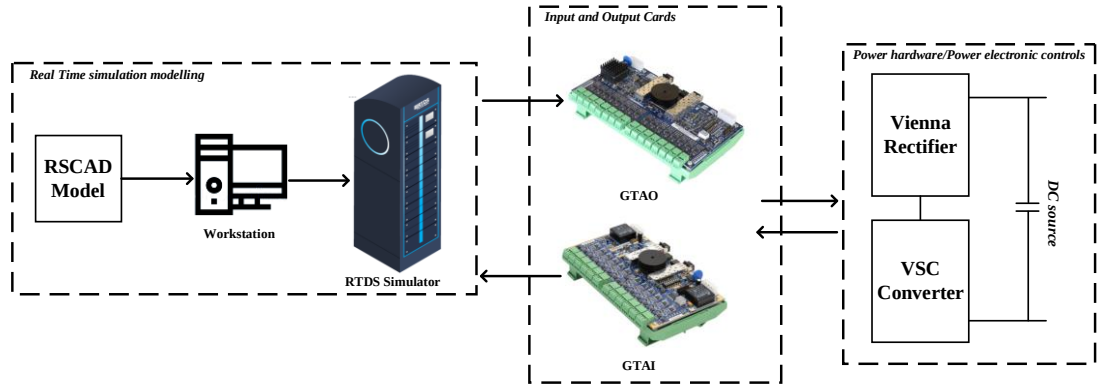

Fig. 6-2 Hardware-in-the-loop

The hardware-in-the-loop testing is also one of the suggestions for future work. There are many real time simulation software that can used for building real time simulation model, like RSCAD software developed by RTDS Technologies [87], and RT-Lab developed by OPAL-RT [88]. Hardware development can prove the hybrid converter can be used in the real-time simulation environment, which improves its Technology Readiness Levels (TRL). Figure 6-2 shows the structure of the hardware-in-the-loop. The references [89, 90] present hardware-in-the-loop testing of the grid-forming converter

6.2.3 Wider applications of using more advanced power electronics in proposed hybrid converter

The MMC converter can be considered an option to replace the 2-level VSC converter of the hybrid converter. The MMC converter can be controlled as a grid-forming converter to regulate offshore AC networks. Meanwhile, the hybrid converter can connect to offshore wind turbines, and wind turbines can perform in the grid-following mode. In addition, the MMC converter can also be considered to limit fault currents in the event of a fault.

6.2.4 Protection and Black Start capability of Hybrid Converter

The hybrid converter is regarded as a unidirectional converter topology, and the black start needs to be considered. In [91], a black-start strategy is proposed that utilizes the low-voltage-ride-through capability of wind turbine converters. With the DR and transformer switches closed, it is possible to avoid current inrush or overvoltage, as well as balance the active power of the system during black-start. In addition, the fault ride-through of the hybrid converter is also worthy of being discussed in future study, like Reference [51] shows a solution to avoid over-voltage during offshore AC faults in the hybrid converter based on FB-MMC and DR.

Reference

[1] Gov.UK. "Net Zero Strategy: Build Back Greener." Department for Energy Security and Net Zero and Department for Business, Energy & Industrial Strategy. https://www.gov.uk/government/publications/net-zero-strategy (accessed 24/07/24, 2023).

[2] European Commission. "A European Green Deal." https://commission.europa.eu/strategy-and-policy/priorities-2019-2024/european-green-deal_en (accessed 24/07/23, 2023).

[3] Gov.UK. "UK becomes first major economy to pass net zero emissions law." Department for Business, Energy & Industrial Strategy and The Rt Hon Chris Skidmore MP. Department for Business, Energy & Industrial Strategy and The Rt Hon Chris Skidmore MP (accessed 24/07, 2023).

[4] Naitonal Grid ESO. "Road to Zero Carbon in numbers." https://www.nationalgrideso.com/future-energy/our-progress-towards-net-zero/road-zero-carbon-numbers (accessed 24/07, 2023).

[5] Wind Europe. "Wind energy in Europe: 2022 Statistics and the outlook for 2023-2027." https://windeurope.org/intelligence-platform/product/wind-energy-in-europe-2022-statistics-and-the-outlook-for-2023-2027/ (accessed 24/07, 2023).

[6] Naitonal Grid TO. "How much of the UK's energy is renewable?" https://www.nationalgrid.com/stories/energy-explained/how-much-uks-energy-renewable (accessed 24/07, 2023).

[7] C.J. Pillay, M. Kabeya and I.E. Davidson, "Transmission systems: HVAC vs HVDC", In Proceedings of the International Conference on Industrial Engineering and Operations Management (IEOM), August 10 – 14, 2020, Detroit, Michigan, USA..

[8] O. Anaya-Lara, N. Jenkins, J. B. Ekanayake, P. Cartwright, and M. Hughes,

"Power Electronics for Wind Turbines," in Wind Energy Generation: Modelling and Control. John Wiley & Sons, 2011,pp. 19-36.

[9] O. Anaya-Lara, D. Campos-Gaona, E. Moreno-Goytia, and G. Adam, *"Offshore Wind Energy Systems"* in Offshore wind energy generation: control, protection, and integration to electrical systems. John Wiley & Sons, 2014,pp1-14.

[10] J. Dakic, M. Cheah-Mane, O. Gomis-Bellmunt and E. Prieto-Araujo, "HVAC Transmission System for Offshore Wind Power Plants Including Mid-Cable Reactive Power Compensation: Optimal Design and Comparison to VSC-HVDC Transmission," in IEEE Transactions on Power Delivery, vol. 36, no. 5, pp. 2814-2824, Oct. 2021, doi: 10.1109/TPWRD.2020.3027356.

[11] M. Qian, D. Zhao, N. Chen, Y. Wang and Z. Hu, "Characteristic Analysis of Overvoltage in Offshore Wind Power Transmission System through HVAC Submarine Cable," 2021 IEEE Sustainable Power and Energy Conference (iSPEC), Nanjing, China, 2021, pp. 366-370, doi: 10.1109/iSPEC53008.2021.9735711.

[12] A. Alassi, S. Bañales, O. Ellabban, G. Adam, and C. MacIver, "HVDC transmission: Technology review, market trends and future outlook," *Renewable and Sustainable Energy Reviews,* vol. 112, pp. 530-554, 2019, doi: 10.1016/j.rser.2019.04.062.

[13] D. Van Hertem, O. Gomis-Bellmunt, and J. Liang, *"HVDC TECHNOLOGY AND TECHNOLOGY FOR OFFSHORE GRIDS"* in HVDC grids: for offshore and supergrid of the future. John Wiley & Sons, 2016, pp 45-107.

[14] H. Xiao, K. Sun, J. Pan, Y. Li, and Y. Liu, "Review of hybrid HVDC systems combining line communicated converter and voltage source converter," *International Journal of Electrical Power & Energy Systems,* vol. 129, p. 106713, 2021, doi: 10.1016/j.ijepes.2020.106713.

[15] A. Stan, S. Costinaș, and G. Ion, "Overview and assessment of HVDC current applications and future trends," *Energies,* vol. 15, no. 3, p. 1193, 2022, doi: 10.3390/en15031193.

[16] Siemens Energy. "High-Voltage Direct Current (HVDC) Transmission Solutions." https://www.siemens-energy.com/global/en/offerings/power-transmission/portfolio/high-voltage-direct-current-transmission-solutions.html (accessed 25/07, 2023).

[17] Rte. International. "Newsletter HVDC." https://www.rte-international.com/newsletter-hvdc/?lang=en (accessed 30/07, 2023).

[18] S. W. Ali et al., "Offshore Wind Farm-Grid Integration: A Review on Infrastructure, Challenges, and Grid Solutions," in IEEE Access, vol. 9, pp. 102811-102827, 2021, doi: 10.1109/ACCESS.2021.3098705.

[19] B. Yang *et al.*, "A critical survey of technologies of large offshore wind farm integration: Summary, advances, and perspectives," *Protection and Control of Modern Power Systems,* vol. 7, no. 1, p. 17, 2022, doi: 10.1186/s41601-022-00239-w.

[20] A. R. Nejad *et al.*, "Wind turbine drivetrains: state-of-the-art technologies and future development trends," *Wind Energy Science,* vol. 7, no. 1, pp. 387-411, 2022, doi: 10.5194/wes-7-387-2022.

[21] M. Q. Duong, F. Grimaccia, S. Leva, M. Mussetta, and E. Ogliari, "Pitch angle control using hybrid controller for all operating regions of SCIG wind turbine system," *Renewable Energy,* vol. 70, pp. 197-203, 2014, doi: 10.1016/j.renene.2014.03.072.

[22] R. Kumar et al., "A Review on Transverse Flux Permanent Magnet Machines for Wind Power Applications," in IEEE Access, vol. 8, pp. 216543-216565, 2020, doi: 10.1109/ACCESS.2020.3041217.

[23] H. Cui, P. Chao, X. Cui, X. Liu and W. Li, "Identification Method for LVRT

Control Parameters of Type-3 wind turbine Based on Short-Circuit Fault Frequency Model," 2023 IEEE 6th International Electrical and Energy Conference (CIEEC), Hefei, China, 2023, pp. 4594-4599, doi: 10.1109/CIEEC58067.2023.10166085.

[24] F. Alatar and A. Mehrizi-Sani, "Frequency scan–based mitigation approach of subsynchronous control interaction in type-3 wind turbines," *Energies,* vol. 14, no. 15, p. 4626, 2021,doi: 10.3390/en14154626.

[25] S. Sang, C. Zhang, X. Cai, M. Molinas, J. Zhang and F. Rao, "Control of a Type-IV Wind Turbine With the Capability of Robust Grid-Synchronization and Inertial Response for Weak Grid Stable Operation," in IEEE Access, vol. 7, pp. 58553-58569, 2019, doi: 10.1109/ACCESS.2019.2914334..

[26] Y. Li, L. Fan and Z. Miao, "Wind in Weak Grids: Low-Frequency Oscillations, Subsynchronous Oscillations, and Torsional Interactions," in IEEE Transactions on Power Systems, vol. 35, no. 1, pp. 109-118, Jan. 2020, doi: 10.1109/TPWRS.2019.2924412.

[27] GE. "HVDC Systems : Connecting Renewable Energy and Power Grids for a Sustainable Future." https://www.gegridsolutions.com/systems_services/catalog/hvdc/ (accessed 28/07, 2023).

[28] O. E. Oni, I. E. Davidson and K. N. I. Mbangula, "A review of LCC-HVDC and VSC-HVDC technologies and applications," 2016 IEEE 16th International Conference on Environment and Electrical Engineering (EEEIC), Florence, Italy, 2016, pp. 1-7, doi: 10.1109/EEEIC.2016.7555677.

[29] ABB. "Evolution of HVDC Light®." https://new.abb.com/news/detail/4224/evolution-of-hvdc-lightr (accessed 28/07, 2023).

[30] P. Sun, Y. Tian, J. Pou and G. Konstantinou, "Beyond the MMC: Extended

Modular Multilevel Converter Topologies and Applications," in IEEE Open Journal of Power Electronics, vol. 3, pp. 317-333, 2022, doi: 10.1109/OJPEL.2022.3175714.

[31] M. A. Perez, S. Ceballos, G. Konstantinou, J. Pou and R. P. Aguilera, "Modular Multilevel Converters: Recent Achievements and Challenges," in IEEE Open Journal of the Industrial Electronics Society, vol. 2, pp. 224-239, 2021, doi: 10.1109/OJIES.2021.3060791.

[32] Y. Tian, H. R. Wickramasinghe, Z. Li, J. Pou, and G. Konstantinou, "Review, classification and loss comparison of modular multilevel converter submodules for HVDC applications," *Energies,* vol. 15, no. 6, p. 1985, 2022, doi: 10.3390/en15061985.

[33] R. Blasco-Gimenez, S. Anó-Villalba, J. Rodriguez-D'Derlée, S. Bernal-Perez and F. Morant, "Diode-Based HVdc Link for the Connection of Large Offshore Wind Farms," in IEEE Transactions on Energy Conversion, vol. 26, no. 2, pp. 615-626, June 2011, doi: 10.1109/TEC.2011.2114886.

[34] J. W. Kolar, U. Drofenik and F. C. Zach, "VIENNA rectifier II-a novel single-stage high-frequency isolated three-phase PWM rectifier system," in IEEE Transactions on Industrial Electronics, vol. 46, no. 4, pp. 674-691, Aug. 1999, doi: 10.1109/41.778214.

[35] J. W. Kolar, U. Drofenik and F. C. Zach, "Current handling capability of the neutral point of a three-phase/switch/level boost-type PWM (VIENNA) rectifier," PESC Record. 27th Annual IEEE Power Electronics Specialists Conference, Baveno, Italy, 1996, pp. 1329-1336 vol.2, doi: 10.1109/PESC.1996.548754.

[36] A. Saadaoui, M. Ouassaid and M. Maaroufi, "Backstepping-Based Control of Vienna Rectifier for Electric Vehicle DC Ultra-Fast Charger," 2022 IEEE 21st Mediterranean Electrotechnical Conference (MELECON), Palermo, Italy,

2022, pp. 360-365, doi: 10.1109/MELECON53508.2022.9842893.

[37] J. L. Monroy-Morales, M. Hernández-Ángeles, D. Campos-Gaona, R. Peña-Alzola, M. Ordonez and W. Mérida, "Modeling and control design of a Vienna rectifier based electrolyzer," 2016 IEEE 7th International Symposium on Power Electronics for Distributed Generation Systems (PEDG), Vancouver, BC, Canada, 2016, pp. 1-8, doi: 10.1109/PEDG.2016.7527093.

[38] X. Jiang, J. Yang, J. Han and T. Tang, "A survey of cascaded multi-level PWM rectifier with VIENNA modules for HVDC system," 2014 International Power Electronics and Application Conference and Exposition, Shanghai, China, 2014, pp. 72-77, doi: 10.1109/PEAC.2014.7037831.

[39] A. Alili, M. B. Camara, and B. Dakyo, "Vienna Rectifier-Based Control of a PMSG Wind Turbine Generator," *Processes,* vol. 10, no. 2, p. 413, 2022.

[40] D. Reddy and S. Ramasamy, "Design of RBFN Controller Based Boost Type Vienna Rectifier for Grid-Tied Wind Energy Conversion System," in IEEE Access, vol. 6, pp. 3167-3175, 2018, doi: 10.1109/ACCESS.2017.2787567.

[41] S. Bozhko, G. Asher, R. Li, J. Clare and L. Yao, "Large Offshore DFIG-Based Wind Farm With Line-Commutated HVDC Connection to the Main Grid: Engineering Studies," in IEEE Transactions on Energy Conversion, vol. 23, no. 1, pp. 119-127, March 2008, doi: 10.1109/TEC.2007.914155.

[42] L. Guanglei, T. Wei, L. Guanyang, W. Hongzhao, W. Yaoyao and L. Guodong, "Research on LCC-MTDC and STATCOM technology for wind farms integration," 2017 IEEE Conference on Energy Internet and Energy System Integration (EI2), Beijing, China, 2017, pp. 1-6, doi: 10.1109/EI2.2017.8244413.

[43] Y. Jiao and H. Nian, "Grid-Forming Control for DFIG Based Wind Farms to Enhance the Stability of LCC-HVDC," in IEEE Access, vol. 8, pp. 156752-156762, 2020, doi: 10.1109/ACCESS.2020.3019691.

[44] L. Yu, "Control and operation of offshore wind farms connected with diode rectifier HVDC systems," 2019.

[45] S. V. Bozhko, R. Blasco-Gimenez, R. Li, J. C. Clare and G. M. Asher, "Control of Offshore DFIG-Based Wind Farm Grid With Line-Commutated HVDC Connection," in IEEE Transactions on Energy Conversion, vol. 22, no. 1, pp. 71-78, March 2007, doi: 10.1109/TEC.2006.889544.

[46] R. Li, S. Bozhko and G. Asher, "Frequency Control Design for Offshore Wind Farm Grid With LCC-HVDC Link Connection," in IEEE Transactions on Power Electronics, vol. 23, no. 3, pp. 1085-1092, May 2008, doi: 10.1109/TPEL.2008.921193.

[47] L. Wang and M. Sa-Nguyen Thi, "Stability Enhancement of a PMSG-Based Offshore Wind Farm Fed to a Multi-Machine System Through an LCC-HVDC Link," in IEEE Transactions on Power Systems, vol. 28, no. 3, pp. 3327-3334, Aug. 2013, doi: 10.1109/TPWRS.2013.2243765.

[48] G. -S. Lee, D. -H. Kwon, Y. -K. Kim and S. -I. Moon, "A New Communication-Free Grid Frequency and AC Voltage Control of Hybrid LCC-VSC-HVDC Systems for Offshore Wind Farm Integration," in IEEE Transactions on Power Systems, vol. 38, no. 2, pp. 1309-1321, March 2023, doi: 10.1109/TPWRS.2022.3171964.

[49] A. Korompili, Q. Wu, and H. Zhao, "Review of VSC HVDC connection for offshore wind power integration," *Renewable and Sustainable Energy Reviews,* vol. 59, pp. 1405-1414, 2016 , doi:10.1016/j.rser.2016.01.064.

[50] Z. Lu, Y. Ye and Y. Qiao, "An Adaptive Frequency Regulation Method With Grid-Friendly Restoration for VSC-HVDC Integrated Offshore Wind Farms," in IEEE Transactions on Power Systems, vol. 34, no. 5, pp. 3582-3593, Sept. 2019, doi: 10.1109/TPWRS.2019.2901986.

[51] R. Li and L. Xu, "A Unidirectional Hybrid HVDC Transmission System Based

on Diode Rectifier and Full-Bridge MMC," in IEEE Journal of Emerging and Selected Topics in Power Electronics, vol. 9, no. 6, pp. 6974-6984, Dec. 2021, doi: 10.1109/JESTPE.2020.3015342.

[52] C. Prignitz, H. -G. Eckel, S. Achenbach, F. Augsburger and A. Schön, "FixReF: A control strategy for offshore wind farms with different wind turbine types and diode rectifier HVDC transmission," 2016 IEEE 7th International Symposium on Power Electronics for Distributed Generation Systems (PEDG), Vancouver, BC, Canada, 2016, pp. 1-7, doi: 10.1109/PEDG.2016.7527013.

[53] A. Nami, J. L. Rodriguez-Amenedo, S. Arnaltes, M. Á. Cardiel-Álvarez and R. A. Baraciarte, "Frequency Control of Offshore Wind Farm With Diode-Rectifier-based HVdc Connection," in IEEE Transactions on Energy Conversion, vol. 35, no. 1, pp. 130-138, March 2020, doi: 10.1109/TEC.2019.2949892.

[54] O. Saborío-Romano, A. Bidadfar, J. N. Sakamuri, L. Zeni, Ö. Göksu and N. A. Cutululis, "Communication-Less Frequency Support From Offshore Wind Farms Connected to HVdc via Diode Rectifiers," in IEEE Transactions on Sustainable Energy, vol. 12, no. 1, pp. 441-450, Jan. 2021, doi: 10.1109/TSTE.2020.3004630.

[55] H. Xiao, X. Huang, Y. Huang and Y. Liu, "Self-Synchronizing Control and Frequency Response of Offshore Wind Farms Connected to Diode Rectifier Based HVDC System," in IEEE Transactions on Sustainable Energy, vol. 13, no. 3, pp. 1681-1692, July 2022, doi: 10.1109/TSTE.2022.3170717.

[56] L. Yu, R. Li and L. Xu, "Distributed PLL-Based Control of Offshore Wind Turbines Connected With Diode-Rectifier-Based HVDC Systems," in IEEE Transactions on Power Delivery, vol. 33, no. 3, pp. 1328-1336, June 2018, doi: 10.1109/TPWRD.2017.2772342.

[57] P. Project. "Progress on Meshed HVDC Offshore Transmission Networks -

EU's Horizon 2020." https://www.promotion-offshore.net/ (accessed 28/07, 2023).

[58] T. H. Nguyen and N. T. Quach, "A hybrid HVDC converter based on M2C and diode rectifiers without DC capacitors for offshore wind farm integration," *International Journal of Electrical Power & Energy Systems,* vol. 133, p. 107260, 2021, doi: 10.1016/j.ijepes.2021.107260.

[59] T. H. Nguyen, D. -C. Lee and C. -K. Kim, "A Series-Connected Topology of a Diode Rectifier and a Voltage-Source Converter for an HVDC Transmission System," in IEEE Transactions on Power Electronics, vol. 29, no. 4, pp. 1579-1584, April 2014, doi: 10.1109/TPEL.2013.2283368.

[60] T. H. Nguyen, Q. A. Le and D. -C. Lee, "A novel HVDC-link based on hybrid voltage-source converters," 2015 IEEE Energy Conversion Congress and Exposition (ECCE), Montreal, QC, Canada, 2015, pp. 3338-3343, doi: 10.1109/ECCE.2015.7310131.

[61] V. Habermann Avila and V. Leite, "Control of grid-connected inverter output current: a practical review," 2020 9th International Conference on Renewable Energy Research and Application (ICRERA), Glasgow, UK, 2020, pp. 232-235, doi: 10.1109/ICRERA49962.2020.9242710.

[62] B. Adineh, R. Keypour, P. Davari and F. Blaabjerg, "Review of Harmonic Mitigation Methods in Microgrid: From a Hierarchical Control Perspective," in IEEE Journal of Emerging and Selected Topics in Power Electronics, vol. 9, no. 3, pp. 3044-3060, June 2021, doi: 10.1109/JESTPE.2020.3001971.

[63] Sha, D.; Wu, D.; Liao, X.: 'Analysis of a hybrid controlled three-phase grid-connected inverter with harmonics compensation in synchronous reference frame', IET Power Electronics, 2011, 4, (7), p. 743-751, DOI: 10.1049/iet-pel.2010.0231 IET Digital Library, https://digital-library.theiet.org/content/journals/10.1049/iet-pel.2010.0231.

[64] L. Yan et al., "Multiple Synchronous Reference Frame Current Harmonic Regulation of Dual Three Phase PMSM With Enhanced Dynamic Performance and System Stability," in IEEE Transactions on Industrial Electronics, vol. 69, no. 9, pp. 8825-8838, Sept. 2022, doi: 10.1109/TIE.2021.3116553.

[65] W. Wang, C. Liu, S. Liu, Z. Song, H. Zhao and B. Dai, "Current Harmonic Suppression for Permanent-Magnet Synchronous Motor Based on Chebyshev Filter and PI Controller," in IEEE Transactions on Magnetics, vol. 57, no. 2, pp. 1-6, Feb. 2021, Art no. 8201406, doi: 10.1109/TMAG.2020.3017671.

[66] T. H. Nguyen, D. -C. Lee and Chan-Ki Kim, "A cost-effective converter system for HVDC links integrated with offshore wind farms," IECON 2013 - 39th Annual Conference of the IEEE Industrial Electronics Society, Vienna, Austria, 2013, pp. 7978-7983, doi: 10.1109/IECON.2013.6700466.

[67] D. Campos-Gaona, E. L. Moreno-Goytia and O. Anaya-Lara, "Fault Ride-Through Improvement of DFIG-WT by Integrating a Two-Degrees-of-Freedom Internal Model Control," in IEEE Transactions on Industrial Electronics, vol. 60, no. 3, pp. 1133-1145, March 2013, doi: 10.1109/TIE.2012.2216234.

[68] H. Zhou, W. Yao, K. Sun, H. Zhao, Q. Zong and J. Wen, "Two-Level Suppressing Controller of Offshore DC Overvoltage Using Zero-Sequence Voltage and GFL-GFM Switching," in IEEE Transactions on Power Delivery, vol. 38, no. 6, pp. 3991-4003, Dec. 2023, doi: 10.1109/TPWRD.2023.3294238.

[69] Y. Xiong et al., "Two-Level Combined Control Scheme of VSC-MTDC Integrated Offshore Wind Farms for Onshore System Frequency Support," in IEEE Transactions on Power Systems, vol. 36, no. 1, pp. 781-792, Jan. 2021, doi: 10.1109/TPWRS.2020.2998579.

[70] Y. Li, S. Liu, J. Zhu, X. Yuan, Z. Xu, and K. Jia, "Novel MTDC droop scheme with decoupled power control for enhancing frequency stabilities of weak AC

systems," *IET Renewable Power Generation,* vol. 14, no. 11, pp. 2007-2016, 2020, doi: 10.1049/iet-rpg.2019.1503.

[71] H. Zhang, W. Xiang and J. Wen, "Dual Grid-Forming Control With Energy Regulation Capability of MMC-HVDC System Integrating Offshore Wind Farms and Weak Grids," in IEEE Transactions on Power Systems, vol. 39, no. 1, pp. 261-272, Jan. 2024, doi: 10.1109/TPWRS.2023.3244807.

[72] F. Kamal, H. M. M. Maruf, B. H. Chowdhury and M. Manjrekar, "DC Voltage Control for Power Sharing in MT-HVDC Connecting Offshore Wind Farm with Onshore Grid," 2019 SoutheastCon, Huntsville, AL, USA, 2019, pp. 1-6, doi: 10.1109/SoutheastCon42311.2019.9020620.

[73] H. Zhang, W. Xiang, Y. He, and J. Wen, "Optimal Energy Utilization of MMC-HVDC System Integrating Offshore Wind Farms for Onshore Weak Grid Inertia Support," *IEEE Transactions on Power Systems,* 2023.

[74] H. Zhang, W. Xiang, Y. He and J. Wen, "Optimal Energy Utilization of MMC-HVDC System Integrating Offshore Wind Farms for Onshore Weak Grid Inertia Support," in IEEE Transactions on Power Systems, vol. 39, no. 1, pp. 1304-1318, Jan. 2024, doi: 10.1109/TPWRS.2023.3239166.

[75] J. D. Irwin and R. M. Nelms, *"Resistive Circuits"* in Basic engineering circuit analysis. John Wiley & Sons, 2020, pp 19-79.

[76] A. S. Satpathy, D. Kastha and N. K. Kishore, "Vienna Rectifier-Fed Squirrel Cage Induction Generator Based Stand-Alone Wind Energy Conversion System," in IEEE Transactions on Power Electronics, vol. 36, no. 9, pp. 10186-10198, Sept. 2021, doi: 10.1109/TPEL.2021.3062694.

[77] J. Moriano, M. Ordonez, M. Rizo and E. Bueno, "Harmonic Compensation Optimization for Multiple Parallel Distributed Generators," in IEEE Transactions on Power Electronics, vol. 34, no. 7, pp. 7103-7112, July 2019, doi: 10.1109/TPEL.2018.2881164.

[78] J. L. Monroy Morales, M. H. Ángeles, D. Campos-Gaona and R. Peña-Alzola, "Control design of a neutral point clamped converter based active power filter for the selective harmonic compensation," 2016 IEEE PES Transmission & Distribution Conference and Exposition-Latin America (PES T&D-LA), Morelia, Mexico, 2016, pp. 1-7, doi: 10.1109/TDC-LA.2016.7805687.

[79] ENTSO-E. "European Network of Transmission System Operators for Electricity." https://www.entsoe.eu/ (accessed 29/07, 2023).

[80] E.-E. AISBL, "Offshore transmission technology," *Report, November,* 2011.

[81] R. Li, L. Yu, and L. Xu, "Operation of offshore wind farms connected with DRU-HVDC transmission systems with special consideration of faults," *Global Energy Interconnection,* vol. 1, no. 5, pp. 608-617, 2018, doi: 10.14171/j.2096-5117.gei.2018.05.010.

[82] L. Yu, L. Xu, J. Zhu and R. Li, "Impedance Modelling and Stability Analysis of Diode-Rectifier based HVDC Connected Offshore Wind Farms," in IEEE Transactions on Power Delivery, vol. 37, no. 1, pp. 591-602, Feb. 2022, doi: 10.1109/TPWRD.2021.3065572.

[83] D. Campos-Gaona, R. Peña-Alzola, J. L. Monroy-Morales, M. Ordonez, O. Anaya-Lara and W. E. Leithead, "Fast Selective Harmonic Mitigation in Multifunctional Inverters Using Internal Model Controllers and Synchronous Reference Frames," in IEEE Transactions on Industrial Electronics, vol. 64, no. 8, pp. 6338-6349, Aug. 2017, doi: 10.1109/TIE.2017.2682003.

[84] S. U. Islam *et al.*, "Design of a proportional resonant controller with resonant harmonic compensator and fault ride trough strategies for a grid-connected photovoltaic system," *Electronics,* vol. 7, no. 12, p. 451, 2018, doi: 10.3390/electronics7120451.

[85] Y. Liao and X. Wang, "Small-Signal Modeling of AC Power Electronic Systems: Critical Review and Unified Modeling," in IEEE Open Journal of

Power Electronics, vol. 2, pp. 424-439, 2021, doi: 10.1109/OJPEL.2021.3104522.

[86] Y. Xu, M. Zhang, L. Fan and Z. Miao, "Small-Signal Stability Analysis of Type-4 Wind in Series-Compensated Networks," in IEEE Transactions on Energy Conversion, vol. 35, no. 1, pp. 529-538, March 2020, doi: 10.1109/TEC.2019.2943578.

[87] RTDS. "RTDS Technologies AMETEK." https://www.rtds.com/ (accessed 29/07, 2023).

[88] OPAL-RT. "OPAL-RT TECHNOLOGIES." https://www.opal-rt.com/ (accessed 29/07, 2023).

[89] Z. Feng, A. Alassi, M. Syed, R. Peña-Alzola, K. Ahmed and G. Burt, "Current-Type Power Hardware-in-the-Loop Interface for Black-Start Testing of Grid-Forming Converter," IECON 2022 – 48th Annual Conference of the IEEE Industrial Electronics Society, Brussels, Belgium, 2022, pp. 1-7, doi: 10.1109/IECON49645.2022.9968517.

[90] A. Alassi, Z. Feng, K. Ahmed, M. Syed, A. Egea-Alvarez, and C. Foote, "Grid-forming VSM control for black-start applications with experimental PHiL validation," *International Journal of Electrical Power & Energy Systems,* vol. 151, p. 109119, 2023, doi: 10.1016/j.ijepes.2023.109119.

[91] Z. Yu et al., "Black-start strategy of the HVDC system based on series-connected hybrid converter for offshore wind farms," 18th International Conference on AC and DC Power Transmission (ACDC 2022), Online Conference, China, 2022, pp. 1153-1157, doi: 10.1049/icp.2022.1364.

Appendix

Appendix A Hybrid Converter Based on the Diode rectifier and VSC Converter

A.1Hybrid Converter

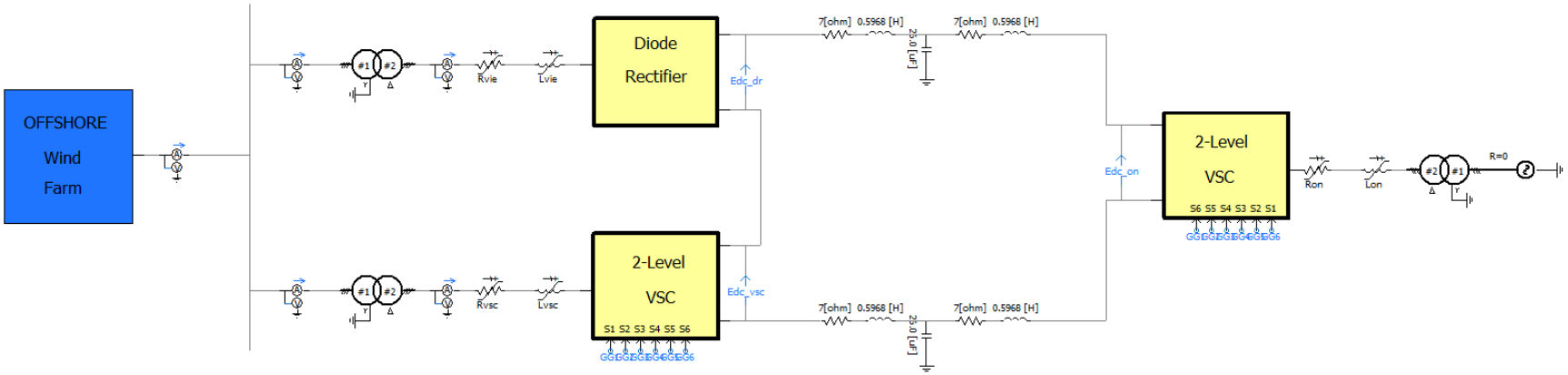

A.2Diode Rectifier

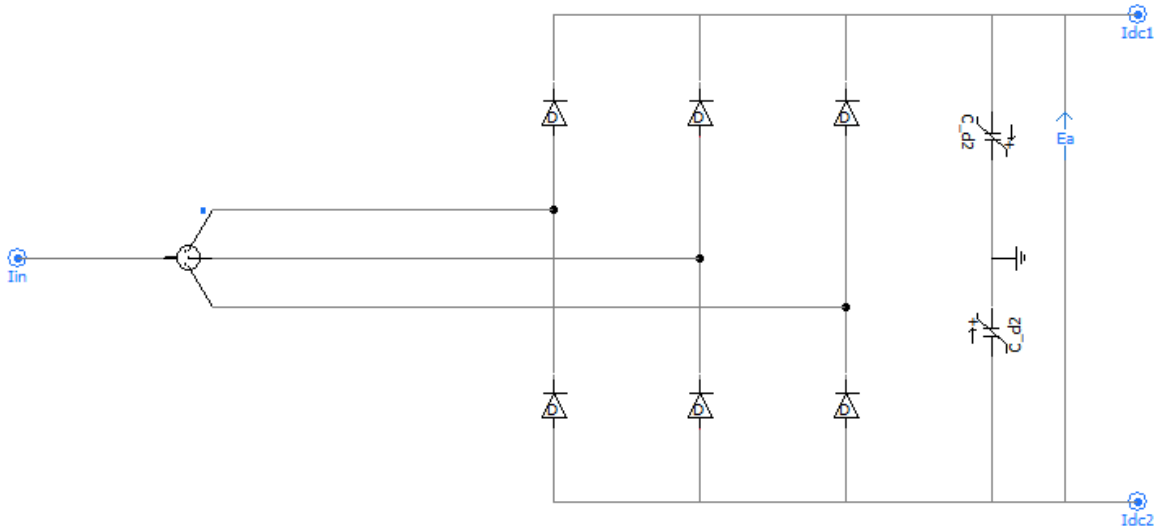

A.3VSC Converter

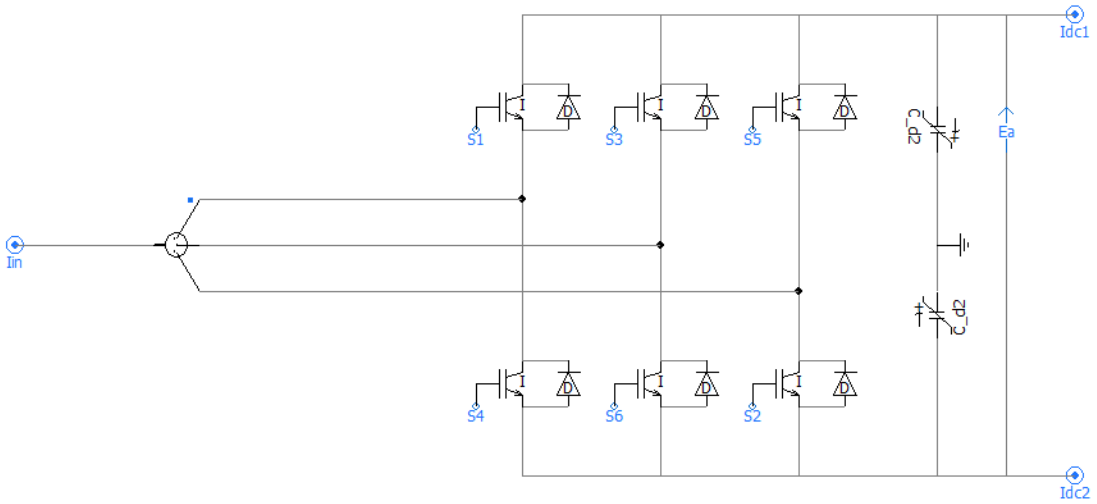

A.4VSC Control System – 1

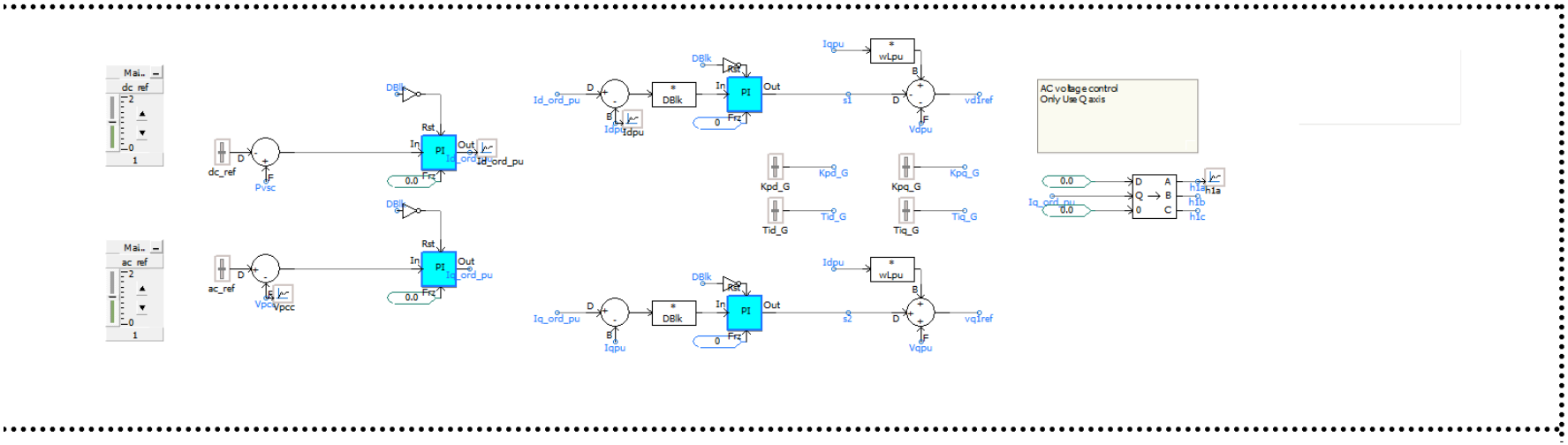

A.5 VSC Control System – 2

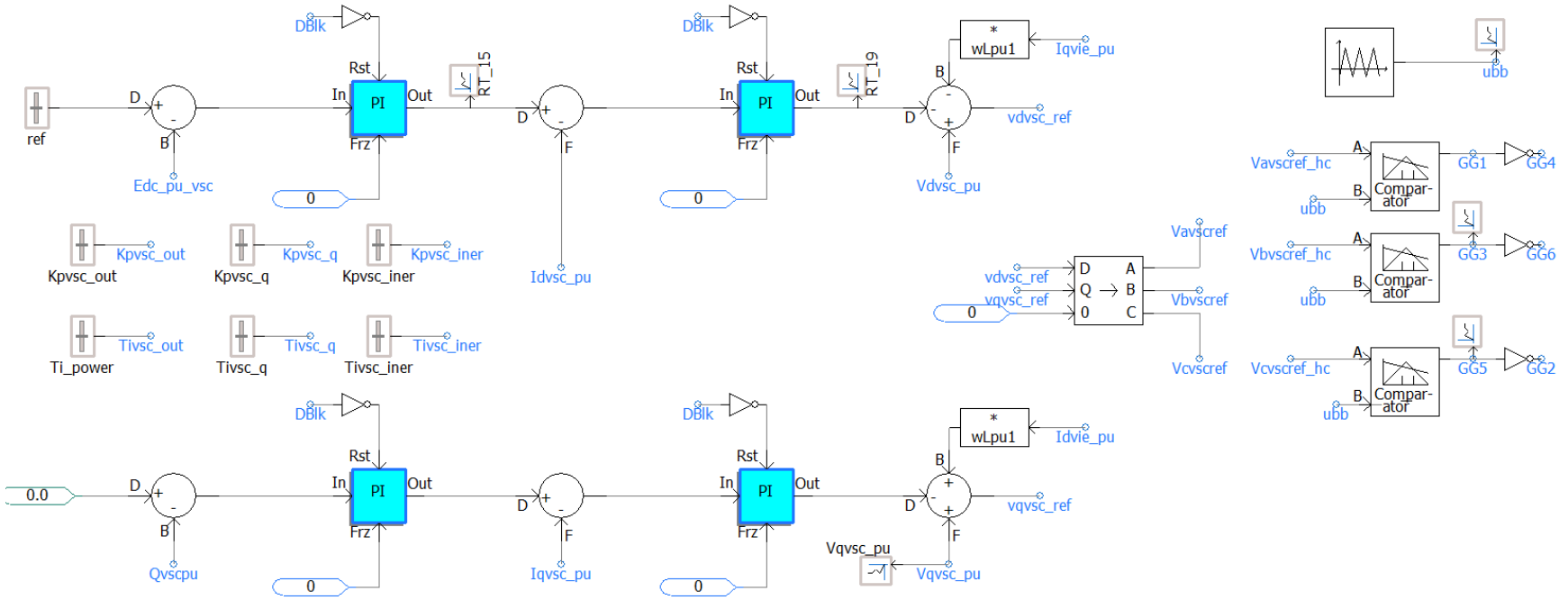

A.6SRF Harmonic Controller

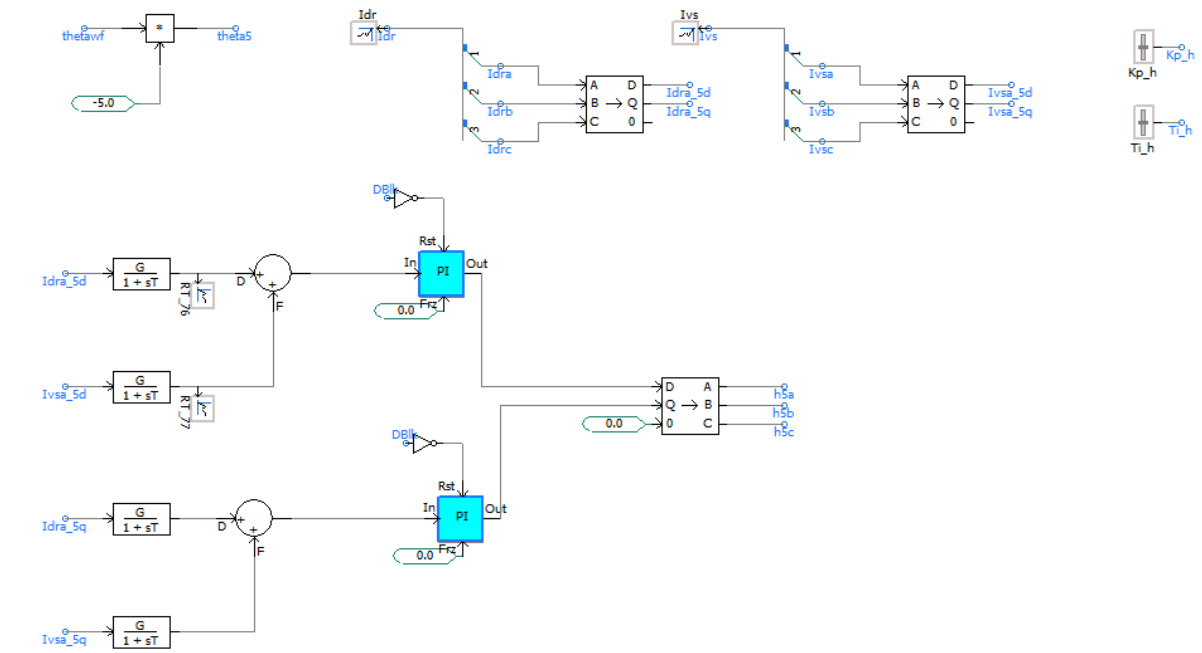

A.7Offshore Wind Farm – 2

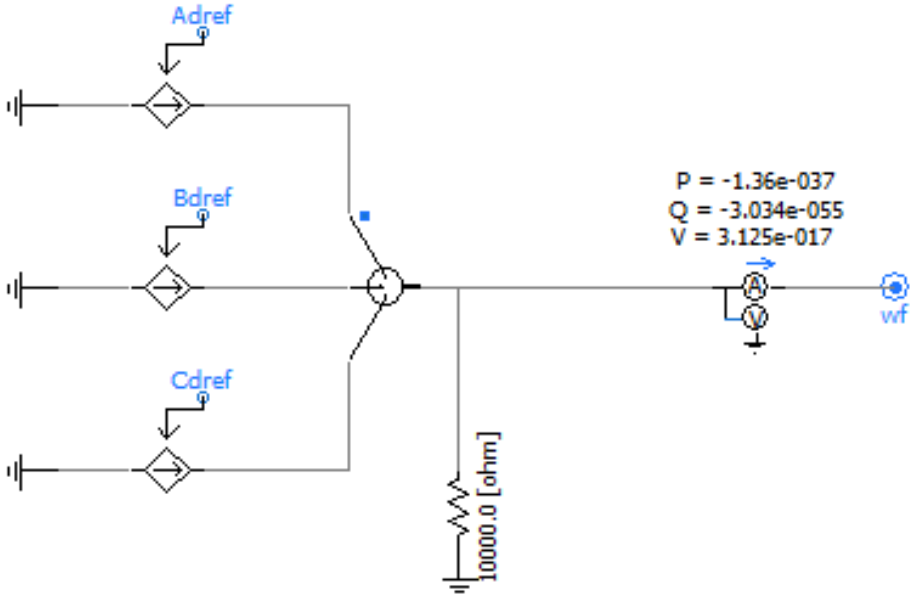

A.8Offshore Wind Farm Control system – 1

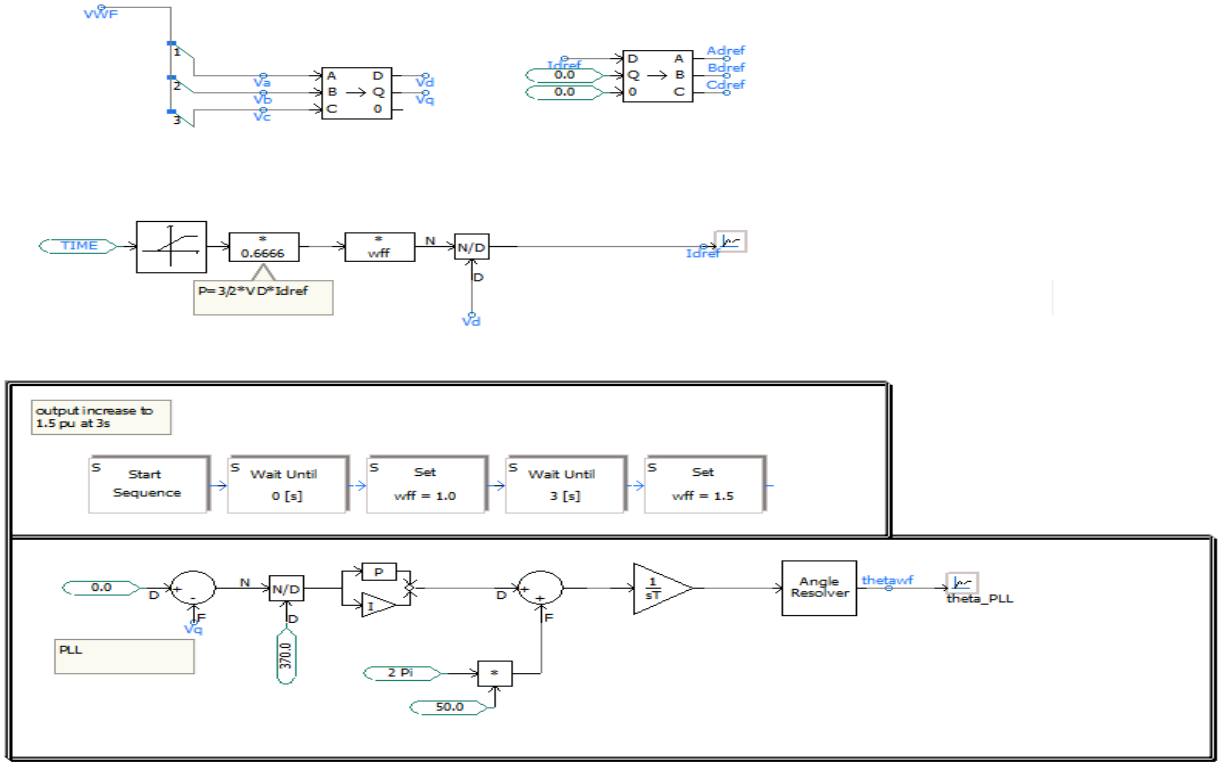

A.9Offshore Wind Farm – 2

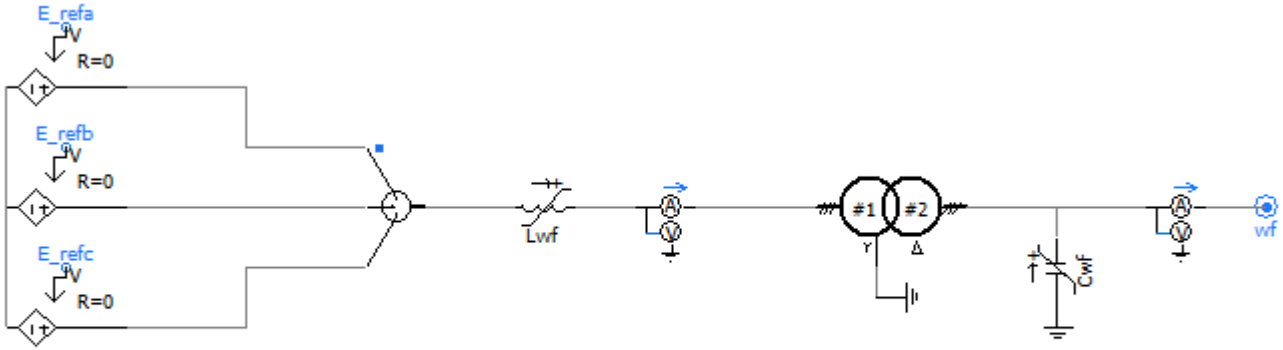

A.10 Offshore Wind Farm Control system – 2

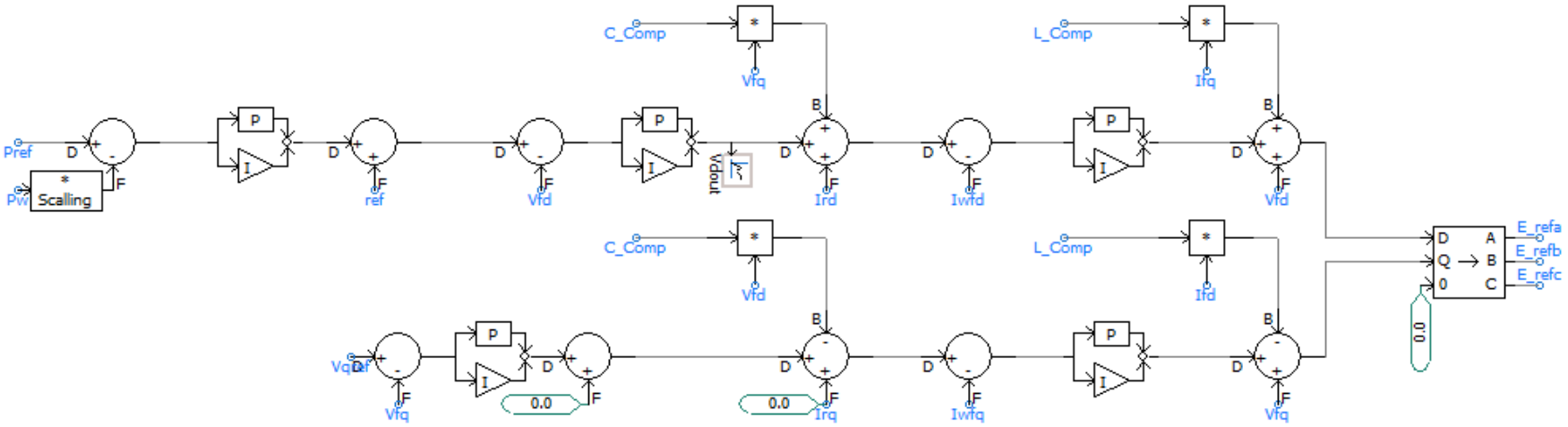

Appendix B Hybrid Converter Based on the Vienna rectifier and VSC

B.1 Hybrid Converter

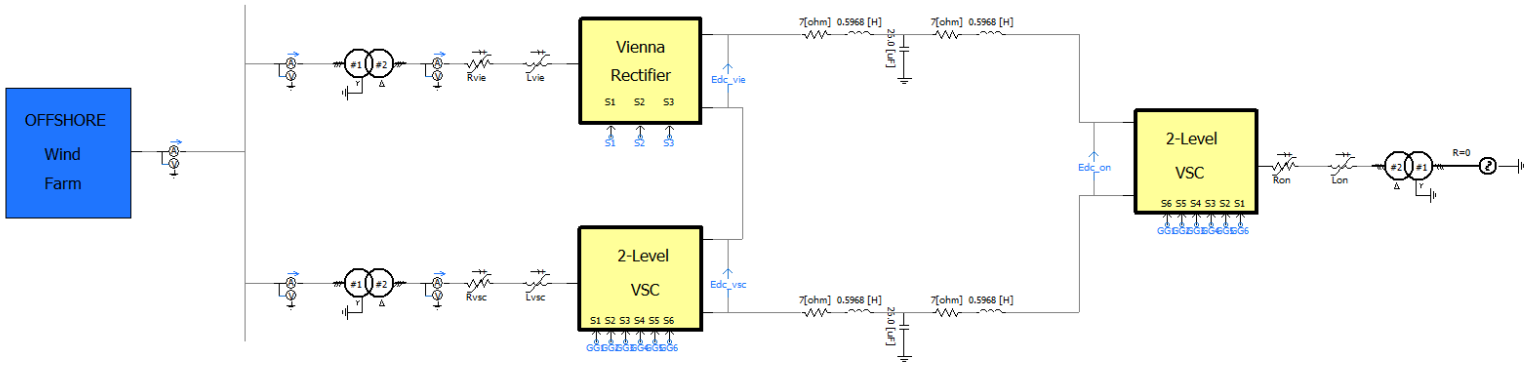

B.2 Vienna Rectifier

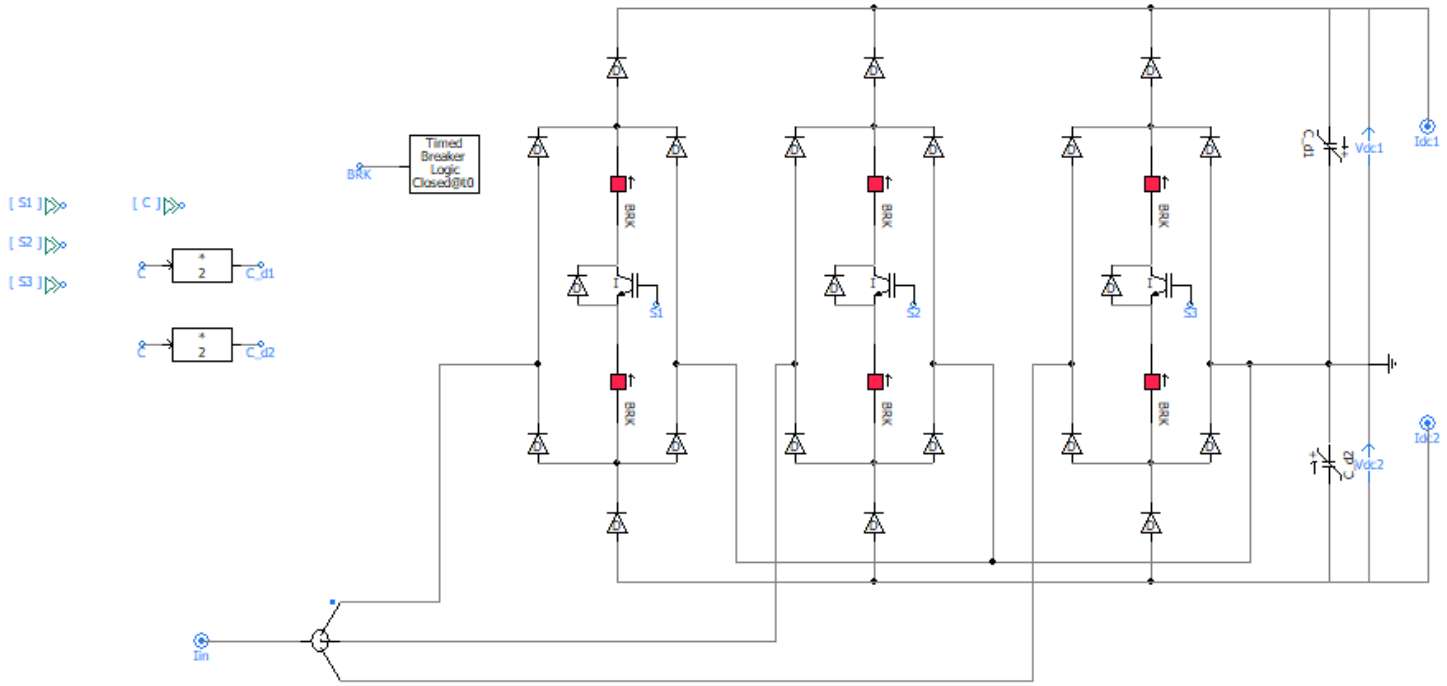

B.3 Vienna Control System

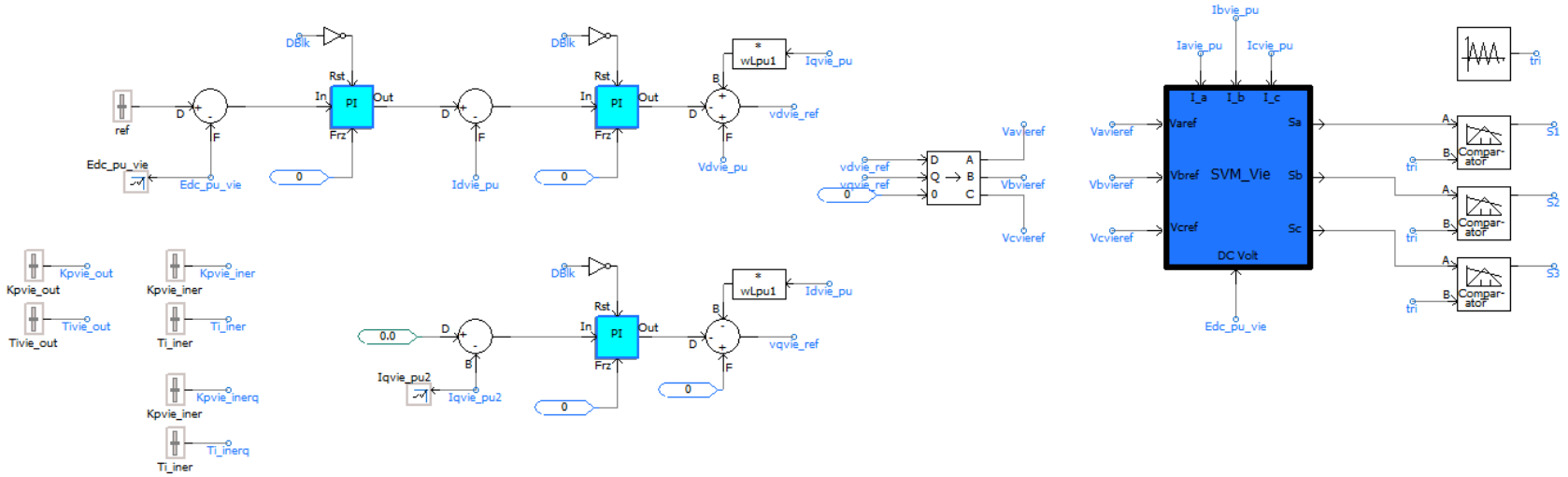

B.4 Vienna Rectifier VSM

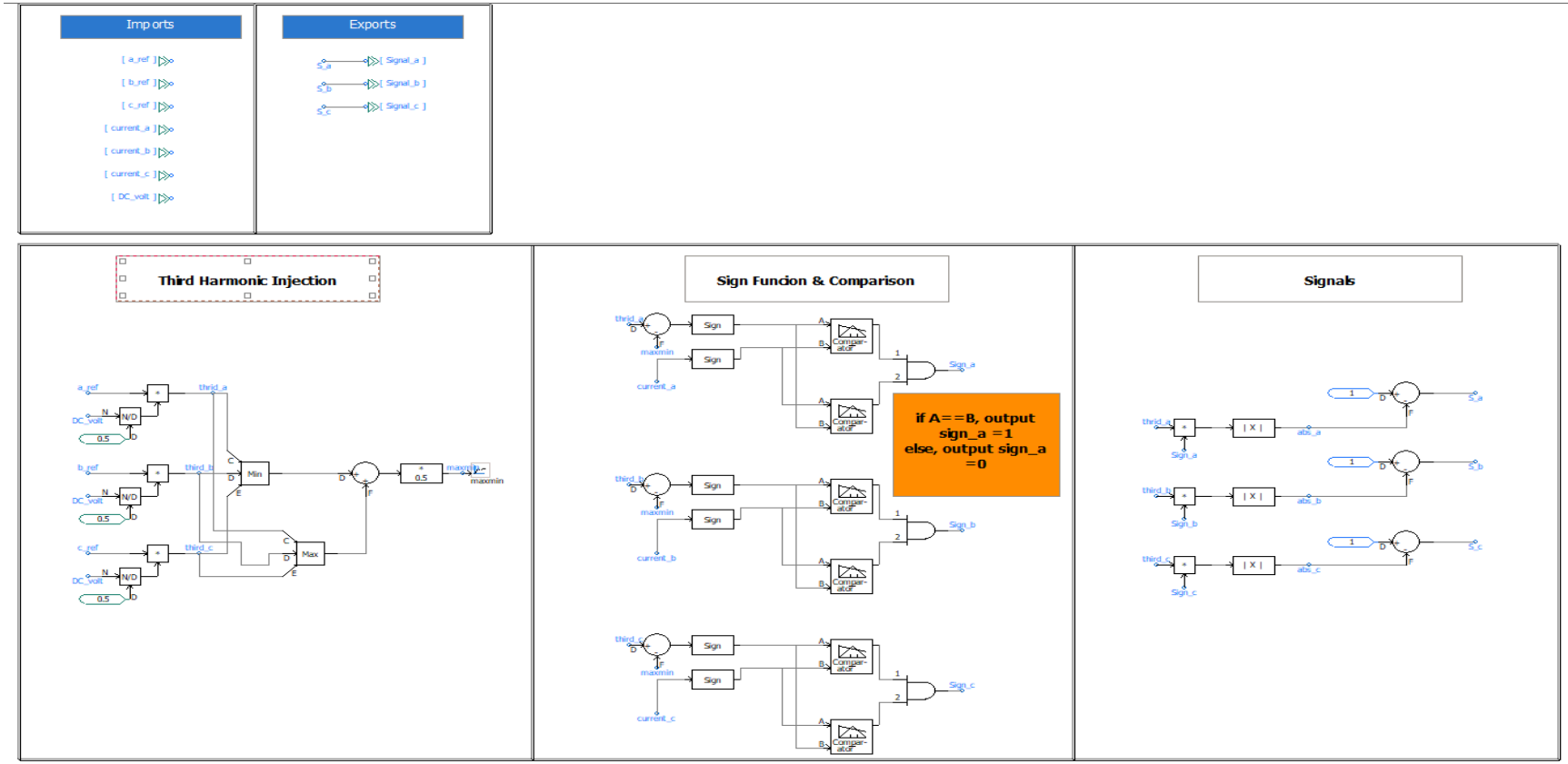

B.5 VSC Converter

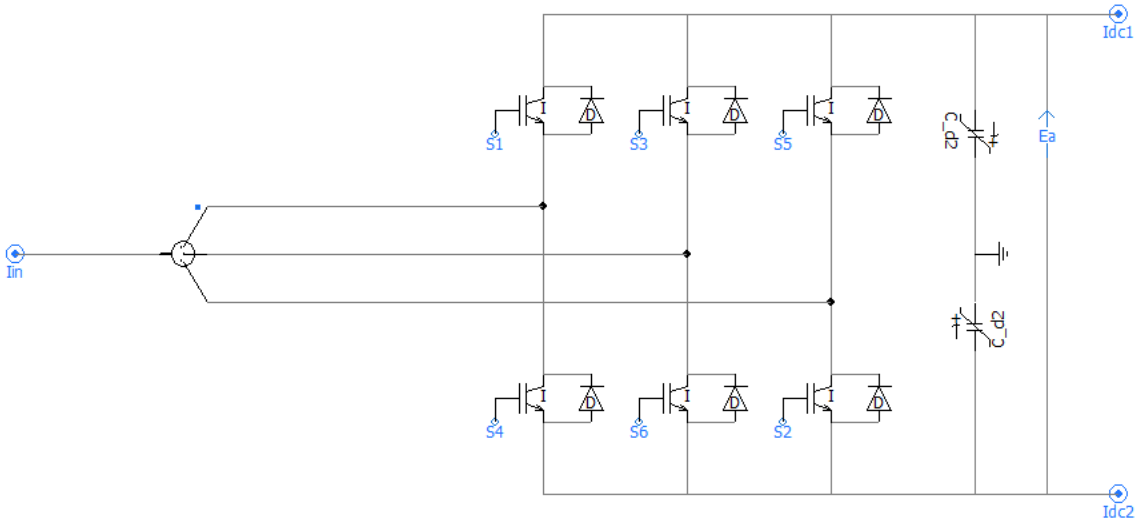

B.6 VSC Control System

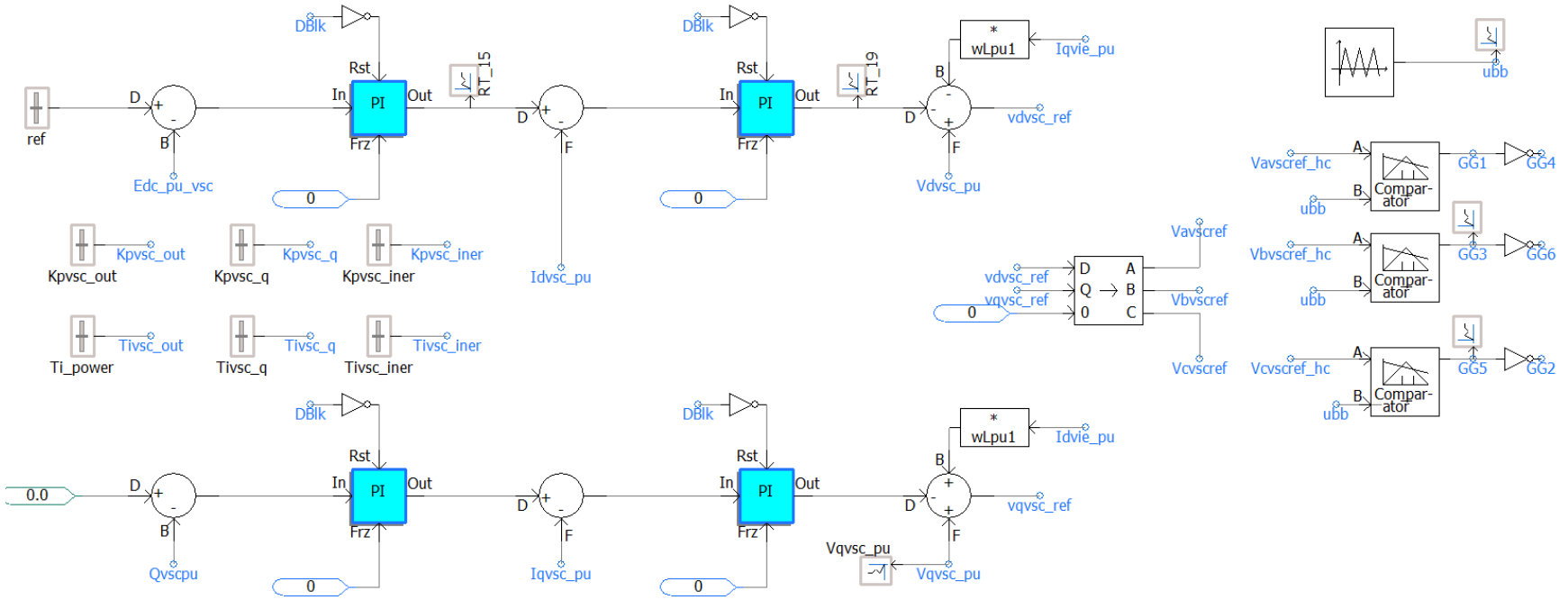

B.7 SRF Harmonic Controller

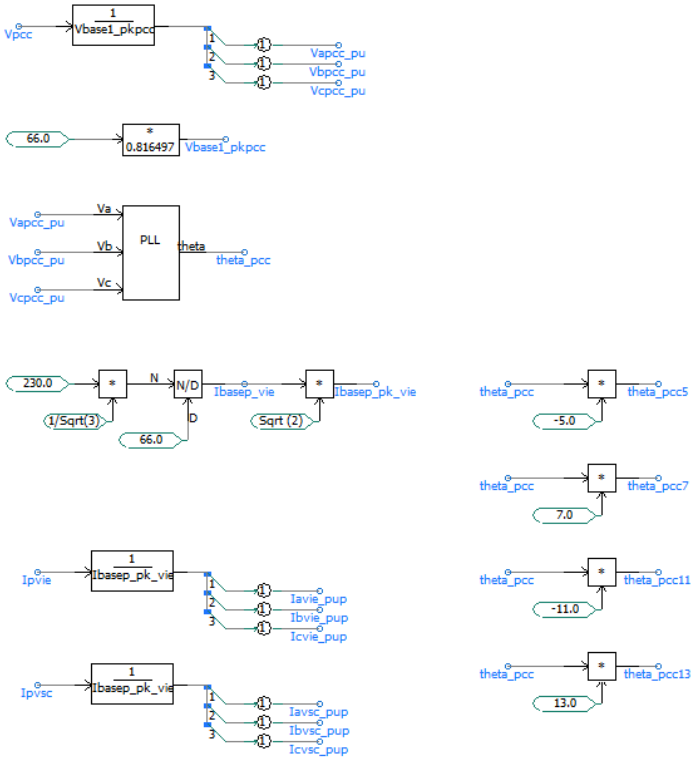

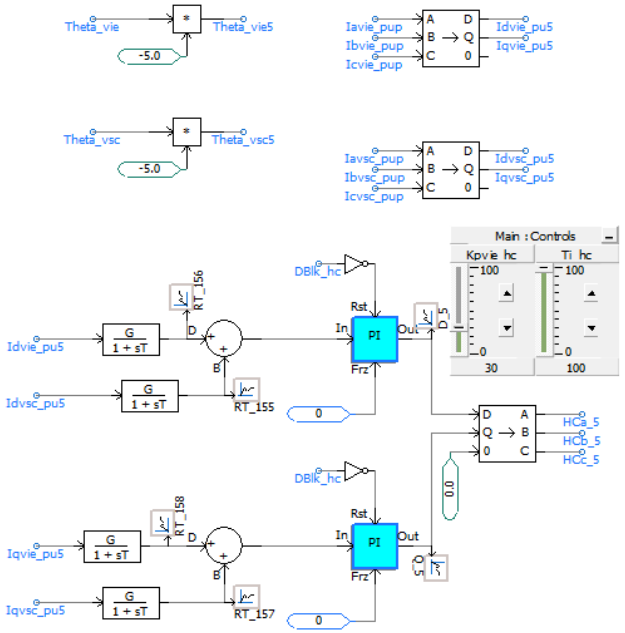

B.8 Offshore Wind Farm

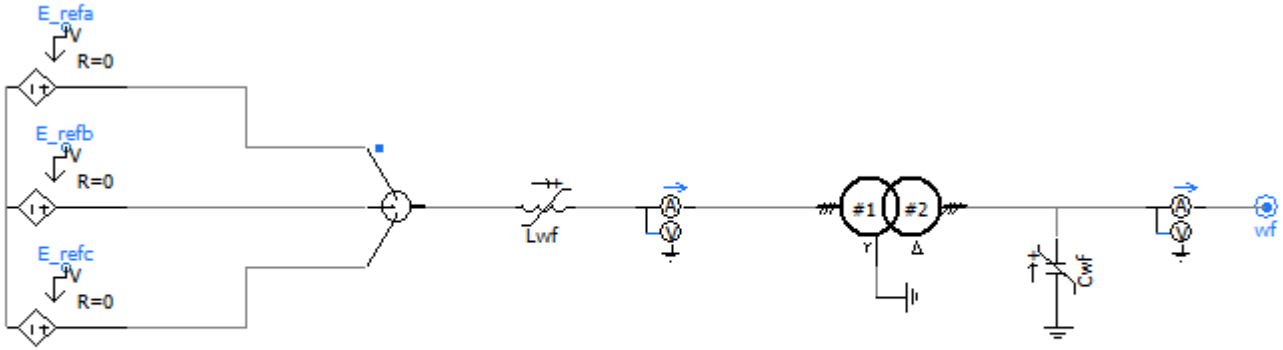

B.9 Offshore Wind Farm Control system

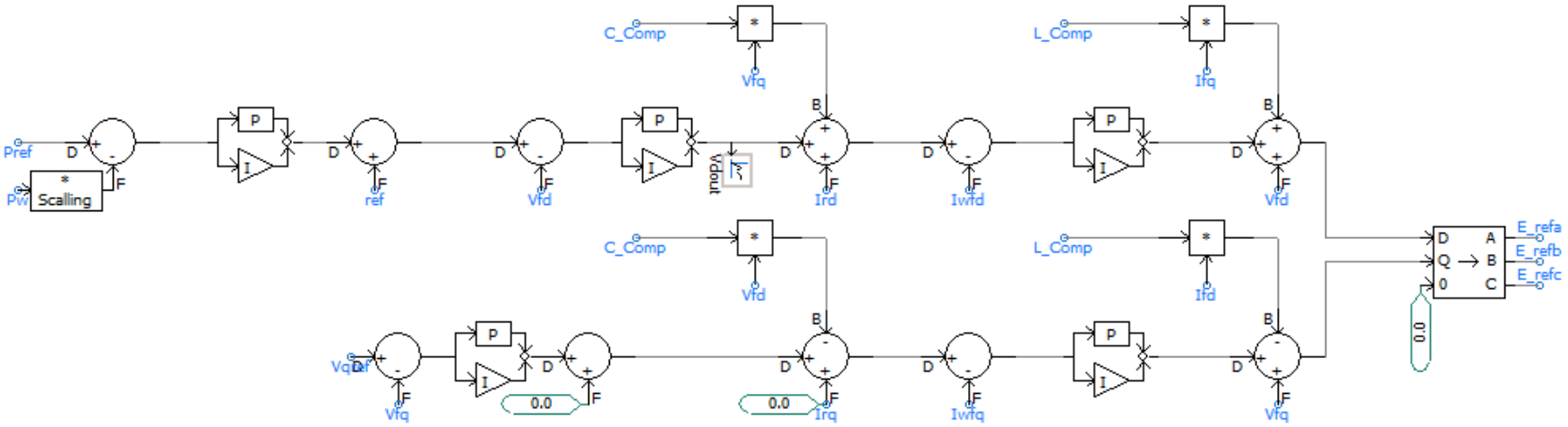

Appendix C

C.1Hybrid Converter

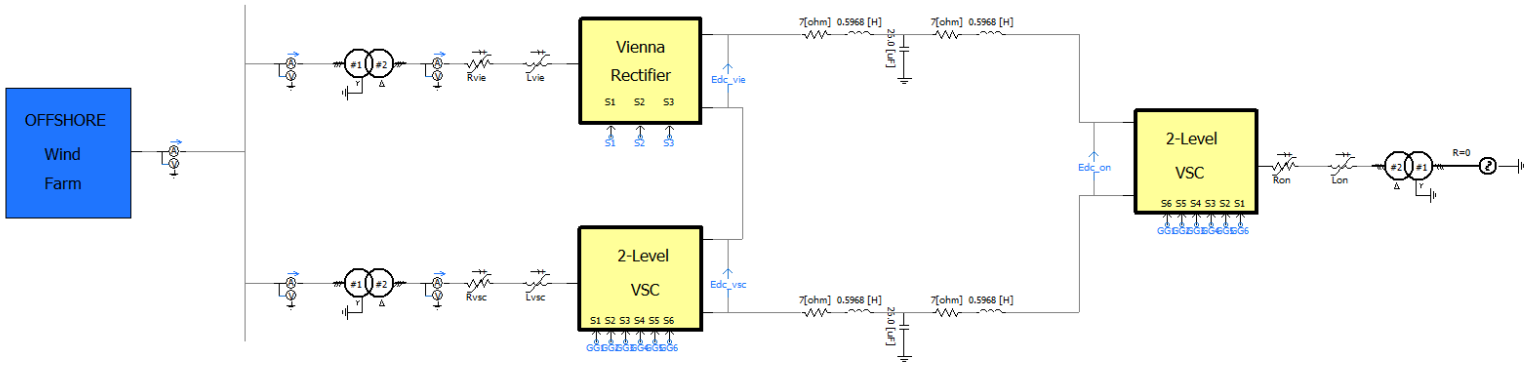

C.2Vienna Rectifier

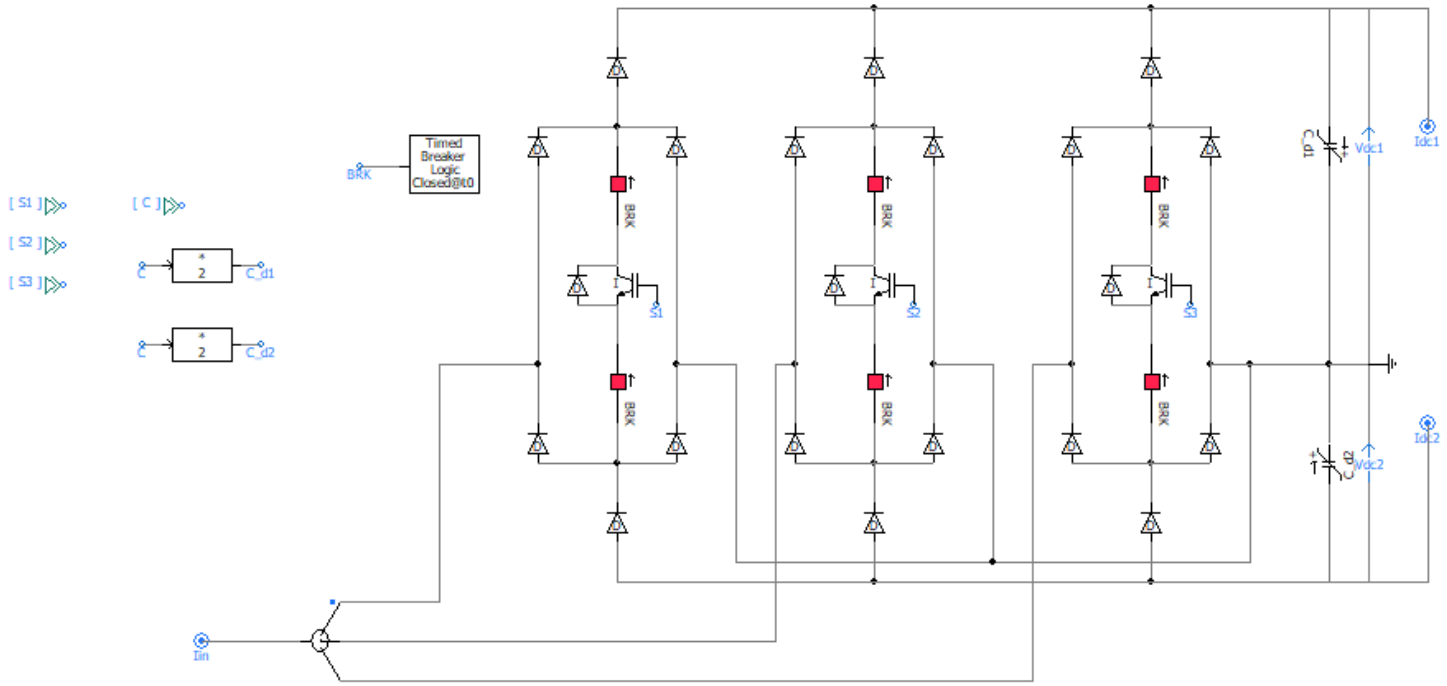

C.3Vienna Control System

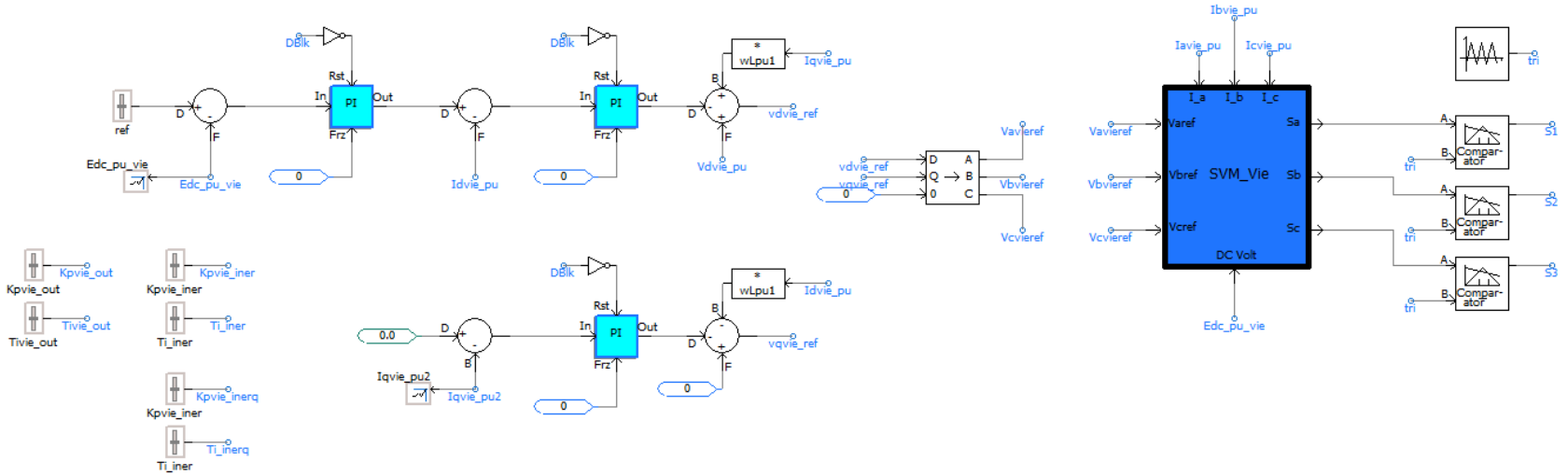

C.4Vienna Rectifier VSM

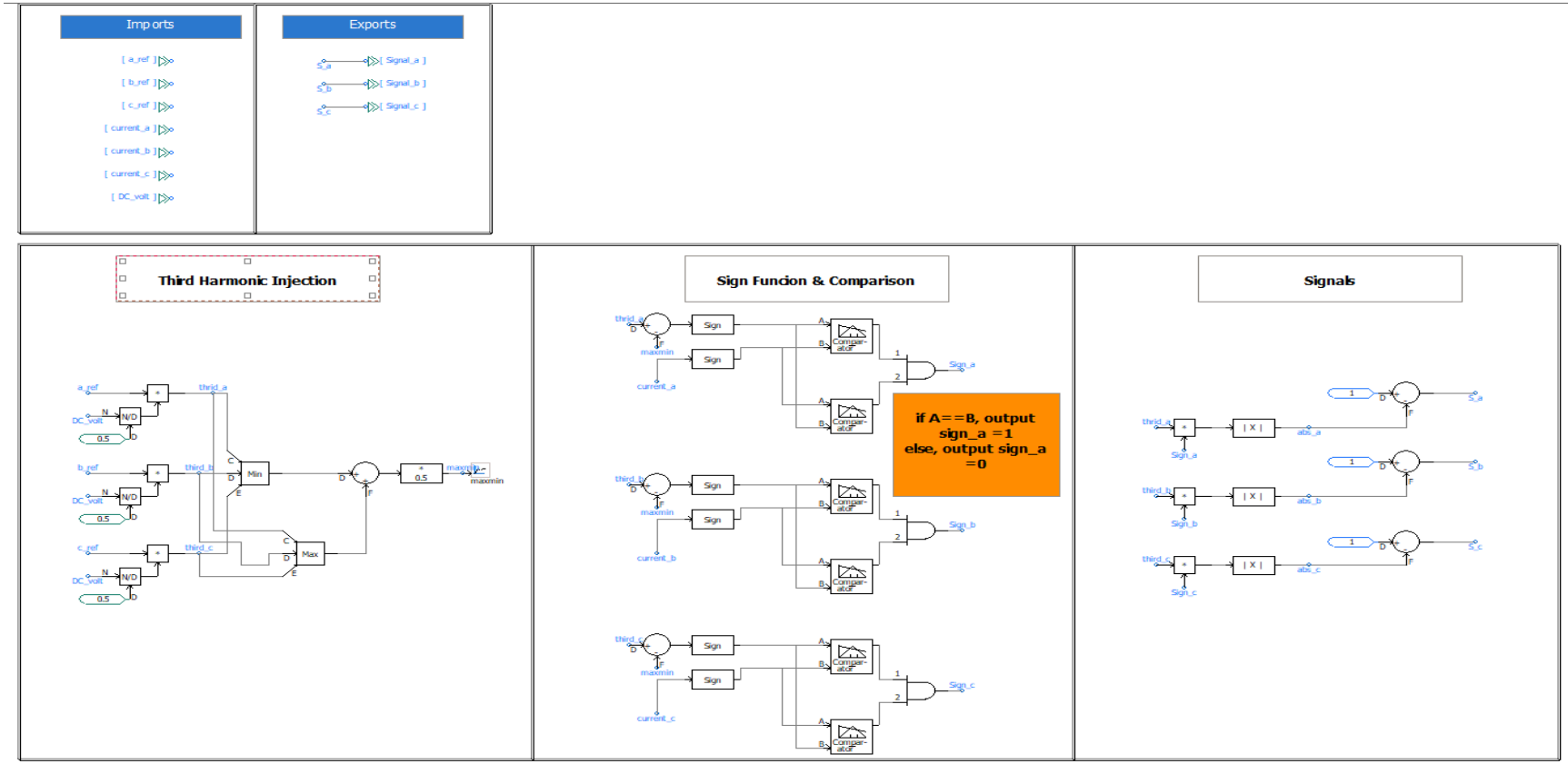

C.5VSC Converter

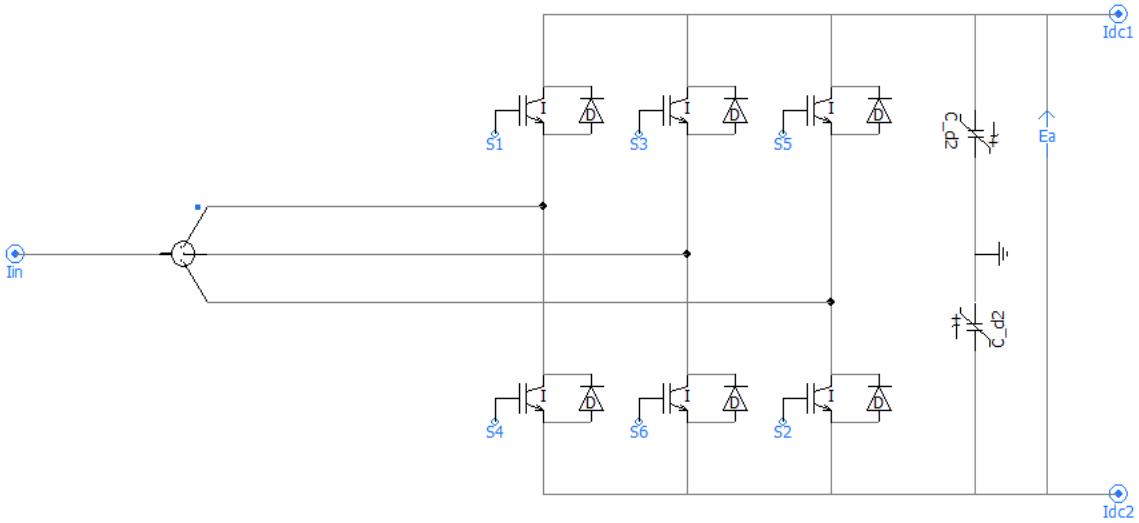

C.6VSC Control System

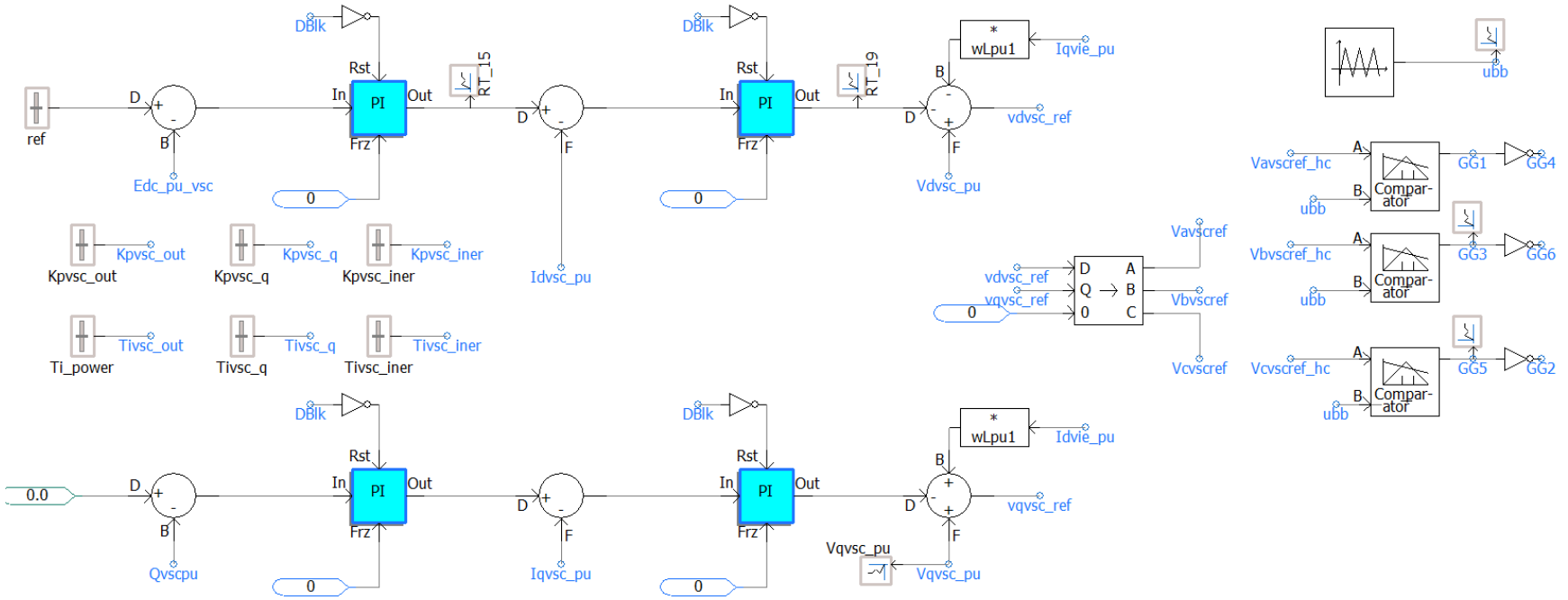

C.7 2DF-IMC SRF Harmonic Controller